

Endothelial TRPV4 channel regulation of pulmonary arterial pressure

Corina Marziano-Willard
Caracas, Venezuela

Master of Science in Biomedical Science
University of Virginia, 2017

Bachelor of Science in Biology
Xavier University, 2014

A Dissertation presented to the Graduate Faculty of the University of Virginia
in Candidacy for the Degree of Doctor of Philosophy

Department of Molecular Physiology and Biological Physics

University of Virginia
August, 2019

ABSTRACT

Pulmonary hypertension is a degenerative disorder affecting the pulmonary circulation and is characterized by increases in pulmonary vascular resistance and pulmonary arterial pressure. Loss of endothelium-dependent vasodilation in resistance vessels contributes to the pathogenesis of pulmonary hypertension. However, the physiological and pathological mechanisms that regulate endothelial function in health and disease remain poorly understood. Spatially localized increases in intracellular endothelial Ca^{2+} in resistance pulmonary arteries regulate vasodilation and overall pulmonary arterial pressure. Endothelial transient receptor potential vanilloid 4 (TRPV4_{EC}) channels are a major source of Ca^{2+} influx in resistance pulmonary arteries but the role of TRPV4_{EC} channel activity on endothelial function has remained unexplored. Work in this thesis investigates the hypothesis that TRPV4_{EC} channel activity promotes vasodilation in resistance pulmonary arteries thereby maintaining a low resting pulmonary arterial pressure.

Our results demonstrate that TRPV4_{EC} channel activity promotes vasodilation in resistance pulmonary arteries through the activation of endothelial nitric oxide synthase and subsequent release of nitric oxide (NO). Furthermore, caveolin-1 (Cav-1) was identified as a novel regulator of TRPV4_{EC} channels which potentiates TRPV4_{EC} channel activity. Loss of Cav-1-dependent activation of TRPV4_{EC} channels leads to endothelial dysfunction and an increase in pulmonary arterial pressure, revealing TRPV4_{EC} channels as important regulators of normal resting pulmonary arterial pressure. In pulmonary hypertension, endothelial Cav-1-TRPV4_{EC} channel signaling is impaired resulting in the

loss of vasodilation, thus increasing pulmonary arterial pressure. Elevated production of the reactive nitrogen species, peroxynitrite, is responsible for the impairment of Cav-1-dependent regulation of TRPV4_{EC} channel activity in pulmonary hypertension. Future studies should investigate the mechanisms by which peroxynitrite modifies Cav-1-dependent potentiation of TRPV4_{EC} channel activity in hopes of developing novel therapeutic targets for the treatment of pulmonary hypertension.

TABLE OF CONTENTS

Abstract.....	ii
List of Figures.....	v
List of Abbreviations	ix
Dedication	xii
Chapter 1: General Introduction	1
1.1 The pulmonary circulation.....	4
1.1.1 Ca ²⁺ regulation of pulmonary endothelial function	8
1.1.2 TRPV _{4EC} channels as a Ca ²⁺ influx pathway in the pulmonary endothelium	11
1.1.3 NO signaling in the pulmonary endothelium.....	14
1.1.4 Caveolin-1 as a regulator of endothelial function.....	16
1.2 Pulmonary Hypertension	17
1.2.1 Pathogenesis of PH.....	18
1.2.2 Endothelial dysfunction in PH.....	19
1.2.3 Animal models of PH	23
1.3 Conclusion	25
Chapter 2: Materials and Methods	27
2.1 Materials and Methods for Chapter 3	28
2.2 Materials and Methods for Chapter 4	38
Chapter 3: Nitric oxide-dependent feedback loop regulates TRPV4 channel cooperativity and endothelial function in small pulmonary arteries.....	49
3.1 Abstract.....	50
3.2 Introduction.....	51
3.3 Results.....	53
3.4 Discussion.....	102
Chapter 4: Impaired endothelial Caveolin-1-TRPV4 channel signaling contributes to endothelial dysfunction in pulmonary hypertension	108
4.1 Abstract.....	109
4.2 Introduction.....	110
4.3 Results.....	112
4.4 Discussion.....	137
Chapter 5: Future Directions.....	141
Chapter 6: Acknowledgements.....	156
Chapter 7: References	157

LIST OF FIGURES**CHAPTER 1**

Figure 1 Blood pressure along the pulmonary circulation7

CHAPTER 3

Figure 2 Native endothelium from small pulmonary arteries (PAs) displays transient receptor potential vanilloid 4 (TRPV4) sparklets with distinct spatial localization57

Figure 3 Specific TRPV4 channel agonists increase the number of sparklet sites per field of view in native ECs from fourth-order PAs61

Figure 4 TRPV4 sparklets increase local, but not whole-cell Ca^{2+} levels in the ECs63

Figure 5 TRPV4 sparklets represent unitary Ca^{2+} influx events through TRPV4 channels in the native endothelium from small PAs.....65

Figure 6 TRPV4 channel activation dilates cannulated, pressurized small PAs through endothelial nitric oxide synthase (eNOS) activation, and small MAs through IK/SK channel activation69

Figure 7 Spermine NONOate, a NO donor, increases DAF-FM fluorescence in ECs and SMCs from small PAs and causes vasodilation in a concentration-dependent manner75

<u>Figure 8</u>	TRPV4-eNOS Ca ²⁺ signaling mechanism regulates nitric oxide levels in small PAs	77
<u>Figure 9</u>	Ca ²⁺ influx via endothelial TRPV4 channels does not increase Ca ²⁺ release from the endoplasmic reticulum (ER) in PAs.....	79
<u>Figure 10</u>	Nitric oxide disrupts cooperative openings of TRPV4 channels and lowers channel activity in small PAs	83
<u>Figure 11</u>	Endothelial NO-guanylyl cyclase (GC)-protein kinase G (PKG) signaling disrupts cooperative openings of TRPV4 channels in small PAs.....	88
<u>Figure 12</u>	NO-GC-PKG signaling impairs Ca ²⁺ -dependent cooperative openings of TRPV4 channels in small PAs	91
<u>Figure 13</u>	Classical activators of endothelial G _q protein-coupled receptors, carbachol (CCh) and bradykinin, do not increase EC TRPV4 Ca ²⁺ sparklet activity in small PAs	95
<u>Figure 14</u>	ATP is an endogenous activator of local TRPV4-eNOS signaling in small PAs	97
<u>Figure 15</u>	Local TRPV4 channel-dependent Ca ²⁺ signaling regulates endothelium-dependent vasodilation in resistance-sized PAs	100

CHAPTER 4

<u>Figure 16</u>	Endothelium-specific TRPV4 knockout (TRPV4 _{EC} ^{-/-}) mice have elevated PAP.....	114
<u>Figure 17</u>	TRPV4 _{EC} channel activity is impaired in PH contributing to elevated PAP.....	118
<u>Figure 18</u>	NO signaling downstream of TRPV4 _{EC} channel activation is unaffected in CH mice.....	120
<u>Figure 19</u>	Cav-1 _{EC} -dependent potentiation of TRPV4 _{EC} channels is impaired in PH.....	124
<u>Figure 20</u>	PN impairs TRPV4 _{EC} channel activity in PH.....	128
<u>Figure 21</u>	Exogenous PN attenuates TRPV4 _{EC} sparklet activity in normal mice.....	130
<u>Figure 22</u>	NOX1-, mitochondria-, and iNOS- dependent signaling impairs TRPV4 _{EC} sparklet activity in CH mice.....	133
<u>Figure 23</u>	Peroxynitrite inhibits Cav-1 _{EC} -PKC-TRPV4 _{EC} signaling in pulmonary hypertension.....	135

CHAPTER 5

<u>Figure 24</u>	ATP increases TRPV4 _{EC} sparklets in a P2Y2R-dependent manner..	144
<u>Figure 25</u>	RVSP of Panx1 _{EC} ^{-/-} mice.....	146
<u>Figure 26</u>	Cysteine oxidation inhibits TPRV4 _{EC} sparklet activity in CH mice..	151

<u>Figure 27</u>	TRPV ₄ ^{EC} sparklet activity and TRPV ₄ ^{EC} channel-dependent vasodilation is impaired in SU + CH mice153
<u>Figure 28</u>	TRPV ₄ ^{EC} sparklet activity is impaired in PAs from PH patients155

LIST OF ABBREVIATIONS

Ca ²⁺	Calcium
CaM	Calmodulin
Cav-1 _{EC}	Endothelial caveolin-1 _{EC}
Cav-1 _{EC} ^{-/-}	Endothelial-specific Cav-1 knockout mice
CH	Chronic hypoxia
CSD	Caveolin-1 scaffold domain
EC	Endothelial cell
EndoMT	Endothelial to mesenchymal transition
eNOS	Endothelial nitric oxide
F/F ₀	Fractional fluorescence
GC	Guanylyl cyclase
GPCR	G-protein coupled receptor
IK	Intermediate conductance K ⁺ channels
iNOS	Inducible nitric oxide synthase
IP ₃	Inositol triphosphate
IP ₃ R	Inositol triphosphate receptor
κ	Coupling coefficient

K ⁺	Potassium
MA	Mesenteric arteries
MEP	Myoendothelial projection
nNOS	Neuronal nitric oxide synthase
NO	Nitric oxide
NOX	NADPH oxidase
O ₂ ⁻	Superoxide
PA	Pulmonary arteries
PAP	Pulmonary arterial pressure
PH	Pulmonary hypertension
PKC	Protein kinase C
PKG	Protein kinase G
PLC	Phospholipase C
PN	Peroxynitrite
P2XR	Purinergic P2X receptor
P2YR	Purinergic P2Y receptor
PVR	Pulmonary vascular resistance
ROS	Reactive oxygen species

RV/LV+S	Right ventricular/left ventricle + septal weight (Fulton Index)
RVSP	Right ventricular systolic pressure
SK	Small conductance K ⁺ channels
SMC	Smooth muscle cell
SOD	Superoxide dismutase
SU-5416	Sugen 5416
SU + CH	Sugen and chronic hypoxia
TRPV4 _{EC}	Endothelial transient receptor potential vanilloid 4
TRPV4 _{EC} ^{-/-}	Endothelial specific TRPV4 knockout mice
TRPV4 ^{-/-}	Global TRPV4 knockout mice

DEDICATION

I would like to dedicate this thesis to everyone who has supported me throughout my life and scientific career. To my parents, for not only their love and support, but also for all the sacrifices they've made in order for me to have the opportunity to pursue my Ph.D. To my Mami, Carolina, for all the love you've given me. To my papito, Francisco, for instilling in me a sense of wonder and curiosity in science, pushing me to learn more and more fun-facts. To my husband and best friend, Jake, for loving and supporting me through everything and always believing that I can accomplish anything I decide to do. Your love has carried me through the crazy experience that is graduate school and I cannot imagine getting through this journey without you. To my sister, Paola, and my bother-in-law, Nick, for their continued and unwavering support. To Oma and Abuelita, for all the laughs, love, and the reminder that nothing is more important than family. To all the Marzianitos and Rufs for the parrillitas and family time that helped me recharge and gave me new energy. To the family I gained through Jake, Dave, Theresa, David, Mary, and Simon for their continued love and support.

To my Ph.D. mentor, Dr. Swapnil Sonkusare, for the guidance and opportunities to grow as a scientist. It is through this experience that I learned what it takes to succeed as a scientist. To all current and past members of the Sonkusare Lab for their support and help throughout my graduate career. To my committee members, Drs. Avril Somlyo, Victor Laubach, and Brant Isakson, for challenging me to look beyond the details and think about how my work fits into the larger spectrum of physiology.

Finally, to my life mentoring committee (a.k.a all the friends I made throughout my life) for all the fun times and experiences outside of lab, all the trivia nights (go Mouse Rat!), and continued advise throughout my life.

CHAPTER 1: GENERAL INTRODUCTION

The cardiovascular system consists of the heart and the network of blood vessels (arteries, capillaries, and veins) responsible for transporting oxygen and nutrients throughout the body. To appropriately meet tissue demand for oxygen and nutrients, the cardiovascular system carefully regulates blood flow to target organs while maintaining a constant blood pressure. Blood pressure is controlled by changes in cardiac output and vascular resistance, with these two factors having differential effects during rest and activity. Cardiac output does not change on a moment to moment basis, and therefore has minimal effects on the dynamic regulation of blood pressure. On the other hand, vascular resistance is much more variable and actively changes in order to maintain a steady blood pressure. Changes in vascular resistance is regulated by the vasoreactivity of resistance arteries which make up a large portion of all the blood vessel cross-sectional area. Therefore, small changes in diameter across resistance vessels greatly impacts vascular resistance and overall resting blood pressure.

Resistance arteries are characterized by their ability to constrict in response to increases in intravascular pressure, a phenomenon known as myogenic vasoconstriction¹. Increases in intravascular pressure depolarizes vascular smooth muscle cells (SMCs) which activates voltage-dependent Ca^{2+} channels causing an influx of Ca^{2+} into the cytosol. Ca^{2+} binds to calmodulin (CaM) promoting actin-myosin crossbridge formation and SMC contraction – and thus vasoconstriction. Large conduit arteries (i.e. aorta, carotid, and main pulmonary artery) lack myogenic tone and therefore exert a minimal effect on blood pressure.

Myogenic vasoconstriction is directly opposed by endothelial cell (EC) Ca^{2+} signaling. Increases in endothelial Ca^{2+} activate vasodilatory pathways through the release of nitric oxide and prostaglandins, or through the opening of Ca^{2+} -sensitive K^+ channels leading to membrane hyperpolarization and vasodilation. By opposing myogenic vasoconstriction, the endothelium lowers vascular resistance and therefore overall blood pressure. Endothelial dysfunction, resulting in part from loss of endothelium-dependent vasodilation, is a contributing factor in vascular pathologies characterized by hypertension. This general introduction will focus on the role of EC regulation of vasodilation in resistance vessels, with a specific focus on the pulmonary circulation.

The pulmonary circulation is a specialized vascular bed important for gas exchange in the lungs. Venous blood is carried through the pulmonary arteries (PAs) to the alveolar capillaries where it is re-oxygenated and returned to the heart by the pulmonary veins before being distributed back to the systemic circulation. Regulation of endothelial function, specifically in resistance PAs, is imperative for maintenance of normal pulmonary vascular resistance and ventilation-perfusion matching. Endothelial dysfunction contributes to the pathogenesis of multiple pulmonary vascular disease including pulmonary hypertension (PH), where loss of endothelium-dependent vasodilation leads to elevated pulmonary arterial pressure (PAP). However, the mechanisms regulating endothelial function in intact resistance PAs have remained elusive. It is critical to decipher the mechanisms regulating endothelial function under normal conditions in order to understand how they may be impaired in pulmonary pathologies.

1.1 The pulmonary circulation

The pulmonary circulation is comprised of PAs which transport deoxygenated blood from the systemic circulation to the alveolar capillaries for re-oxygenation and pulmonary veins which transport oxygenated blood back to the heart. For this reason, the anatomy of the pulmonary circulation closely parallels the airways. PAs are highly compliant vessels able to withstand high volumes of blood flow. Large PAs have multiple layers of elastic lamina throughout the media²⁻⁵. Elastin and collagen fibers in the media allows the vessel to expand and accommodate the pulsatile flow emerging from the right ventricle. Further down the vascular tree, at the level of resistance PAs, the number of elastic layers decrease to a single layer of internal and external elastic lamina³. These resistance vessels are fully muscularized by a single SMC layer and respond to physiological signals to modulate arterial diameter³. Partial de-muscularization of the PAs begins to occur at the pre-capillary arterioles which parallel the terminal bronchi^{2,6,7}. Partial de-muscularization of the terminal arterioles maximizes the surface area available for gas exchange, thereby increasing oxygen saturation efficiency^{3,8}. The primary site of gas exchange is the pulmonary capillaries which are made up of only an EC layer and form a network of vessels that completely surround the alveoli. The abundance of capillaries surrounding each alveolus and the structure of the capillary ECs are perfectly designed to maximize the amount of surface area available for gas exchange while minimizing the distance gas needs to travel from the air space to the blood. Blood from the capillaries drain into the pulmonary veins which are similar in structure to PAs, although they have 30-60% less SMC covering compared to equal sized PAs^{2,3}. Loss of SMC layers in veins is

compensated by a thicker extracellular matrix comprised mainly of collagen fibers^{3,9}. Overall, the anatomy of the pulmonary circulation is perfectly structured to withstand high volumes of blood flow and optimize gas exchange.

Contrary to the systemic circulation, the pulmonary circulation is characterized as a high flow and low resistance system. With each heartbeat, the entirety of the right ventricular cardiac output is transferred into the pulmonary circulation making it a high flow system, unlike in systemic arteries where the cardiac output is distributed throughout multiple target organs¹⁰. To accommodate high blood flow, PAs are elastic and exhibit lower vascular resistance than systemic arteries. This is evident by the differences in diastolic blood pressure where the PAP is approximately 10 times lower than systemic arterial pressure (8 vs. 80 mmHg, respectively, Figure 1). Although PAs are highly compliant, they are not passive vessels void of vasoreactivity. In fact, inhibition of vasodilatory signals increases PAP¹¹. Increases in basal vascular tone is also observed in pulmonary vascular pathologies, like PH, where EC and SMC function are disrupted, indicating that there is a baseline regulation of vascular tone¹². However, the mechanisms regulating resting PAP are not fully understood and are an important ongoing area of research in the field. My dissertation work, in part, contributes to the understanding of pulmonary EC function and regulation of resting PAP by investigating the mechanisms controlling endothelium-dependent vasodilation in resistance PAs.

Vasoreactivity of resistance PAs maintains optimal ventilation/perfusion (V/Q) matching and resting PAP. The V/Q ratio measures the efficiency of gas exchange within the alveoli, where V represents alveolar gas filling and Q represents blood flow through

the capillaries. Under normal conditions, most alveoli are continuously perfused with blood. When alveolar ventilation is disrupted, localized hypoxia manifests in the alveolar region, referred to as V/Q mismatching, ensuing vasoconstriction resulting in blood shunted away from the damaged alveoli to restore the V/Q ratio^{13,14}. This phenomenon is termed hypoxic vasoconstriction and is unique to the pulmonary circulation. Hypoxic vasoconstriction is regulated by Ca²⁺-dependent mechanisms in pulmonary SMCs^{13,14}. Similarly, Ca²⁺ signaling in ECs regulate endothelium-dependent vasodilation to counteract pulmonary vasoconstriction. Impairment in endothelial Ca²⁺ signaling results in excessive vasoconstriction and elevation of PAP.

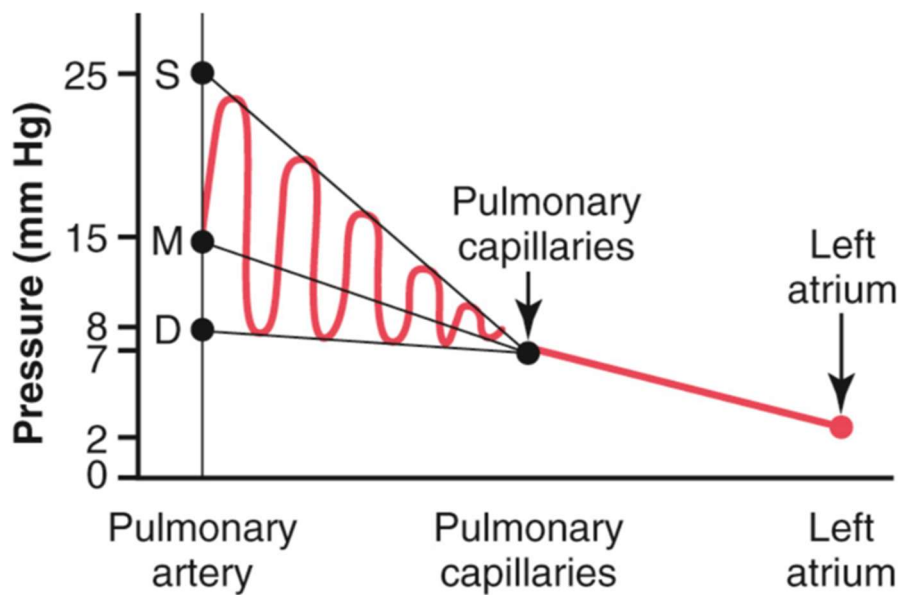
FIGURE 1. BLOOD PRESSURE ALONG THE PULMONARY CIRCULATION.

Figure 1. Blood pressure along the pulmonary circulation. Mean blood pressure (mmHg) along the pulmonary circulation. Red curve represents changes in pressure. D, S, and M represent diastolic, systolic, and mean pressure respectively. Figure obtained from Guyton and Hall Textbook of Medical Physiology¹⁵.

1.1.1 Ca²⁺ regulation of pulmonary endothelial function

The endothelium is the innermost layer of all PAs and is critical for the regulation of vasoreactivity and capillary barrier integrity. Endothelial dysfunction is common in the pathogenesis of multiple pulmonary vascular diseases including PH and pulmonary edema. The endothelium responds to physiological stimuli including; mechanical forces¹⁶⁻¹⁸, paracrine and autocrine signals^{19,20}, and neuronal input to regulate vascular function²¹⁻²³. This activation of ECs regulates vascular resistance, permeability, inflammation, and angiogenesis. It is important to note that endothelial heterogeneity throughout the vascular tree contributes to differences in response to similar physiological stimuli in resistance PAs and capillaries^{24,25}. These differences are in part due to variances in Ca²⁺ signaling mechanisms between PAs and capillaries. Increased intracellular Ca²⁺ is an important intermediate signaling molecule responsible for regulating EC function, including vasoreactivity and barrier integrity. The sources of Ca²⁺, its spatial localization within individual ECs, and the location of the ECs within the vascular tree, determines the overall effect on vascular function^{24,25}. Therefore, it is imperative to understand Ca²⁺ dynamics in the context of the vessel being studied.

EC Ca²⁺ can increase through two main pathways: internal release of Ca²⁺ from the endoplasmic reticulum (ER) and Ca²⁺ influx through membrane ion channels. Internal release of Ca²⁺ from the ER occurs through inositol triphosphate receptor (IP₃R)-dependent activation. Gq-protein coupled receptor (GqPCR)-signaling results in the formation of diacylglycerol (DAG) and inositol triphosphate (IP₃) from phosphatidylinositol 4,5-bisphosphate (PIP₂). IP₃ activation of IP₃R, ionotropic channels on the ER membrane,

causes the release of Ca^{2+} into the cytosol²⁶. IP_3R opening is also facilitated by direct binding of Ca^{2+} to the receptor. However, at higher concentrations, Ca^{2+} inhibits IP_3R activity, supporting a biphasic role for Ca^{2+} in the regulation of IP_3R signaling^{27,28}. ER Ca^{2+} stores are replenished through the activity of Ca^{2+} -ATPases on the ER membrane that transport Ca^{2+} back into the ER against its concentration gradient. Ca^{2+} release from the ER is present in the native endothelium of resistance PAs, however, the signaling targets downstream of IP_3R -dependent Ca^{2+} release and its contribution to endothelial function remain unknown²⁹.

Ca^{2+} influx in pulmonary ECs can also occur through openings of cell membrane cation channels, which are activated by direct agonist ligation, mechanical forces, or G-protein coupled receptor (GPCR) signaling. Purinergic P2X receptors are ligand gated ion channels present in the pulmonary endothelium serving as a direct Ca^{2+} influx pathway. P2X receptors are activated by direct binding of ATP, a prominent signaling molecule that is released by shear stress in the pulmonary circulation^{30,31}. P2X4 receptors (P2X4R) are the main subtype of P2X receptors responsible for shear stress-induced increases of intracellular Ca^{2+} in cultured human pulmonary EC³⁰. Shear stress-induced activation of P2X4R was dependent on ATP signaling and was unaffected by inhibition of GqPCR signaling or ER Ca^{2+} depletion, suggesting that the results observed were Ca^{2+} influx events through a ligand gated ion channel. The contribution of P2X4R as Ca^{2+} influx channels was confirmed by attenuation in Ca^{2+} increases in response to shear stress after P2X4R knockdown. However, the physiological role of P2X4R signaling in intact resistance PAs remains an open area of study. It is important to note that Ca^{2+} increases in response to

shear stress was not completely blocked by knocking down P2X4R, suggesting the presence of other membrane Ca^{2+} channels which contribute to the shear-stress response.

Recently, Piezo channels have been identified as mechanosensitive cation channels present in multiple cell types including vascular ECs³². Piezo channels are trimeric transmembrane channels containing a large blade-like structure on the extracellular portion of the cell membrane, which is hypothesized to be the mechanosensitive region of the channel³³. So far two isoforms of Piezo have been identified, Piezo 1 and Piezo 2, with Piezo 1 more highly expressed in the vascular endothelium, including PAs^{32,33}. In a perfused lung system, pressure-induced activation of Piezo 1 disrupted endothelial adherens junction leading to fluid extravasation and edema formation³⁴. Mice with endothelium specific deletion of Piezo 1 (Piezo 1_{EC}^{-/-}) were protected from pressure-induced edema formation highlighting the mechanosensitive regulation of pulmonary endothelial function by Piezo 1³⁴. However, the possible contribution of Piezo 1 in shear stress sensing in the endothelium of resistance arteries and its possible regulation on PAP remain unknown. Interestingly, Piezo 1_{EC}^{-/-} mice develop systemic hypertension supporting the possibility of Piezo 1-dependent regulation of resting PAP.

Finally, members of the large TRP (transient receptor potential) channel family, which are activated by GPCR signaling, are key sources of Ca^{2+} influx in the pulmonary endothelium. Of specific interest to this dissertation, endothelial TRPV4 (TRPV4_{EC}) channels have been found to be the main Ca^{2+} influx pathway in resistance PAs²⁹. TRPV4_{EC} channel activity promotes endothelium-dependent vasodilation through the activation of endothelial nitric oxide synthase (eNOS) and subsequent release of nitric oxide (NO)²⁹.

The following sections of this introduction will focus on the current knowledge of role of TRPV4_{EC} channels in resistance PAs and their contribution to the regulation of vasodilation.

1.1.2 TRPV4_{EC} channels as a Ca²⁺ influx pathway in the pulmonary endothelium.

TRPV4 (transient receptor potential vanilloid 4) channels are non-selective cation channels belonging to the larger family of TRP channels. TRPV4 channels are homotetramers with each subunit containing a cytosolic C- and N-terminal domain and 6 transmembrane spanning regions (TMs)³⁵⁻³⁸. The channel pore is made up of the transmembrane loop between TM5 and TM6³⁵⁻³⁸. The N-terminal contains three consecutive ankyrin repeats that facilitate channel interaction with other proteins as well as anchoring of the channel to the cell membrane³⁵. There are several PKC phosphorylation sites in the N-terminal tail and one PKA phosphorylation site in the C-terminal that contribute to PKC- and PKA- dependent potentiation of channel activity^{35,39}. The C-terminal tail contains a CaM binding site that is important for Ca²⁺-dependent potentiation of channel activity⁴⁰. Ca²⁺-bound CaM enhances channel activity by increasing the open state probability of the channel⁴⁰⁻⁴². At high concentrations, Ca²⁺ inhibits TRPV4 channel activity⁴⁰⁻⁴², however, the mechanism for Ca²⁺-dependent inhibition are not fully understood.

TRPV4 channels are preferentially permeable to divalent ions with 10- and 6-times higher permeability to Ca²⁺ and Mg²⁺ over Na⁺, respectively^{36,37,40,41,43,44}. Mutation of

D682 in the pore forming loop of the channel significantly lowers the Ca^{2+} permeability, indicating that D682 is important for the high Ca^{2+} conductance exhibited by TRPV4 channels^{45,46}. TRPV4 channels have a high single channel conductance of 60 pS, which results in a large influx of Ca^{2+} into the cytosol with the opening of single TRPV4 channels^{37,40,47,48}. In fact, once opened, approximately 100 times more Ca^{2+} flow through TRPV4 channels than a voltage-gated L-type Ca^{2+} channels, making TRPV4 channels a major source of Ca^{2+} influx in ECs⁴⁹. A current area of interest in the field focuses on understanding the structure of TRPV4 channels, specifically changes in the pore forming region that may dictate ion selectivity through the channel.

TRPV4 channels can be activated by a variety of physiological stimuli including temperature, shear stress, and GPCRs. TRPV4 channels are activated by temperatures ranging between 27-35°C^{48,50,51}. However, there have been some conflicting studies in patch clamp systems suggesting that TRPV4 channels may not be directly thermosensitive⁵². Shear stress has also been investigated as a mode of TRPV4 channel activation^{48,53}. One study suggests that the ankyrin repeat region is responsible for the mechanosensitive properties of TRPV4 channels³⁶. Deletion of the ankyrin repeats attenuates hypotonic-dependent activation of TRPV4 channels³⁶. However, more studies are needed to demonstrate that shear stress is a direct activator of TRPV4 channels. For instance, shear stress could indirectly activate TRPV4 channels through the release of ATP and activation of GPCR-dependent signaling²⁹. GPCR signal through DAG- or cyclic AMP (cAMP)- dependent pathways, which can enhance TRPV4 channel activity through PKC- and PKA-dependent phosphorylation, respectively^{23,39,49,53,54}.

In the lungs, TRPV4 channels are expressed within the bronchiolar epithelium, SMCs, and ECs^{11,55-57}. TRPV4_{EC} channel activity promotes vasodilation in resistance PAs and may also contribute to endothelial barrier dysfunction when overactivated^{29,58}. It should be noted that the ultimate effect of TRPV4_{EC} channel signaling may be determined by the concentration of the agonist used and the size of the blood vessel under consideration. Overactivation of TRPV4_{EC} channels by high concentrations of the agonist may lead to Ca²⁺ toxicity and cell death, thereby causing breakdown of the EC barrier. Administration of the specific TRPV4 channel agonist, GSK1016790A, to anesthetized mice induced edema, both at the arteriolar and capillary level, measured by perivascular cuff formation and alveolar flooding, respectively¹¹. Similarly, in isolated lung system, perfusion with 4 α -PDD, another TRPV4 channel agonist, induced edema as measured by alveolar flooding and an increased filtration coefficient (K_f), a measurement of fluid extravasation in *ex vivo* perfused lungs⁵⁵. Interestingly, lungs from global TRPV4^{-/-} mice were protected against edema⁵⁵. Although these studies suggest that TRPV4 channel activity is detrimental to barrier integrity, they fail to discern the relative contributions from individual cell types (EC, SMC, or airway epithelium). Currently there is a lack of understanding of the physiological role of TRPV4_{EC} channels throughout the pulmonary vascular network.

Activation of TRPV4_{EC} channels decreases RVSPs in anesthetized mice, suggesting that TRPV4 channel activity is important for the regulation of resting PAP¹¹. In larger PAs, TRPV4_{EC} channel activity promotes vasorelaxation through a NO-dependent mechanism⁵⁹. Consistently, inhibition of NOS caused a slight increase in RVSPs in mice¹¹.

These data suggest that TRPV4_{EC}-eNOS signaling regulates resting PAP. Chapter 3 and 4 of this dissertation will focus on the novel findings of TRPV4_{EC}-eNOS signaling in resistance PAs and its contribution to the regulation of PAP.

1.1.3 NO signaling in the pulmonary endothelium

NO is a major signaling molecule in the pulmonary vasculature. NO is formed by nitric oxide synthase (NOS) as a product of L-arginine hydrolysis. There are three isoforms of NOS: endothelial NOS (eNOS), neuronal NOS (nNOS), and inducible NOS (iNOS). eNOS is mainly expressed in ECs, but has also been identified in cardiac myocytes and platelets⁶⁰. Similarly, nNOS expression is not restricted to neurons, although that is where it is predominantly expressed. nNOS has also been identified in epithelial cells, kidneys, pancreatic islet cell, and SMCs⁶¹. The third NOS isoform, iNOS is ubiquitously expressed at low levels in all cell types. During inflammation, iNOS expression and activity increases^{11,62}. All three isoforms of NOS enzymes are homodimers, with each subunit containing a reductase and oxygenase domain. Several cofactors bind NOS to facilitate enzyme activity, including; flavin adenine dinucleotide (FAD), flavin mononucleotide (FMN), tetrahydrobiopterin (BH4), CaM, and heat shock protein 90 (HSP90). Inability of these cofactors to associate with NOS leads to NOS uncoupling and the subsequent release of superoxide radicals ($O_2^{\cdot-}$)^{60,63}.

NOS-dependent production of NO begins when reduced NADPH molecules, bound to the NOS reductase domain, transfers an electron to the heme on the oxygenase domain, via

FAD and FMN. At the heme site, L-arginine is oxidized to L-citrulline and reduced oxygen is converted to NO^{64,65}. Ca²⁺-bound CaM (Ca²⁺-CaM) promotes enzyme activity by facilitating the transfer of electrons from the reductase domain to the oxygenase domain⁶⁶. Both eNOS and nNOS activity is potentiated by increases in cytosolic Ca²⁺. Normally, eNOS and nNOS are bound to caveolin-1 (Cav-1), a negative regulator of enzyme activity. Increases in intracellular Ca²⁺, and subsequent Ca²⁺-CaM interaction, displaces the enzyme from Cav-1 promoting NO synthesis⁶⁶. Conversely, iNOS is considered to be calcium-independent because it does not require increases in intracellular Ca²⁺ to become active^{66,67}.

eNOS is expressed throughout the pulmonary vasculature, and is an important regulator of vascular tone⁶⁸⁻⁷⁰. After birth, eNOS expression in the pulmonary arteries increases reaching a maximum level at approximately two weeks post birth⁷¹. The increase in eNOS expression correlates with elevated NO production and decreased pulmonary vascular resistance (PVR) and is important for the transition of the pulmonary circulation from a high resistance system in the fetus, to a low resistance system in the adult⁷². Consistent with these findings, reduced NO signaling after birth is associated with the development of newborn PH^{73,74}. In the adult circulation, NO signaling continues to be important for the regulation of resting PAP. Global eNOS^{-/-} mice have elevated PVR that is rescued by re-expressing eNOS⁷⁵. It is important to note that eNOS^{-/-} mice have normal systemic blood pressures, further highlighting the importance of eNOS signaling specifically in the pulmonary vasculature. However, the Ca²⁺ signals that regulate eNOS activation in the pulmonary endothelium remain unknown. Chapter 3 contains the first evidence of TRPV4_{EC} channel- dependent activation of eNOS in pulmonary resistance arteries.

1.1.4 Caveolin-1 as a regulator of endothelial function

Caveolae are membrane invaginations involved in a multitude of cellular processes including: transcellular transport, cell survival, apoptosis, proliferation, migration, and vascular reactivity⁷⁶. Caveolin-1 (Cav-1) is the main structural protein in caveolae and is expressed throughout the vasculature, including the pulmonary endothelium. Cav-1 serves as a membrane scaffold protein, localizing cell signaling components for efficient signal transduction. Because of its interactions with key signaling molecules in the endothelium, Cav-1 is an important regulator of EC function and vasodilation. In fact, changes in Cav-1 expression is associated with multiple pulmonary diseases, including PH⁷⁷⁻⁸⁰.

One of the mechanisms by which Cav-1 regulates endothelium-dependent vasodilation is through the interaction with eNOS at the caveolin-1 scaffold domain (CSD), the main scaffolding site on Cav-1 for protein interaction^{81,82}. eNOS binding to the CSD of Cav-1 inhibits enzyme activity⁸³⁻⁸⁵. Once intracellular Ca^{2+} increases, Ca^{2+} -CaM displaces eNOS from the CSD and activates the enzyme⁶⁶. Although the Cav-1-eNOS binding prevents NO synthesis, this interaction is required for proper enzyme association with its cofactors (L-arginine and BH4) and facilitates localizing eNOS at the cell membrane where it can be activated. Inhibition of this association prevents the ability of cofactors to bind to eNOS, leading to the uncoupling of the protein and formation of superoxides (O_2^-)⁷⁶.

Loss of Cav-1 is associated with pulmonary vascular diseases including PH. One of the leading hypotheses in the field is that loss of Cav-1 expression results in eNOS uncoupling and endothelial dysfunction, contributing to the pathogenesis of PH⁷⁹. This hypothesis is supported in myocardial infarction rat models of PH, which demonstrate a decrease in Cav-

1 expression taken from whole tissue homogenates⁸⁰. Furthermore, global Cav-1^{-/-} mice develop spontaneous PH which can be prevented by re-expressing Cav-1 in the endothelium, suggesting that endothelial Cav-1 is an important regulator of resting PAP⁸⁶⁻⁸⁸. It is essential to note that studies showing loss of Cav-1 expression in models of PH were measured from whole lung tissue homogenates and were not representative of only pulmonary ECs. Consistent with these results, decreases in Cav-1 expression is only observed in the plexiform lesions of PH patients⁷⁸. Plexiform lesions are formed in areas of the pulmonary vasculature where ECs are undergoing endothelial-mesenchymal cell transitions⁷⁸. It is likely that the arteries containing plexiform lesions are not vasoactive and may not have a direct impact on PAP. Therefore, it is imperative to understand the cell-specific changes in Cav-1 expression and, more importantly, regulation in the development of PH. Chapter 4 describes, for the first time, a Cav-1-dependent regulation of TRPV4_{EC} channel activity in resistance PAs.

1.2 Pulmonary Hypertension

Pulmonary hypertension (PH) is a progressive debilitating disease affecting approximately 1,000 new people each year in the United States alone (NHLBI). This vaso-occlusive disease is characterized by impaired vasodilation and vascular remodeling of resistance PAs leading to sustained elevated PAP (> 25 mmHg). Elevated PAP leads to right ventricular (RV) hypertrophy and ultimately right heart failure in PH patients. Even with therapeutic intervention, such as vasodilators and vasoconstrictor inhibitors, PH patients continue to have a 30% mortality rate 5 years after diagnosis⁸⁹. This fact highlights

the need for the discovery of novel therapeutic targets for improving patient outcome. PH can be classified into one of five categories: 1. Idiopathic/heritable PH (also referred to as pulmonary arterial hypertension), 2. PH secondary to left heart failure, 3. PH secondary to lung disease/hypoxia, 4. PH secondary to chronic thromboembolisms and, 5. PH resulting from unclear mechanisms (blood, systemic, or metabolic disorders)⁹⁰. Despite different triggers, all classes of PH present with similar pathologies of endothelial dysfunction, vascular remodeling, and increased inflammation in resistance PAs.

1.2.1 Pathogenesis of PH

Although a number of factors can trigger PH, the underlying cellular mechanisms that lead to disease development remain inconclusive. Changes in flow/shear stress have been shown to promote vascular dysfunction in animal models of PH, suggesting that hemodynamic changes are a secondary contributor to the pathogenesis of PH⁹¹. This likely occurs through shear stress promotion of EC apoptosis and inflammatory cell recruitment causing a loss of vasodilation and impaired EC function^{12,92}. Additionally, circulatory cytokine levels are increased in PH patients and correlate with severity of the disease^{93,94}. Cytokines and chemokine signaling (TNF α - , IL-1 β , IL-6) promote SMC proliferation and migration into previously partially de-muscularized arterioles ultimately increasing PVR leading to PH. Inflammatory signaling also promote apoptotic-resistant EC transition to mesenchymal-like cells, further contributing to the medial thickening and perivascular cuff formation in resistance vessels¹². PAs that do not form obstructive lesions have impaired endothelial function leading to reduced vasodilatory capacity and sustained

vasoconstriction. Together, these changes increase PVR and PAP. The following sections of the introduction will further examine mechanism leading to endothelial dysfunction in PH.

1.2.2 Endothelial dysfunction in PH.

Endothelial dysfunction refers to loss of endothelium-dependent vasodilation of resistance PAs and increased EC proliferation in plexiform lesions. Impairment in endothelium-dependent vasodilation is caused by a loss of eNOS-NO signaling. PH patients have lowered NO bioavailability and treatment with inhaled NO temporarily lowers PAP, indicating that impaired eNOS-NO signaling significantly contributes to increased PAP in PH^{95,96}. Initial studies attributed reduced NO bioavailability to decreased eNOS expression⁷⁰. These studies were supported by evidence in global eNOS^{-/-} mice which spontaneously develop PH⁹⁷. However, recent findings have challenged this idea by showing no change in eNOS expression in lung sampled from PH patients⁹⁸. In fact, eNOS expression was increased within the plexiform lesions of PH patients⁹⁹, revealing that expression levels may not always correlate with enzyme activity. This was further highlighted in a study on fetal lambs with PH which showed eNOS uncoupling, not changes in eNOS expression, resulting in reduced NO bioavailability¹⁰⁰. Uncoupled eNOS leads to the preferential synthesis of O₂⁻ over NO¹⁰¹. Scavenging O₂⁻ restored endothelium-dependent vasodilation suggesting that formation of reactive oxygen species (ROS), such as O₂⁻, attenuates vasodilatory signaling in pulmonary ECs thereby contributing to endothelial dysfunction in PH¹⁰⁰.

ROS are oxygen containing radicals which play an important role in cell homeostasis and disease pathogenesis. Endogenous antioxidants serve as a counterbalance to ROS signaling by metabolizing oxidative molecules. Under pathological conditions, an imbalance of oxidative and reductive signaling leads to the overproduction of ROS, inducing maladaptive changes to cell signaling and cell death. Elevated ROS production is associated with a multitude of vascular diseases, including PH¹⁰². Specifically, elevated ROS in pulmonary ECs leads to impaired vasodilation, cell proliferation, and elevation in PAP¹⁰². Several ROS are elevated in pulmonary pathologies including hydrogen peroxide (H₂O₂), hydroxyl (HO[•]), and O₂^{•-}. Chemical reaction of O₂^{•-} with NO, a major signaling molecule in the pulmonary endothelium, forms the reactive nitrogen species peroxynitrite (PN; ONOO⁻). Post-translational modification of signaling molecules by PN inhibits vasodilation leading to endothelial dysfunction in PH.

The two main sources of ROS in the pulmonary endothelium, apart from eNOS uncoupling mentioned previously, are the mitochondria and NADPH oxidases (NOXs). O₂^{•-} is released from the mitochondria during aerobic respiration as a byproduct of ATP synthesis. O₂^{•-} is released from the mitochondria by complex I and III and is quickly metabolized into H₂O₂ by superoxide dismutase 1 (SOD1)¹⁰³⁻¹⁰⁵. Changes in mitochondrial bioenergetics contributes to excess O₂^{•-} release in PH¹⁰⁶. Mitochondrial function is highly susceptible to changes in O₂ levels, therefore it is conceivable that changes in mitochondrial activity contributes to EC dysfunction in hypoxia-induced PH. In support of this, exposure of pulmonary ECs to acute hypoxia increases mitochondrial ROS

production¹⁰⁷. However, the role of EC mitochondrial-derived ROS in the pathogenesis of PH is still unclear.

The second source of O_2^- in the pulmonary endothelium is O_2^- release from endothelial NOX. Three main NOX isoforms have been identified contributing to the pathogenesis of PH: NOX1, NOX2 and NOX4. Increased NOX1 and 2 activity are maladaptive and lead to EC damage, while NOX4-mediated signaling is protective against EC dysfunction. NOX1 and NOX2 expression are increased in lung samples from PH patients and in rodent models of PH, and contribute to endothelial dysfunction and EC proliferation¹⁰². A loss of function mutation of p22phox, a subunit of NOX1, is protective against the development of PH in animal models¹⁰⁸. Similarly, deletion of the NOX2 subunit gp91phox is protective against hypoxia-induced PH, highlighting the role of NOX1 and NOX2 signaling in the pathogenesis of PH^{109,110}. Recently, NOX3 has been identified as a source of ROS in the pulmonary endothelium regulating EC death and lung injury¹¹¹. However, the contribution of NOX3 signaling in PH remain unknown. Unlike all other NOX isoforms, NOX4 has an associated SOD subunit, which immediately catalyzes any O_2^- produced into H_2O_2 . NOX4 is also unique in that it displays protective functions within the pulmonary vasculature. Release of H_2O_2 from NOX4 promotes the synthesis of NO¹¹². Furthermore, global NOX4^{-/-} mice have lower NOS expression leading to worsened EC dysfunction in angiotensin II models of oxidative stress¹¹².

Increased ROS signaling contributes to the development of endothelial dysfunction by inhibiting EC-dependent vasodilation and promoting EC proliferation. Cultured ECs

obtained from lung tissue homogenate of PH rats showed enhanced TRPV4_{EC}-dependent Ca²⁺ signaling which promoted EC migration and proliferation⁵⁸. Administration of the mitochondrial antioxidant, MitoQ, lowered TRPV4_{EC}-dependent Ca²⁺ increases in cultured ECs, supporting a role for ROS-dependent regulation of TRPV4_{EC} channel activity in microvascular ECs. However, mechanistic studies are still necessary to truly understand the role of local ROS signaling in the native pulmonary endothelium of resistance PAs. We address this in work shown in Chapter 4 of this dissertation which discusses a novel mechanism wherein ROS-dependent inhibition of TRPV4_{EC} channel activity in resistance PAs lead to impaired vasodilation and elevated PAP in PH.

Recently, endothelial to mesenchymal transition (EndoMT), has emerged an important contributing factor to endothelial dysfunction in PH. EndoMT is a transition state where ECs lose traditional EC markers and begin to exhibit a mesenchymal cell-like phenotype, partly characterized by expression of α -SMA¹¹³. These mesenchymal-like cells are hyperproliferative and contribute to perivascular cuff formation in PH. In lung samples from PH patients, there is an increase in α -SMC positive cells in the arterial lesions¹¹⁴. Some of these α -SMC positive cells also express EC markers identifying them as ECs undergoing EndoMT^{113,115,116}. EndoMT is caused by increased inflammatory signaling (TNF- α and IL-1 β) promoting the upregulation of mesenchymal cell genes such as (i.e. α -SMC, vimentin, fibronectin), while simultaneously suppressing EC genes (i.e. VE-cadherin, vWF, and CD-31)^{113,115}. This increased inflammatory signaling triggered by changes in flow/shear stress, matrix stiffness, and metabolic dysregulation in pulmonary

ECs¹¹³. Cells undergoing EndoMT have impaired vasodilatory signaling and promote vascular stiffening, both of which results in elevated PVR in PH.

1.2.3 *Animal models of PH*

Several animal models are used to study the pathogenesis of PH, although none entirely recapitulates the pathobiology of human PH. The following section contains a brief overview the predominant animal models of PH. A comprehensive table of all the available models of PH has previously been published by *de Jesus Perez*¹².

Chronic Hypoxia Model. Exposure to chronic hypoxia (CH; 3-4 weeks, 10% O₂) in both mice and rats most closely recapitulates Group 3 PH¹². CH induces sustained vasoconstriction and medial hypertrophy, due to SMC proliferation, in both murine models. However, the phenotype is less severe in mice than rats¹¹⁷⁻¹²⁰. CH also induces muscularization of previously de-muscularized precapillary arterioles. These novel SMC-like cells arise from migratory SMC, pericytes, and cells undergoing EndoMT^{117,121,122}. Animals challenged with CH also develop fibrosis in the large PAs contributing to vascular stiffness and increased PAP. This model is highly reproducible, consistently causing an increase in PAP (30-40 mmHg vs. 20 mmHg in normal mice) and moderate RV hypertrophy without heart failure. However, this model fails to promote the development of perivascular cuff formation and inflammatory cell infiltration seen in the clinical presentation of PH. Importantly, this model is reversible as animals lose PH pathological hallmarks once returned to normoxic conditions.

Sugen (SU-5416) Hypoxia Model. The Sugen-hypoxia (SuHx) model promotes the sustained vasoconstriction observed in the CH model while also inducing plexiform lesion formation in resistance vessels¹²³. Like the CH model, mice are exposed to chronic hypoxia (10% O₂) for 3-4 weeks and are injected with SU-5416 weekly. Normoxic mice treated with SU-5416 develop mild PH, which is worsened with a CH challenge – PAP up to 60 mmHg and worse medial and RV hypertrophy compared to CH alone treated rats¹². As seen in the CH model, rats develop a more severe phenotype compared to mice¹²⁴. SU-5416 is a VEGF receptor inhibitor, which promotes EC apoptosis and vascular remodeling. EC apoptosis promotes the recruitment of inflammatory cells, which release cytokines and chemokines that lead to SMC remodeling and increased PVR. Apoptotic-resistant ECs undergo EndoMT giving rise to plexiform lesions in the resistance vasculature. Interestingly, and important for our studies, the effects of SU-5416 are specific to the pulmonary circulation and no adverse effects are observed in the systemic circulation after treatment¹¹⁷. This model most closely resembles the human pathology and is used to test novel therapeutic options. However, the phenotype of this model is less consistent than the CH model, particularly in mice, and is usually used in conjunction with another murine model of PH.

Monocrotaline Model. The monocrotaline model is the most widely used rat model of PH. Administration of a single dose of monocrotaline, a pyrrolizidine alkaloid, induces the development of severe PH. Rats treated with monocrotaline display elevated PAP (40-60 mmHg), medial thickening, SMC proliferation, and plexiform lesion formation. Rats also develop severe RV hypertrophy, which can lead to heart failure in 65% of animals¹²⁵⁻¹²⁷.

However, the exact mechanism by which monocrotaline promotes PH development is not known. The vascular damaging effects of monocrotaline are not restricted to the pulmonary circulation. Damage to the systemic circulation has been reported in some rats, which leads to the development of hepatic veno-occlusive disease¹²⁸. Despite these non-pulmonary effects, the monocrotaline model has been used to test novel therapeutics with great effectiveness in rats. However, few of the treatments have been translatable to humans, suggesting key differences in the pathogenesis of PH between species.

1.3 Conclusion

The pulmonary circulation is a specialized vascular bed that is both structurally and functionally distinct from the systemic circulation. Vascular reactivity, in part regulated by the endothelium of resistance PAs, is important for maintaining stable blood perfusion and resting PAP. Loss of endothelial function is one of the primary injuries leading to the development of vascular diseases including PH. Oxidative damage to pulmonary ECs prevents the release of vasodilatory signals, contributing to sustained vasoconstriction. Furthermore, EC de-differentiation into mesenchymal-like cells increases inflammation and fibrosis in resistance PAs creating vaso-occlusive lesions. Together, these changes increase PVR leading to sustained elevation in PAP. Current therapies include vasodilators to help alleviate the increased PAP, but patients continue to have a high morbidity rate, even with continued therapeutic interventions. Therefore, it is imperative to understand the signaling mechanisms that regulate EC function in resistance PAs under normal and pathological conditions in order to generate better therapeutic options for PH patients. This

dissertation elucidates a novel TRPV₄^{EC} channel-dependent regulation of vasodilation in resistance PAs (Chapter 3) which is impaired by oxidative stress in PH contributing to loss of endothelium-dependent vasodilation and increasing PAP (Chapter 4).

CHAPTER 2: MATERIALS AND METHODS

2.1. Materials and Methods for Chapter 3:

Drugs and chemical compounds.

Apamin, cyclopiazonic acid (CPA), GSK2193874, GSK1016790A, HC067047, NS309, 1400W, N ω -Propyl-L-arginine hydrochloride, ODQ, RN1747, Rp-8-Br-PET-cGMPS, Suramin, and Tram 34 were purchased from Tocris Bioscience (Minneapolis, MN). ATP and N^o-nitro-L-arginine were obtained from Sigma-Aldrich (St. Louis, MO). DAF-FM diacetate, Fluo-4AM (Ca²⁺ indicator) and EGTA-AM (Ca²⁺ chelator) were purchased from Fischer Scientific (Pittsburgh, PA). Spermine NONOate and U46619 were purchased from Cayman Chemical (Ann Arbor, MI). All other chemicals were obtained from Sigma-Aldrich (St. Louis, MO).

Animal Procedures.

All animal protocols were approved by the Animal Care and Use Committee of the University of Virginia. Male C57BL6/J, transgenic GCaMP2^{Cx40}, TRPV4^{-/-}, and eNOS^{-/-} (The Jackson Laboratory, Bar Harbor, ME) mice (10–14 weeks old) were used for all the studies. GCaMP2^{Cx40} mice express GCaMP2, a Ca²⁺-specific biosensor under the connexin 40 promoter thereby limiting its expression to only ECs^{129,130}. Mice were euthanized with pentobarbital (90 mg/kg; intraperitoneal) followed by decapitation. Third-order mesenteric arteries (MAs; ~100 μ m in diameter), fourth-order pulmonary arteries (PAs, ~100-200 μ m), and second-order PAs (~400 μ m) were isolated in cold HEPES-buffered physiological salt solution (HEPES-PSS, in mmol/L, 10 HEPES, 134 NaCl, 6 KCl, 1 MgCl₂ hexahydrate, 2 CaCl₂ dihydrate, and 7 dextrose, pH adjusted to 7.4 using 1 mol/L NaOH). Data were collected from at least three different arteries from at least three mice.

Pressure Myography.

Isolated PAs and MAs were cannulated on glass pipettes mounted on an arteriography chamber (The Instrumentation and Model Facility, University of Vermont, Burlington, VT) at areas lacking branching points and pressurized to physiological pressure (15 mmHg for PA and 80 mmHg for MA). Arteries were superfused with physiological salt solution (PSS) (in mmol/L, 119 NaCl, 4.7 KCl, 1.2 KH₂PO₄, 1.2 MgCl₂ hexahydrate, 2.5 CaCl₂ dihydrate, 7 dextrose, and 24 NaHCO₃) at 37°C and bubbled with 20% O₂/ 5% CO₂ to maintain the pH at 7.4. All drug treatments were added to the superfusing PSS. Because PAs do not develop myogenic tone at 15 mmHg, they were precontracted with 100 nmol/L U46619 (a thromboxane A₂ agonist). In functional studies with PAs, all other pharmacological treatments were performed in the presence of U46619. Prior to measurement of vascular reactivity, arteries were treated with NS309 (1 μmol/L), a direct opener of endothelial IK/SK channel, to assess endothelial health. Arteries that failed to dilate to NS309 were discarded. Endothelial denudation was performed by passing an air bubble through the artery for ~ 60 seconds. Complete removal of the endothelial layer was verified by the absence of dilation to NS309. Changes in arterial diameter were recorded at 60 ms frame rate using a CCD (charge-coupled device) camera and edge-detection software (IonOptix LLC, Westwood, MA)^{22,23}. All drug treatments were incubated for 10 min. At the end of each experiment Ca²⁺-free PSS (in mmol/L, 119 NaCl, 4.7 KCl, 1.2 KH₂PO₄, 1.2 MgCl₂ hexahydrate, 7 dextrose, 24 NaHCO₃, and 5 EGTA) was applied to assess the maximum passive diameter. Percent constriction was calculated by:

$$[(\text{Diameter}_{\text{before}} - \text{Diameter}_{\text{after}}) / \text{Diameter}_{\text{before}}] \times 100 \quad (1)$$

where $\text{diameter}_{\text{before}}$ is the diameter of the artery before a treatment and $\text{Diameter}_{\text{after}}$ is the diameter after the treatment. Percent dilation was calculated by:

$$[(\text{Diameter}_{\text{dilated}} - \text{Diameter}_{\text{basal}}) / (\text{Diameter}_{\text{Ca-free}} - \text{Diameter}_{\text{basal}})] \times 100 \quad (2)$$

where $\text{Diameter}_{\text{basal}}$ is the stable diameter before drug treatment, $\text{Diameter}_{\text{dilated}}$ is the diameter after drug treatment, and $\text{Diameter}_{\text{Ca-free}}$ is the maximum passive diameter.

NO imaging.

PAs and MAs were surgically opened and pinned down on a Sylgard block in *en face* preparation for NO imaging from intact EC and SMC layers. NO levels were assessed using 5 $\mu\text{mol/L}$ DAF-FM (4-amino-5 methylamino-2',7'-difluorofluorescein diacetate) prepared in HEPES PSS with 0.02% pluronic acid¹³¹. DAF-FM forms a fluorescent triazole compound after binding to NO. *En face* PAs or MAs were pre-treated with GSK101, L-*N*^G-nitroarginine (L-NNA), or GSK219 in HEPES-PSS for 5 minutes at 30°C. Arteries were then incubated with DAF-FM containing the drug under consideration for 20 minutes at 30°C in the dark. Validity of DAF-FM as an NO indicator was tested by treating PAs with NO donor Spermine NONOate (NONOate, 3-30 $\mu\text{mol/L}$), and recording the DAF-FM fluorescence (Figure 8). Spermine NONOate was selected because it has a long half-life (~39 min) and releases a controlled amount of NO in solution. The experiments using NONOate were performed in the presence of L-NNA to eliminate the effect of endogenous

release of NO in response to TRPV4 channel activation. The arteries were incubated with either Hepes-PSS (baseline) or 30 nmol/L GSK101 in the absence or presence of 200 $\mu\text{mol/L}$ L-NNA to determine whether localized Ca^{2+} influx through EC TRPV4 channels contributes to NO release through NOS activation. DAF-FM fluorescence was imaged using Andor Revolution WD (with Borealis) spinning-disk confocal imaging system (Andor Technology, Belfast, UK) comprised of an upright Nikon microscope with a 60X water dipping objective (numerical aperture (NA) 1.0) and an electron multiplying charge coupled device (CCD) camera. DAF-FM fluorescence was recorded using an excitation wavelength of 488 nm and emitted fluorescence was captured with a 525/36-nm band-pass filter. Images were obtained along the z-axis at a slice size of 0.05 microns from the top of the ECs to the bottom of the SMCs. DAF-FM fluorescence was analyzed using custom-designed SparkAn software by Dr. Adrian D. Bonev (University of Vermont, Burlington, VT). An outline was drawn around each EC or SMC to obtain the arbitrary fluorescence intensity of that cell. The background fluorescence was then subtracted from the recorded fluorescence. The fluorescence numbers from all the cells in a field of view were averaged to obtain single fluorescence number for that field. Relative changes in DAF-FM fluorescence were obtained by dividing the fluorescence in the treatment group by that in the control group. Each field of view was considered as $n=1$, and several fields of view from at least three arteries from at least three mice were included in the final analysis.

Ca²⁺ imaging.

Measurement of Ca^{2+} events in the native ECs from PAs was performed as previously described^{22,23}. Briefly, Andor Revolution WD (with Borealis) spinning-disk confocal

imaging system described above was used to record Ca^{2+} influx events in *en face* PAs. Ca^{2+} events were recorded at 30 ms per image before and after 5 minutes of each treatment. The arteries were loaded with fluo-4 AM (10 $\mu\text{mol/L}$) in the presence of pluronic acid (0.04%) at 30°C for 30 minutes for PAs and 45 minutes for MAs. The majority of experiments were carried out in the presence of cyclopiazonic acid (CPA, 20 $\mu\text{mol/L}$, a sarco-endoplasmic reticulum Ca^{2+} -ATPase inhibitor) in order to eliminate the interference from Ca^{2+} release from intracellular stores. Ca^{2+} binding-induced changes in emitted fluorescence were observed by exciting at 488 nm with a solid-state laser and collecting emitted fluorescence using a 525/36-nm band-pass filter. In the studies examining whether S-nitrosylation of TRPV4 channels mediated the effect of NO on channel activity, flash photolysis using Ultraviolet (UV) light pulse of 10 ms (Andor Mosaic 3 Infinity, Andor Technology, and pE-4000, CoolLED Ltd, Andover, UK) was conducted to dissociate the S-NO bonds on TRPV4 channels. The experiments using NONOate were performed in the presence of L-NNA to eliminate the effect of endogenous release of NO in response to TRPV4 channel activation. TRPV4 Ca^{2+} sparklets and Ca^{2+} release events from the ER in ECs were analysed using custom-designed SparkAn software. To generate fractional fluorescence (F/F_0) traces, a region of interest (ROI) defined by a 1.7 μm^2 (5 x 5 pixels) box was placed at a point corresponding to peak sparklet amplitude. Each field of view was $\sim 110 \times 110$ μm and covered approximately 15 ECs. Representative F/F_0 traces were filtered using a Gaussian filter and a cut-off corner frequency of 4 Hz. Sparklet activity, all-points histograms, and coupling coefficients were determined as described previously using the custom-designed SparkAn software, Clampfit and OriginPro7.5^{22,23}.

Localization of sparklets at myoendothelial projections (MEPs).

To determine the localization of sparklets at MEPs, the arteries were incubated with 100 $\mu\text{mol/L}$ Alexa Fluor 633 hydrazide. Alexa 633 hydrazide cannot penetrate into the cells, but preferentially binds to elastin-containing internal elastic lamina (IEL), thereby illuminating the IEL^{132,133} for 15 minutes following Ca^{2+} imaging experiment. The images were then acquired in the fields of view from which Ca^{2+} signals were recorded, using excitation wavelengths of 640 nm (for IEL staining) and 488 nm (for fluo-4), and capturing the emitted fluorescence using 685/40- and 525/36-nm band-pass filters, respectively. ROIs ($1.7 \mu\text{m}^2$) corresponding to the peak sparklet fluorescence were overlaid onto the IEL staining image. The ROIs within 5 μm from the centre of the holes in the IEL were counted as MEP sparklet sites and the remaining ROIs were counted as non-MEP sparklet sites, as we have done previously²³. A sparklet site displays spread of calcium away from the site of initiation. In 88% of sparklet sites, the site of sparklet initiation coincided with the peak sparklet amplitude. Therefore, the ROI corresponding to the peak sparklet amplitude was used to analyze the sparklet localization data.

Calculation of sparklet activity per site and sparklet activity per field.

Activity of TRPV4 Ca^{2+} sparklets was evaluated as described previously^{22,23}. Area under the curve (AUC) for all the events at a site was determined using trapezoidal numerical integration ($[\text{F} - \text{F}_0]/\text{F}_0$ over time, in seconds). The average number of active TRPV4 channels, as defined by NP_O (NP_O , where N is the number of channels at a site and P_O is the open state probability of the channel), was calculated by

$$NP_O = (T_{\text{level1}} + 2T_{\text{level2}} + 3T_{\text{level3}} + 4T_{\text{level4}}) / T_{\text{total}} \quad (3)$$

where T is the dwell time at each quantal level detected at TRPV4 sparklet sites and T_{total} is the duration of the recording. NP_O was determined using Single Channel Search module of Clampfit and quantal amplitudes derived from all-points histograms ($\Delta F/F_0$ of 0.29 for Fluo-4-loaded PAs). NP_O for all the sites in a field was averaged to obtain NP_O per site. For the studies on baseline sparklet activity (without GSK101), some of the fields showed no sparklet activity at the baseline but L-NNA still increased the sparklet activity. Therefore, we used NP_O per field instead of NP_O per site to estimate the effect of L-NNA on baseline sparklet activity. All NP_O per site values for all the sites in a field were summated to calculate NP_O per field.

Construction of all-points histograms.

As described previously²², all-points amplitude histograms were constructed by first filtering Ca^{2+} images with a Kalman filter (adopted from an ImageJ plug-in written by Christopher Philip Mauer, Northwestern University, Chicago, IL; acquisition noise variance estimate=0.05; filter gain=0.8) to assess quantal amplitudes of Ca^{2+} influx events (i.e., equal increments of fluorescence signals over increasing numbers of TRPV4 channels). All sparklet events with at least five steady baseline points and a steady peak of at least five data points were used for the construction of all points histograms, whereas channel openings with either unstable baseline or shorter duration of opening (e.g., fewer than five data points at the peak) were excluded from this analysis. The analysis was undertaken with Ca^{2+} images obtained from 3-5 fields from 3-5 PAs from C57BL6/J or

GCaMP2 mice. F/F_0 traces were exported to ClampFit10.3 for constructing all-points histograms, which were then fit with multiple Gaussian function:

$$f(F/F_0) = \sum_{i=1}^N \frac{a_i}{\sqrt{2\pi}\sigma_i} \exp \left[-\frac{(F/F_0 - \mu_i)^2}{2\sigma_i^2} \right] \quad (4)$$

where F/F_0 , a , μ , and σ^2 represent the fractional fluorescence, area, mean value, and variance of the Gaussian distribution, respectively. Statistical differences in the quantal levels of TRPV4 mediated Ca^{2+} sparklets between diverse treatment regimens were evaluated based on a 95% confidence interval calculated from the mean and standard error for each peak.

Determination of coupling coefficients.

Coupling coefficients for the coupling among TRPV4 channels at a cluster were determined using a coupled Markov chain model in MATLAB, as previously described^{23,134-137}. $[F-F_0]/F_0$ traces showing steady baseline (i.e., at least 30s duration) were selected for analyzing the cooperative gating of TRPV4 channels. Each TRPV4 sparklet site was examined separately. The coupled Markov chain model developed by Chung and Kennedy¹³⁵ was used to simulate and fit independent records of partially coupled channels. Openings of single TRPV4 channel were identified using a single channel amplitude (i.e., quantal level) of $0.29 \Delta F/F_0$ for mouse PAs loaded with fluo-4 and a half-amplitude protocol in a program written in MATLAB. TRPV4 channel activity was considered as a first-order and discrete Markov chain. The built-in Hidden Markov parameter estimation

function in MATLAB was utilized to estimate a Markovian transition matrix based on the TRPV4 sparklet data and their corresponding channel opening time course. The estimated transition matrix was modeled as a partially coupled Markov chain, suggesting the coupling coefficient (κ) values varying from 0 (no coupling or independent gating) to 1 (maximum coupling).

Immunostaining for AKAP150 and PKG in ECs of the intact PAs and MAs.

Immunostaining assay was performed as described previously²³. Briefly, mouse intact PAs and MAs cut longitudinally and pinned down on SYLGARD blocks were rapidly fixed with ice-cold acetone for 10-min and then washed 3 times with phosphate-buffered saline (PBS). The arteries were permeabilized with 0.2% Triton-X for 30-min, blocked with 5% normal donkey serum (ab7475, Abcam, Cambridge, MA) for 1 hour, and incubated with a goat polyclonal AKAP150 antibody (sc-6445, 1:250, Santa Cruz Biotechnology, Dallas, TX, USA) or a rabbit polyclonal anti-cGKI antibody (ab37709, 1:100, Abcam, Cambridge, MA) overnight at 4°C. After 5 washes with PBS, PAs and MAs were incubated with Alexa Fluor® 568-conjugated donkey anti-goat (A11057, 1:500, Life Technologies, Carlsbad, CA) or anti-rabbit secondary antibody (A10042, 1:500, Life Technologies) for 1 hour at room temperature in a dark room. Immunostaining images were acquired using Andor imaging system described above. Images were obtained along the z-axis from the top of ECs to the bottom of SMCs with a slice size of 0.05- μm . Connective tissue autofluorescence was evaluated by exciting at 488 nm with a solid-state laser and collecting emitted fluorescence with a 525/36-nm band-pass filter. AKAP150 and PKG immunostaining (i.e., red-pseudo color images) was assessed by exciting at 561 nm and

collecting emitted fluorescence with a 607/36 -nm band-pass filter. The specificity of the antibodies was tested using competing peptides and by substitution with PBS. AKAP150 or PKG-associated staining was absent under these conditions.

Statistics.

The n number represents the unit of analysis, and has been specified in each figure legend. The data in this manuscript were normally distributed, therefore, parametric statistics were performed and mean \pm SEM were used to describe the data set. P value of less than 0.05 was considered significant. The n numbers and P values are indicated in each figure legend. Two-tailed, paired (for paired observations) or independent two sample t-test was used for comparisons between two groups. One-way ANOVA with *post hoc* Tukey test (comparing different means) or Dunnett test (comparisons with control group) or 2-way ANOVA with post hoc Tukey test was used for comparing 3 or more groups. Statistical analysis was performed using OriginPro7.5. For all the calculations of TRPV4 sparklet activity per site and activity per field, n value represents number of fields²². For the coupling coefficient analysis, n value represents number of sites^{22,23}. Only 1 artery from a mouse was used for 1 experimental treatment. Within an experimental treatment group, activity per site did not change significantly among different fields from the same artery ($P > 0.05$), or among fields from different arteries as determined using 1-way ANOVA. Moreover, the coupling coefficient values also did not change significantly among different fields from the same artery, or among fields from different arteries under the same experimental treatment group. In some cases, activity per field was calculated instead of

activity per site to account for fields with no active sites, and was not significantly different among different arteries from the same experimental treatment group.

2.2. Materials and Methods for Chapter 4:

Animal models and procedures.

All animal protocols were approved by the University of Virginia Animal Care and Use Committee. Male C57BL6/J and endothelium-specific TRPV4 (TRPV4_{EC}^{-/-}) and Cav-1 (Cav-1_{EC}^{-/-}) knockout mice (10-14 weeks) were used for all the studies. TRPV4_{EC}^{-/-} and Cav-1_{EC}^{-/-} mice were generated by crossing TRPV4^{lox/lox} or Cav-1^{lox/lox} mice with tamoxifen-inducible VE-Cadherin (Cdh5) Cre mice. Mice were euthanized with pentobarbital (90 mg/kg; intraperitoneal) followed by decapitation. Lungs and heart were taken out *en block* and placed in cold Hepes-buffered physiological salt solution (Hepes-PSS; concentration in mmol/L, 10 HEPES, 134 NaCl, 6 KCl, 1 MgCl₂ hexahydrate, 2 CaCl₂ dihydrate, and 7 dextrose, pH adjusted to 7.4 using 1 mol/L NaOH).

Generation of TRPV4_{EC}^{-/-} and Cav-1_{EC}^{-/-} mice.

TRPV4^{lox/lox} (Wolfgang Liedtke, Duke University) and Cav-1^{lox/lox} (Richard Minshall, University of Illinois, Chicago) were crossed with VE-Cadherin (Cdh5) Cre mice (Ralf Adams). TRPV4^{lox/lox} and Cav-1^{lox/lox} Cre⁻ mice were used as wild-type (WT) controls. Knockout of TRPV4 or Cav-1 were induced by injecting 6 week-old TRPV4^{lox/lox} Cre⁺ or Cre⁻ and Cav-1^{lox/lox} Cre⁺ or Cre⁻ mice with tamoxifen (40 mg/kg i.p. per day for 10 days). Mice were used after a two-week washout period. Specific deletion of TRPV4 or

Cav-1 from ECs was confirmed using immunostaining and mRNA levels on freshly isolated endothelial cells (described below).

Genotyping.

Genomic DNA was extracted from mouse ear clip samples treated with HotSHOT lysis buffer (25 mM NaOH, 0.2 mM EDTA) followed by equal volume of neutralization solution (40 mM Tris-HCl). Polymerase chain reactions were performed using 1 unit Bioline MangoTaq Polymerase and buffer (London, England), 1.5 mM MgCl₂, 200 μM of each dNTP, 1 μM 5' and 3' primers, and approximately 100-250 ng genomic DNA, and run on a Bio-Rad T100 Thermal Cycler (Hercules, CA). Reaction products were run on a 1% agarose gel containing 0.2 μg/μL ethidium bromide in TAE Buffer (40 mM Tris Base, 20 mM Acetic Acid, 1 mM EDTA) at 90V using a Bio-Rad PowerPac HC High-Current Power Supply. Gels were visualized by exposing to 302 nm UV light and compared to a New England BioLabs 100 bp DNA Ladder (Ipswich, MA). The genotyping primers included: Cdh5 Cre, 5' GCCTGCATTACCGGTCGATGCAACGA, 3' GTGGCAGATGGCGCGGCAACACCATT;TRPV4^{loxP}, 5' TGAAATCTGACCTCTTGTCCCC, 3' TTGTGTACTGTCTGCACACCAGGC; Cav-1^{loxP}, F1'' 5'-TTCTGTGTGCAAGCCTTTCC-3', R1'' 5'-GTGTGCGCGTCATACACTTG-3' All primers were ordered from Eurofins Genomics (Louisville, KY).

Quantitative polymerase chain reaction (qPCR).

For whole artery isolation, PAs were dissected and placed in 500 μL RTL buffer (Qiagen RNeasy Mini Kit, Hilden, Germany) with 5 μL β-mercapto ethanol and

homogenized using a Standard Microhomogenizer (PRO Scientific Inc., Oxford, CT, USA). For freshly isolated ECs, PAs were enzymatically digested in dissociation solution (55 mM NaCl, 80 mM Na-glutamate, 6 mM KCl, 2 mM MgCl₂, 0.1 mM CaCl₂, 10 mM glucose, 10 mM HEPES, pH 7.3) containing Worthington neutral protease (0.5 mg/mL) 60 minutes at 37°C. Isolated ECs (~2000) were transferred to RTL buffer with β-mercapto ethanol and snap frozen in liquid nitrogen. RNA was isolated using the Qiagen RNeasy Mini Kit (Hilden, Germany). Samples were purified using the Invitrogen DNA-free DNA Removal Kit (Waltham, MA). RNA was converted to cDNA with the Bio-Rad iScript cDNA Synthesis Kit. The qPCR reaction mixes were prepared using Bio-Rad 2X SYBR Green Master Mix, 200 nM 5' and 3' primers, and 20 nM cDNA. Samples were run on a Bio-Rad CFX96 qPCR Detection System. Data were analyzed using the $\Delta\Delta C_t$ method. qPCR primers for TRPV4, Cav-1, and GAPDH (internal control) were ordered from GeneCoeppia Inc. (Rockville, MD, USA). The remaining qPCR primers included iNOS, and NOX1 were ordered from Eurofins Genomics (Louisville, KY).

Right ventricular systolic pressure (RVSP) measurement.

Mice were anesthetized with pentobarbital (50 mg/kg BW; i.p.) and bupivacaine HCl (100 μ l of 0.25% solution, s.c.) was used to numb the dissection site on the mouse. Right ventricular systolic pressures (RVSPs) were measured as an indicator of pulmonary arterial pressure. A Mikro-Tip pressure catheter (SPR-671; Millar Instruments, Huston, TX) connected to a bridge amp (FE221), and a PowerLab 4/35 4-channel recorder (Instruments, Colorado Springs, CO) was cannulated through the external jugular vein into the right ventricle. Right ventricular pressure and heart rate were acquired and analyzed

using LabChart8 software (ADInstruments, Colorado Springs, CO). A stable 3-minute recording was acquired for all the animals, and 1 minute continuous segment was used for data analysis. Drugs were administered through an intraperitoneal injection following a baseline recording. Changes in RVSP to drug administration were recorded 10 minutes post-injection. When necessary, traces were digitally filtered using a low-pass filter at a cut-off frequency of 50 Hz. At the end of the experiments, mice were euthanized, and the hearts were isolated for right ventricular hypertrophy analysis. Right ventricular hypertrophy was determined by calculating the Fulton Index, a ratio of the right ventricular (RV) heart weight over the left ventricular (LV) plus septum (S) heart weight (RV/ LV+S).

Pressure myography.

Pressure myography experiments were conducted as described previously²⁹. Briefly, fourth-order PAs (~150-100 μm) were cannulated on glass pipettes mounted on an arteriography chamber (The Instrumentation and Model Facility, University of Vermont, VT) and pressurized to a physiological pressure of 15 mmHg. PAs were superfused with PSS (in mmol/L, 119 NaCl, 4.7 KCl, 1.2 KH₂PO₄, 1.2 MgCl₂ hexahydrate, 2.5 CaCl₂ dihydrate, 7 dextrose, and 24 NaHCO₃) at 37°C and bubbled with 20% O₂/5% CO₂ to maintain the pH at 7.4. PAs were precontracted with the thromboxane A₂ (receptor) agonist (U46619, 100 nM). Endothelium health was confirmed by a dilation to the IK and SK channel opener (NS309, 1 μM). Vascular reactivity was tested by addition of specific pharmacological treatments directly to the superfused PSS and incubated for 5-10 min. Changes in the internal diameter were recorded using a charge-coupled device camera set to a 60-ms frame rate and edge detection software (IonOptix LLC, Westwood, MA). At

the end of each experiment, PAs were incubated with Ca²⁺ free-PSS (in mmol/L, 119 NaCl, 4.7 KCl, 1.2 KH₂PO₄, 1.2 MgCl₂ hexahydrate, 7 dextrose, 24 NaHCO₃, and 5 EGTA) to assess the maximum passive diameter. Percent vasoconstriction was calculated by:

$$\left[\frac{(Diameter_{initial} - Diameter_{final})}{Diameter_{initial}} \right] * 100$$

where *Diameter_{initial}* is the internal diameter of the PA before the drug treatment and *Diameter_{final}* is the diameter after the drug treatment. Percent vasodilation was calculated by:

$$\left[\frac{(Diameter_{dilated} - Diameter_{basal})}{(Diameter_{Ca^{2+} free} - Diameter_{basal})} \right] * 100$$

where *Diameter_{dilated}* is the internal diameter after drug treatment, *Diameter_{basal}* is the internal diameter before drug treatment, and *Diameter_{Ca²⁺ free}* is the maximum passive internal diameter.

Ca²⁺ imaging.

Ca²⁺ imaging experiments were performed as described previously²⁹. Fourth-order PAs were pinned *en face* on SYLGARD blocks and incubated with fluo-4 AM (10 μM) and pluronic acid (0.04 %) dissolved in HEPES-PSS and incubated at 30° C for 45 min in the dark. PAs were superfused with PSS warmed to 37 °C and bubbled with 20% O₂/ 5% CO₂ to maintain pH at 7.4. Images were recorded before and 5-10 minutes after the addition of a pharmacological treatment to the superfusing PSS. PAs were treated with the sarcoplasmic reticulum (SR/ER) Ca²⁺-ATPase inhibitor, cyclopiazonic acid (CPA; 20 mM)

for 15 min. Ca^{2+} images were acquired at 30 frames per second using Andor Revolution WD (with Borealis) spinning-disk confocal imaging system (Andor Technology, Belfast, UK) comprising of an upright Nikon microscope with a 60X water dipping objective (numerical aperture 1.0) and an electron multiplying charge coupled device camera. Fluo-4 fluorescence was imaged at an excitation of 488 nm solid-state laser and emitted fluorescence was captured using a 525/36 nm band-pass filter.

Analysis of TRPV4_{EC} Ca^{2+} sparklets.

Ca^{2+} influx through TRPV4_{EC} (TRPV4_{EC} sparklets) were analyzed using a custom-designed SparkAn software developed by Dr. Adrian Bonev (University of Vermont) as described previously²⁹. Fractional fluorescence traces (F/F_0) were obtained by selecting a region of interest (ROI; $1.7 \mu\text{m}^2$, 5×5 pixels) on individual sparklet sites. Representative F/F_0 traces were filtered using a Gaussian Filter and a cutoff corner frequency of 4 Hz. TRPV4_{EC} sparklets were measured using the increase in fluorescence over the averaged fluorescence obtained from 10 images. The averaged TRPV4_{EC} sparklet activity is defined as NP_O (where N is the number of TRPV4 channels per site and P_O is the open state probability of the channel) and was calculated using the Single Channel Search module of Clampfit quantal amplitudes derived from the all-points histogram ($0.29 \Delta F/F_0$ for fluo-4 loaded PAs) and the following equation:

$$\text{NP}_O = \left[\frac{(T_{\text{level}} + 2T_{\text{level}} + 3T_{\text{level}3} + 4T_{\text{level}})}{T_{\text{total}}} \right]$$

where T is the dwell time at each quantal level detected at each TRPV4 sparklet site, and T_{total} is the recording duration. Averaged NP_O per site was calculated by averaging the NP_O

for all the sites in a field. Total number of sites per field was calculated by the number of TRPV₄^{EC} sparklet sites per field averaged over all the fields in different PAs. All the sparklets in a field were added to obtain the total number of sites per field of view.

Immunostaining.

Immunostaining was performed on fourth-order PAs pinned *en face* on SYLGARD blocks. PAs were fixed using 4% paraformaldehyde (PFA) at room temperature for 15 minutes and then washed 3 times with phosphate-buffered saline (PBS) solution. The tissue was permeabilized with 0.2% Triton-X for 30 minutes, blocked with 5% normal donkey serum (ab7475, Abcam, Cambridge, MA) or normal goat serum (ab7475, Abcam, Cambridge, MA), depending on the host of the secondary antibody used, for one hour at room temperature. Primary antibodies (Table 1) were incubated with overnight at 4 °C. Afterwards, PAs were incubated secondary antibody for one hour at room temperature in the dark room. For nuclear staining, PAs were washed with PBS and then incubated with 0.3 μM DAPI (Invitrogen, Carlsbad, CA, USA) for 10 minutes at room temperature. Images were acquired along the z-axis starting at the top of the ECs with a slice size of 0.02 μm using the Andor microscope described above. The internal elastic lamina (IEL) autofluorescence was evaluated using an excitation of 488 nm with a solid-state laser and collecting the emitted fluorescence with a 525/36 nm band-pass filter. Immunostaining for the protein of interest was evaluated using an excitation of 561 nm and collecting the emitted fluorescence with a 607/36 nm band-pass filter. DAPI immunostaining was evaluated using an excitation of 409 nm and collecting the emitted fluorescence with a 447/69 nm band-pass filter. Imaris 9.3 was used to render 3D images of the *en face* PA.

Proximity Ligation Assay (PLA).

Fourth order PAs were pinned *en face* on SYLGARD blocks. PAs were fixed with 4% paraformaldehyde (PFA) for 15 minutes followed by three washes with PBS. PAs were permeabilized with 0.2% Triton X for 30 minutes at room temperature followed by blocking with 5% normal donkey serum (Abcam plc, Cambridge, MA, USA) and 300 mM glycine for one hour at room temperature. After three washes with PBS, PAs were incubated with the primary antibody overnight at 4 °C. The PLA protocol from Duolink PLA Technology kit (Sigma-Aldrich, St. Louis, MO, USA) was followed for the detection of co-localized proteins. Lastly, PAs were incubated with 0.3 μM DAPI nuclear staining (Invitrogen, Carlsbad, CA, USA) for 10-min at room temperature in the dark room. PLA images were acquired using the Andor Revolution spinning-disk confocal imaging system along the z-axis at a slice size of 0.02 mm from the top of the EC to the bottom of the SMC. Images were analyzed by normalizing the number of positive puncta in the endothelium per number of nuclei in a field.

Table 1. List of antibodies used for immunostaining and PLA on *en face* PAs.

Protein	Product no.	Company	Address	Concentration
TRPV4	LSC 94498	LifeSpan BioScience INC	Seattle, WA, USA	1:200
Cav-1	ab2910	Abcam plc.	Cambridge, MA, USA	1:500
PKC	SC-17769	Santa Cruz Biotechnology, Inc.	Dallas, TX, USA	1:250

Nitric oxide (NO) measurements.

PAs were pinned *en face* on SYLGUARD blocks and incubated with DAF-FM (4-amino-5 methylamino-2',7'-difluorofluorescein diacetate, 5 μ M) in Hepes-PSS with 0.02% pluronic acid for 20 min at 30 °C in the dark. DAF-FM forms a fluorescent triazole compound after binding to NO. DAF-FM fluorescence was imaged using an excitation of 488 nm solid state laser and collecting the emitted fluorescence was captured with a 525/36 nm band-pass filter using the Andor Revolution spinning disk confocal imaging system. Images were obtained along the z-axis at a slice size of 0.02 μ m from the top of the endothelial cells to the bottom of the smooth muscle cell. DAF-FM fluorescence was analyzed using the custom-designed SparkAn software by placing region of interest outlining each EC and obtaining the arbitrary fluorescence intensity for each cell. The background fluorescence was subtracted from the average cell fluorescence. EC fluorescence was averaged to all the other cells in a field to obtain a single fluorescence number for each field.

Plasmid generation and transfection into HEK293 cells.

The TRPV4 coding sequence without stop codons was amplified from mouse heart cDNA. The amplified fragment was inserted into a plasmid backbone containing a CMV promoter region for expression and in addition, is suitable for lentiviral production by Gibson assembly. The in-frame FLAG tag was inserted into the 3'-primer used for amplification. Cav-1 plasmids were obtained from Origene Technologies (Montgomery County, MD). Constructs were verified by sequencing the regions that had been inserted into the plasmid backbone. HEK293 cells were seeded (7×10^5 cells per 100 mm dish) in Dulbecco's Modified Eagle Medium with 10% fetal bovine serum (Thermo Fisher

Scientific Inc. Waltham, MA, USA) one day prior to transfection. Cells were transfected using the LipofectamineLTX protocol (Thermo Fisher Scientific Inc. Waltham, MA, USA). Patch clamp experiments were conducted 48 hours after transfection.

Patch clamp in HEK293 cells.

HEK293 cell currents were recorded using whole-cell patch configuration. Cells were kept at room temperature in a bathing solution consisting of 10 mM Hepes, 134 mM NaCl, 6 mM KCl, 2 mM CaCl₂, 10 mM glucose, and 1 mM MgCl₂ (adjusted to pH 7.4 with NaOH). The intracellular solution consisted (in mM) 20 CsCl, 100 Cs-aspartate, 1 MgCl₂, 4 ATP, 0.08 CaCl₂, 10 BAPTA, 10 Hepes, pH 7.2 (adjusted with CsOH). Currents were measured using a voltage clamped protocol where a voltage-ramp pulses (-100 mV to +100 mV) was applied over 200 ms with a holding potential of -50 mV. TRPV4 currents were measured before or five minutes after treatment with peroxynitrite (5 μM).

Drugs and chemical compounds.

Cyclopiazonic acid, GSK1016790A, GSK2193874, NS309, and tempol were purchased from Tocris Bioscience (Minneapolis, MN, USA). DAF-FM were purchased from Thermo Fisher Scientific Inc. (Waltham, MA, USA). PN, UA, FeTPPS, ML171, and 1400w were purchased from Cayman Chemical (Ann Arbor, MI, USA). All other chemicals were purchased from Sigma-Aldrich (St. Louis, MO, USA).

Statistical analysis.

All results are presented as mean ± SEM. Data figures were made using CorelDraw Graphic Suite X7 (Ottawa, ON, Canada). Statistical analysis was performed using OriginPro 7.5 (Northampton, MA, USA). A two-tailed, paired or independent t-test (for

comparison of data collected from two different treatments) or one-way ANOVA (to investigate statistical differences among more than two different treatments) were performed to determine statistically significant differences between groups. If significant, Tukey correction was performed for *post hoc* testing. Statistical significance was determined as a *p* value less than 0.05.

**CHAPTER 3. NITRIC OXIDE-DEPENDENT FEEDBACK LOOP REGULATES
TRPV4 CHANNEL COOPERATIVITY AND ENDOTHELIAL FUNCTION IN
SMALL PULMONARY ARTERIES**

3.1 Abstract

Recent studies demonstrate that spatially restricted, local Ca^{2+} signals are key regulators of endothelium-dependent vasodilation in systemic circulation. There are drastic functional differences between pulmonary arteries (PAs) and systemic arteries, but the local Ca^{2+} signals that control endothelium-dependent vasodilation of PAs are not known. Localized, unitary Ca^{2+} influx events through TRPV4 (transient receptor potential vanilloid 4) channels, termed TRPV4 sparklets, regulate endothelium-dependent vasodilation in resistance-sized mesenteric arteries via activation of Ca^{2+} -dependent K^+ channels. The objective of this study was to determine the unique functional roles, signaling targets, and endogenous regulators of TRPV4 sparklets in resistance-sized PAs. Using confocal imaging, custom image analysis, and pressure myography in fourth-order PAs in conjunction with knockout mouse models, we report a novel Ca^{2+} signaling mechanism that regulates endothelium-dependent vasodilation in resistance-sized PAs. TRPV4 sparklets exhibit distinct spatial localization in PAs when compared to mesenteric arteries, and preferentially activate endothelial nitric oxide synthase (eNOS). Nitric oxide released by TRPV4-eNOS signaling not only promotes vasodilation, but also initiates a guanylyl cyclase-protein kinase G-dependent negative feedback loop that inhibits cooperative openings of TRPV4 channels, thus limiting sparklet activity. Moreover, we discovered that adenosine triphosphate (ATP) dilates PAs through a P2 purinergic receptor-dependent activation of TRPV4 sparklets. Our results reveal a spatially distinct TRPV4-eNOS signaling mechanism and its novel endogenous regulators in resistance-sized PAs.

3.2 Introduction

Endothelial cells (ECs) from small, resistance-sized arteries are key controllers of vascular resistance. Recent studies in systemic arteries—including mesenteric, cremaster, and cerebral arteries—have demonstrated that endothelium-dependent vasodilation is controlled by local, spatially restricted increases in endothelial Ca^{2+} while the whole-cell Ca^{2+} level remains unchanged^{22,23,132,138,139}. In contrast to systemic arteries, pulmonary arteries (PAs) comprise a low pressure, high flow circulation. Moreover, systemic and pulmonary vascular resistances can be regulated independently¹⁴⁰. The distinct signaling mechanisms that regulate endothelial function in small PA are poorly understood. Unraveling the local Ca^{2+} signals in small PAs may be necessary for understanding endothelial regulation of pulmonary vascular resistance (PVR) under normal and disease conditions.

In mesenteric, cremaster, and cerebral arteries TRPV4 channels are key regulators of endothelium-dependent vasodilation^{22,132,141}. In mesenteric arteries, local, unitary Ca^{2+} influx events through endothelial TRPV4 (transient receptor potential vanilloid 4) channels, termed “TRPV4 sparklets”, activated endothelial IK/SK (Ca^{2+} -activated intermediate and small conductance K^+) channels to cause vasodilation^{22,23}. The biophysical properties, signaling targets, and endogenous regulators of TRPV4 sparklets in small PAs remain unknown. Endothelium-derived nitric oxide (NO) is thought to be the predominant vasodilator in the pulmonary circulation^{101,142-145}. Increase in global Ca^{2+} has long been associated with activation of endothelial nitric oxide synthase (eNOS). Whether a specific local Ca^{2+} signal can activate eNOS has not been elucidated. In this study, we

explored the possibility that local, unitary Ca^{2+} influx through TRPV4 channels activates eNOS in small PAs, a signaling mechanism different from small mesenteric/cremaster/cerebral arteries^{22,132,141}.

NO can alter the activity of several ion channels by S-nitrosylation or activation of guanylyl cyclase-protein kinase G (GC-PKG) signaling¹⁴⁶⁻¹⁵⁰. In cultured cells, S-nitrosylation of TRPV4 channels increased the channel function¹⁵¹, and activation of GC-PKG signaling reduced the channel activity¹⁵². Therefore, in PAs, TRPV4-eNOS signaling could activate a bidirectional regulation, where TRPV4 channels promote NO release, which in turn regulates TRPV4 channel function. Ca^{2+} -dependent cooperative opening of TRPV4 channels in a cluster has emerged as a key mechanism for modulating TRPV4 channel function^{22,23,153,154}. We postulated that TRPV4-induced NO release modulates TRPV4 channel activity by altering cooperative openings of TRPV4 channels.

Discovering the endogenous activators of TRPV4 channels in small PAs is central to deciphering the unique physiological roles of TRPV4 channels in pulmonary circulation. In this regard, purinergic receptor agonist ATP (adenosine triphosphate) has been shown to increase endothelial Ca^{2+} and cause vasodilation in large, conduit PAs¹⁵⁵⁻¹⁵⁷. ATP can be released into the circulation by ECs, smooth muscle cells, and red blood cells^{158,159}. Circulatory ATP may, therefore, serve as an important regulator of pulmonary vascular resistance. We hypothesized that ATP is a novel, endogenous activator of TRPV4 channels in small PAs.

In the current study we provide the first evidence that local Ca^{2+} signals–TRPV4 sparklets–regulate baseline and induced eNOS activity to dilate small PAs. Moreover, we

report ATP as a novel endogenous activator of TRPV4 channels that promotes TRPV4-eNOS signaling through P2 purinergic receptors. NO is another endogenous regulator of TRPV4 channels that limits TRPV4 channel activity by disrupting the coupling among TRPV4 channels via activation of endothelial GC-PKG mechanism. These results reveal distinct, novel local Ca^{2+} signaling mechanisms that regulate endothelial function in small PAs.

3.3 Results

Native endothelium from small PAs exhibits unitary TRPV4 sparklets with distinct spatial properties.

We recently discovered localized, unitary Ca^{2+} influx events through TRPV4 channels in the endothelium from small mesenteric arteries (MAs), and termed them TRPV4 sparklets^{22,23}. Because of the structural and functional differences between systemic and pulmonary circulations¹⁴⁰, we hypothesized that TRPV4 sparklets from small PAs exhibit unique biophysical properties. Local Ca^{2+} signals were studied in the intact endothelium from small (~100-200 μm), fourth-order PAs (Figure 2A, *top panel*). Cyclopiazonic acid (CPA, 20 $\mu\text{mol/L}$, sarcoplasmic/endoplasmic reticulum Ca^{2+} -ATPase inhibitor) was employed to deplete intracellular stores of Ca^{2+} and to eliminate the interference from Ca^{2+} release from intracellular stores in *en face* PAs. In the presence of CPA alone, there were ~ 2 TRPV4 sparklet sites per field of view (~ 15 ECs, Figure 2A, *top panel*) within a recording duration of 1 minute (Figure 3A). The number of TRPV4 sparklet sites per field was increased 2- and 7-fold by the selective channel agonists, GSK1016790A (GSK101; 3

nmol/L) and RN1747 (1 μ mol/L), respectively (Figure 3A and B). The TRPV4 sparklet activity was almost entirely inhibited by selective TRPV4 inhibitors GSK2193874 (GSK219; 100 nmol/L) and HC067047 (HC067; 1 μ mol/L) (Figure 2A, *middle and bottom panels*; Figure 3A). The Ca^{2+} sparklets elicited by GSK101 and RN1747 were absent in arteries from TRPV4^{-/-} mice (Figure 2A, *bottom panel* – Figure 3A). The Ca^{2+} sparklets elicited by GSK101 were immediately abolished as the external Ca^{2+} was changed from 2 mmol/L to 0 mmol/L (Figure 2A, *bottom panel*; Figure 3C), confirming that the TRPV4 sparklets represented the influx of extracellular Ca^{2+} through TRPV4 channels on EC membrane. Moreover, the increase in fluorescence at a sparklet site was not accompanied by an increase in whole-cell fluorescence (Figure 4), indicating that TRPV4 sparklets did not alter whole-cell Ca^{2+} levels. The surface area encompassed by EC outlines was \sim 45-fold higher than the spatial spread of TRPV4 sparklets, further supporting the local nature of sparklets (Figure 4C).

The fractional fluorescence (F/F_0) traces revealed square, discrete amplitudes of TRPV4 sparklets, reminiscent of single-channel openings from a patch clamp experiment (Figure 2A, *middle panel*). Therefore, we used the following single-channel opening criteria to determine whether Ca^{2+} sparklets in PAs are unitary events^{22,160} - 1) small recording volumes; 2) high Ca^{2+} permeability and single channel conductance; 3) quantal amplitudes, and 4) dependence of the sparklet amplitude on Ca^{2+} electrochemical gradient but not on the concentration of the agonist or inhibitor¹⁶⁰. Regarding the first criterion, ECs from small PAs are \sim 1 μ m thick, corresponding to a recording volume of 1.2 fL. TRPV4 channels have been demonstrated to have a large single channel conductance and Ca^{2+}

permeability¹⁶¹, satisfying the second criterion. A multiple Gaussian fit to all-points histogram of the fractional fluorescence established a stepwise increase in amplitude, with the quantal level being $0.29 \Delta F/F_0$ for the arteries loaded with fluo-4 (Figure 2B), and $0.19 \Delta F/F_0$ for the arteries from GCaMP2^{Cx40} mice (Figure 5A - *top*). Increasing the extracellular Ca^{2+} from 2 mmol/L to 10 mmol/L produced a 70% increase in the quantal level of Ca^{2+} sparklets (Figure 5A - *middle*). Reducing the electrochemical gradient for Ca^{2+} influx by depolarizing EC membranes using 100 mmol/L extracellular K^+ decreased the amplitude of these events by 50% (Figure 5A - *bottom*), satisfying the third criterion. Moreover, the quantal amplitude did not change with the use of different agonists, with increasing concentration of an agonist, or with the use of TRPV4 inhibitor (Figure 5B), satisfying the fourth criterion. These results supported the concept that TRPV4 sparklets in PA endothelium represent unitary Ca^{2+} influx events through TRPV4 channels.

In small MAs, the majority (~ 60%) of TRPV4 sparklet sites occurred at endothelial projections to smooth muscle cells (SMCs) or myoendothelial projections (MEPs)²³, where IK channels were also localized^{23,132}. In small PAs, however, a small percentage of sparklet sites ($25 \pm 3\%$; n=5 PAs) occurred at the MEPs. To confirm the spatial differences in sparklet localization between small PAs and MAs, internal elastic lamina (IEL) was stained with Alexa Fluor 633 (a marker for extracellular matrix)¹³³ immediately after Ca^{2+} imaging experiments. Overlay of sparklet site ROIs with IEL staining images showed that only ~ 28% of the sparklet sites overlapped with MEPs in small PAs, whereas ~65% sparklet sites overlapped with MEPs in small MAs (Figures 2C, 2D). The total number of holes per field of view was, however, higher in PAs compared to MAs (Figure 2D). These results

established the spatial differences in TRPV4 sparklet activity between small PAs and MAs. We previously showed that MEP-localized A-kinase anchoring protein 150 (AKAP150) was required for localization of TRPV4 sparklets at MEPs in MAs. Consistent with the non-MEP localization of sparklets in PAs, only ~ 5% of holes in the IEL showed identifiable AKAP150 staining in PAs when compared to ~90% of the MEPs in MAs (Figure 2E).

FIGURE 2. NATIVE ENDOTHELIUM FROM SMALL PULMONARY ARTERIES (PAS) DISPLAYS TRANSIENT RECEPTOR POTENTIAL VANILLOID 4 (TRPV4) SPARKLETS WITH DISTINCT SPATIAL LOCALIZATION.

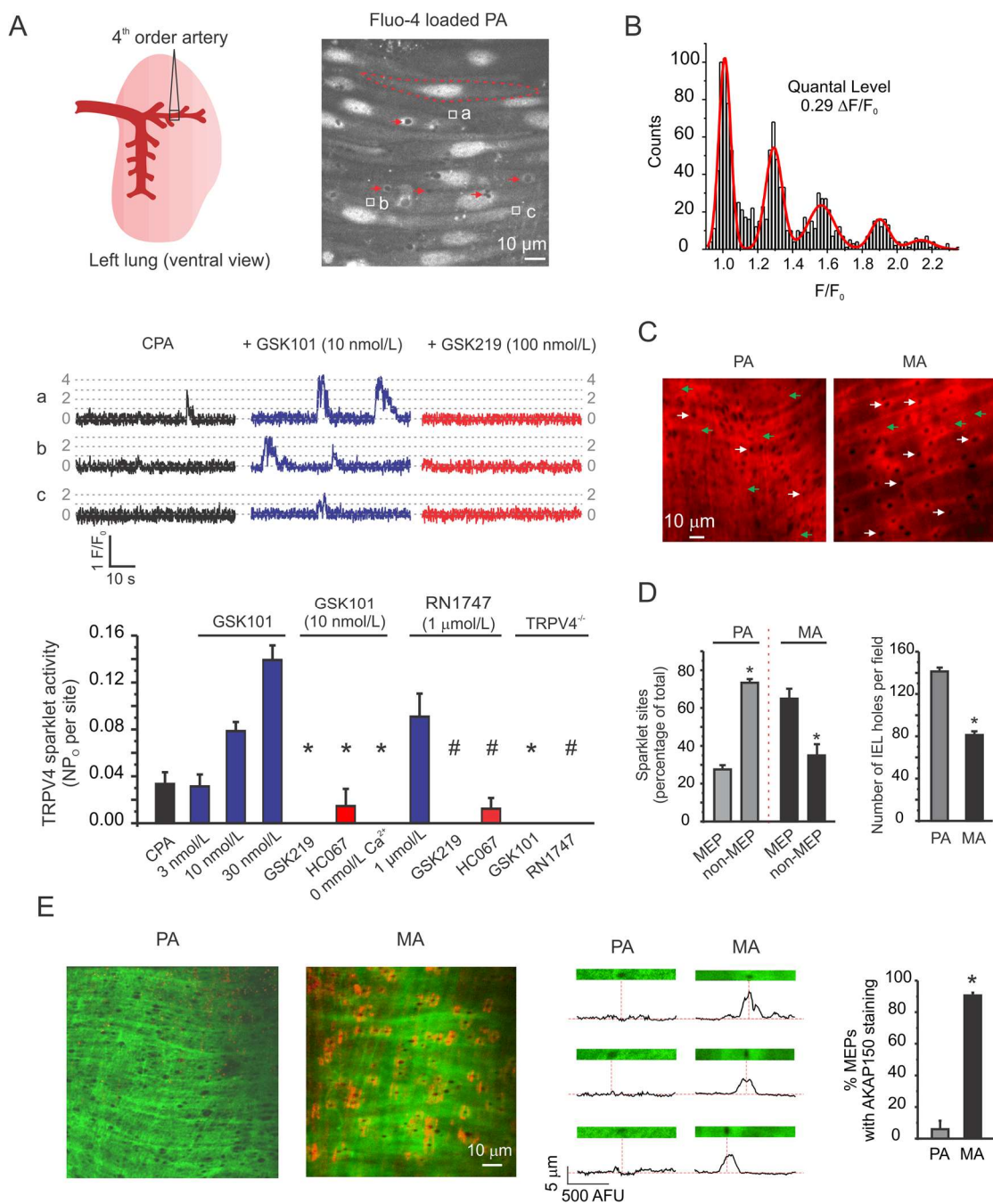


Figure 2. Native endothelium from small pulmonary arteries (PAs) displays transient receptor potential vanilloid 4 (TRPV4) sparklets with distinct spatial localization.

Local Ca^{2+} influx events through TRPV4 channels (TRPV4 sparklets) were recorded in *en face* fourth-order PAs and third-order mesenteric arteries (MAs) loaded with fluo-4AM (10 $\mu\text{mol/L}$). Cyclopiazonic acid (CPA, 20 $\mu\text{mol/L}$) was used in order to eliminate interference from Ca^{2+} release from the endoplasmic reticulum (ER). **A.** *Top*, the cartoon indicates a fourth-order PA from left lung that was used in this study (*left*). A grayscale image of a field of view with ~ 15 endothelial cells (ECs; *right*). The dotted line indicates the outline of a single EC. Square boxes represent the regions of interest (ROIs) placed at the sparklet sites detected within a recording duration of 1 minute. Arrows point to the holes in internal elastic lamina (IEL) that represent myoendothelial projections (MEPs). *Middle*, fractional fluorescence (F/F_0) traces were obtained from the ROIs shown in the *top* panel. The traces indicate sparklet activity under basal conditions (CPA), with the TRPV4 agonist GSK1016790A (GSK101) alone and in the presence of TRPV4 inhibitor GSK2193784 (GSK219). Dotted lines represent the single-channel levels derived from all-points histogram in B. *Bottom*, averaged TRPV4 sparklet activity under basal conditions (CPA), in the presence of TRPV4 agonist GSK101, GSK101 in the absence or presence of two different TRPV4 channel inhibitors (GSK219, 100 nmol/L and HC067047 or HC067, 1 $\mu\text{mol/L}$) or 0 mmol/L extracellular Ca^{2+} , another TRPV4 channel agonist RN1747 in the absence or presence of TRPV4 inhibitors GSK219 (100 nmol/L) and HC067 (1 $\mu\text{mol/L}$), and GSK101 (10 nmol/L) and RN1747 (1 $\mu\text{mol/L}$) in the PAs from TRPV4^{-/-} mice. Data are mean \pm SEM; TRPV4 sparklet activity (NP_0 per site) was calculated using the quantal

amplitude derived from Figure 1B; N represents the number of channels at a site and P_o is the open state probability of the channels (n=5 fields; $P < 0.0001$ using one-way ANOVA and *post hoc* Tukey test; * and # indicate statistical significance ($P < 0.05$) versus 10 nmol/L GSK101 and 1 $\mu\text{mol/L}$ RN1747, respectively). **B.** All-points histogram was constructed from F/F_0 traces pooled from three PAs and was fit with a multi-Gaussian curve. The quantal levels (single-channel amplitudes) were derived from the peaks of the multi-Gaussian curve. **C.** Experiments were performed in arteries loaded with fluo-4AM and Alexa Fluor 633 hydrazide. Representative images show black holes in the IEL that represent MEPs. Sparklet ROIs were superimposed with IEL staining. Arrows indicate MEP sites in the IEL (white) and non-MEP sites (green) that overlapped with sparklet sites. **D.** (*Left*) Averaged data for localization of sparklet sites at MEPs in PAs and MAs. Data are mean \pm SEM (n=10 fields; $P < 0.001$ using two-way ANOVA and post hoc Tukey test; * $P < 0.05$ versus MEP). (*Right*) Average number of IEL holes per field in PAs and MAs. Data are mean \pm SEM (n=10 fields; $P < 0.05$ using two-sample t-test). **E.** AKAP150 staining was performed in *en face* third-order MAs and fourth-order PAs as described in the Methods section. (*Left*) Representative AKAP150 staining images from PAs and MAs, where green color indicates the autofluorescence of the internal elastic lamina (IEL), black holes in the IEL indicate MEPs, and red color indicates AKAP150-staining. (*Middle*) Plot profiles of AKAP150 immunostaining for representative horizontal transects. Dotted lines indicate the positions of MEPs located at the holes in IEL. Images were acquired along the z-axis (0.05 μm optical slice). (*Right*) Averaged AKAP150 localization from MAs and

PAs; AKAP150 immunostaining within 5 μm from the center of the holes in IEL was considered to be localized at the IEL (n= 5 arteries; *P<0.0001 using independent t-test).

FIGURE 3. SPECIFIC TRPV4 CHANNEL AGONISTS INCREASE THE NUMBER OF SPARKLET SITES PER FIELD OF VIEW IN NATIVE ECS FROM FOURTH-ORDER PAS.

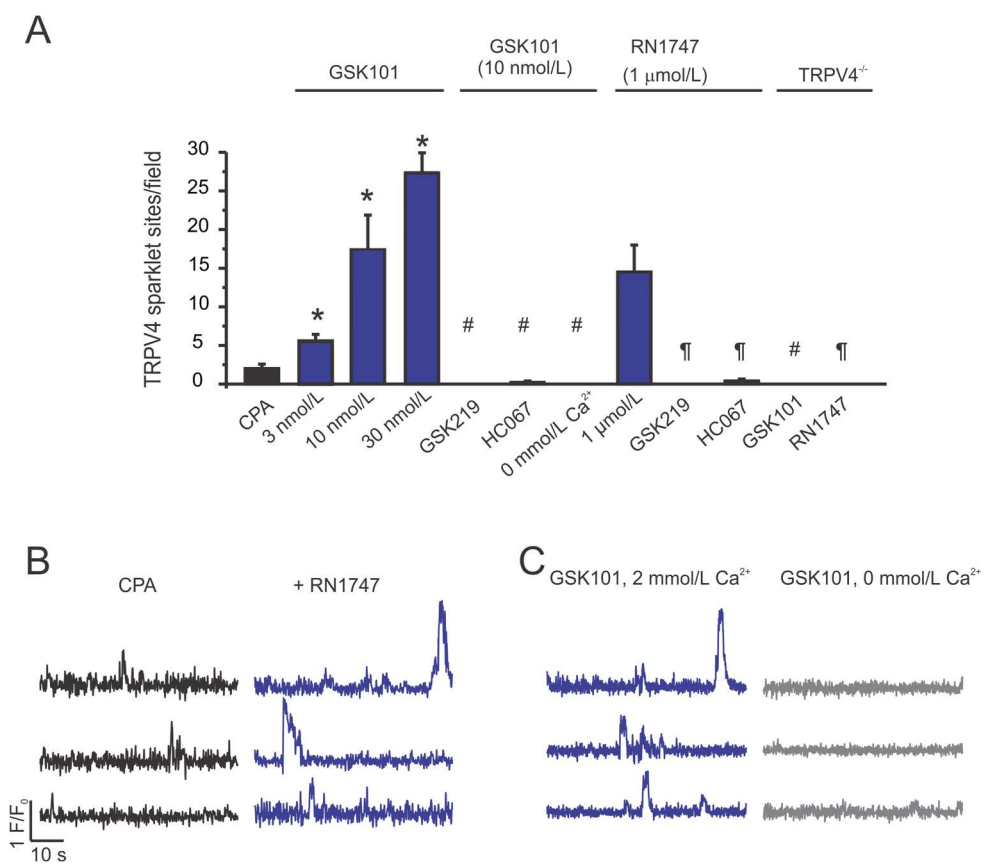


Figure 3. Specific TRPV4 channel agonists increase the number of sparklet sites per field of view in native ECs from fourth-order PAs. TRPV4 Ca^{2+} sparklets were recorded in *en face* fourth-order PAs loaded with fluo-4AM (10 $\mu\text{mol/L}$). Cyclopiazonic acid (CPA, 20 $\mu\text{mol/L}$) was used in order to eliminate the interference from ER Ca^{2+} release. **A.** Averaged number of TRPV4 sparklet sites per field under basal conditions (CPA), in the presence of TRPV4 agonist GSK101 (3-30 nmol/L), GSK101 (10 nmol/L) in the absence or presence of two different TRPV4 channel inhibitors (GSK219, 100 nmol/L and HC067047 or HC067, 1 $\mu\text{mol/L}$) or 0 mmol/L extracellular Ca^{2+} , another TRPV4 channel agonist RN1747 (1 $\mu\text{mol/L}$) in the absence or presence of TRPV4 inhibitors GSK219 (100 nmol/L) and HC067 (1 $\mu\text{mol/L}$), and GSK101 (10 nmol/L) and RN1747 (1 $\mu\text{mol/L}$) in the PAs from TRPV4^{-/-} mice. Data are presented as mean \pm SEM (n=5 PAs; P<0.0001 using one-way ANOVA; *, #, ¶ indicate significance (P<0.05) versus CPA, 10 nmol/L GSK101, and 1 $\mu\text{mol/L}$ RN1747, respectively). **B.** Representative fractional fluorescence (F/F₀) traces of three distinct TRPV4 sparklet sites in a field of view in the absence (*left*) or presence (*right*) of the TRPV4 agonist RN1747 (1 $\mu\text{mol/L}$). **C.** Representative fractional fluorescence (F/F₀) traces of three distinct GSK1016790A (GSK101, 10 nmol/L)-induced TRPV4 sparklet sites in the presence (*left*) or absence (*right*) of extracellular Ca^{2+} (2 mmol/L).

FIGURE 4. TRPV4 SPARKLETS INCREASE LOCAL, BUT NOT WHOLE-CELL Ca^{2+} LEVELS IN THE ECS.

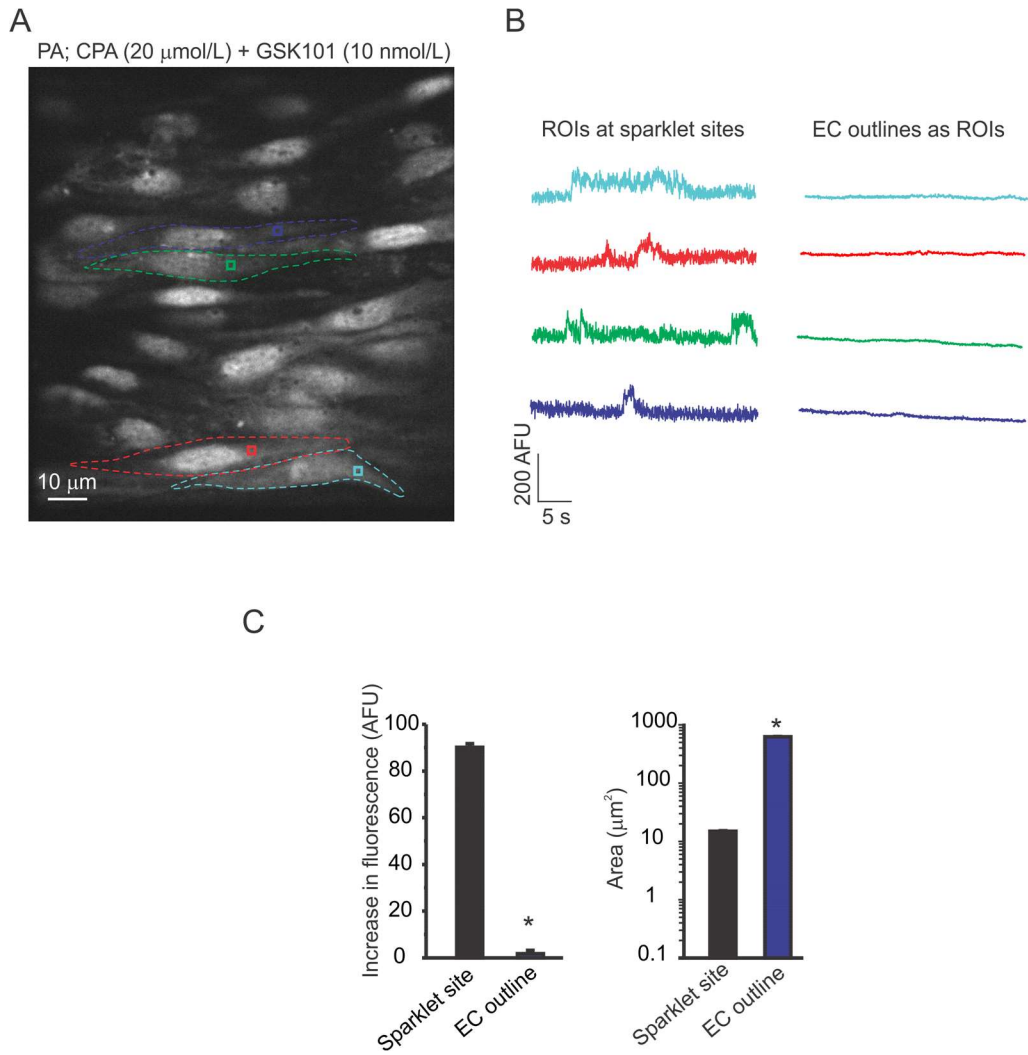


Figure 4. TRPV4 sparklets increase local, but not whole-cell Ca²⁺ levels in the ECs.

Changes in fluorescence were recorded in *en face* fourth-order PAs loaded with fluo-4AM (10 $\mu\text{mol/L}$) in the presence of GSK101 (10 nmol/L). Cyclopiazonic acid (CPA, 20 $\mu\text{mol/L}$) was used in order to eliminate the interference from Ca²⁺ release from intracellular stores. **A.** A greyscale image of a field of view with ~ 15 ECs; the dotted lines indicates the outlines of ECs. Square boxes represent the regions of interest (ROIs) placed at the sparklet sites. **B.** Representative fluorescence traces of TRPV4 sparklets using square ROIs (*left*) and whole-cell fluorescence using whole-cell outlines as ROIs (*right*). **C.** Averaged increase in fluorescence (arbitrary fluorescence units; AFU) for ROIs placed at sparklet sites and whole cell ROIs following TRPV4 channel activation with GSK101 (3 nmol/L ; *left*); average spatial spread of sparklets and area encompassed by whole cell outlines (*right*). Data are presented as mean \pm SEM (n=24 sparklet sites and 24 ECs; *P<0.0001 using independent t-test).

Figure 5. TRPV4 sparklets represent unitary Ca^{2+} influx events through TRPV4 channels in the native endothelium from small PAs. Localized Ca^{2+} influx events through TRPV4 channels (TRPV4 sparklets) were recorded in *en face* fourth-order PAs from $\text{GCaMP2}^{\text{Cx40}}$ mice. Cyclopiazonic acid (CPA, 20 $\mu\text{mol/L}$) was used to eliminate the interference from Ca^{2+} release from the endoplasmic reticulum (ER). Experiments were performed using 3 nmol/L GSK101 to increase the activity of TRPV4 sparklets in PAs from GCaMP2 mice. All-points histograms were constructed from the F/F_0 traces and were fit with a multiple Gaussian curve. The quantal levels (single-channel amplitudes) were derived from the peaks of the multiple Gaussian curve. The data were pooled from three PAs. Dotted lines represent the quantal levels (number of channels open) at a site. **A.** All-points histogram and representative traces in the presence of 2 mmol/L extracellular Ca^{2+} (*top*) 10 mmol/L extracellular Ca^{2+} (*middle*) and 10 mmol/L extracellular Ca^{2+} and 100 mmol/L KCl (*bottom*). **B.** All-points histograms in the presence of a TRPV4 channel agonist GSK101 (10 nmol/L , *top*), a different TRPV4 channel agonist RN1747 (1 $\mu\text{mol/L}$, *middle*), and with the addition of a TRPV4 channel inhibitor HC067047 (1 $\mu\text{mol/L}$, *bottom*) in the presence of GSK101. The data were pooled from 3 PAs for each histogram.

TRPV4 sparklets cause vasodilation in small PAs via eNOS activation

Administration of TRPV4 channel agonist GSK101 lowered PAP in rats¹⁶². At the level of small PAs, however, the functional effect of endothelial TRPV4 channel activation and the Ca²⁺-sensitive targets have not been identified. PAs are normally exposed to intravascular pressures of 10-20 mmHg. We therefore cannulated and pressurized fourth-order PAs at 15 mmHg to assess the effect of TRPV4 channel activation on PA diameter. PAs were precontracted with U46619 (100 nmol/L), a thromboxane A2 receptor agonist (32 ± 2 % constriction; n=30 PAs). NS309, a highly specific activator of endothelial IK and SK channels¹⁶³, induced dilations in PAs that were absent in endothelium-denuded PAs, confirming the presence of functional IK and SK channels in PA endothelium (Figure 6A, 6B). PAs were then treated with GSK101 (3–30 nmol/L), which caused a concentration-dependent vasodilation (Figures 6A, 6B). GSK101-induced dilation was absent in endothelium-denuded PAs, PAs from TRPV4^{-/-} mice, and in the presence of TRPV4 channel inhibitor GSK219 (Figures 6A, 6B), confirming that endothelial TRPV4 channel activation dilated small PAs.

We previously showed that endothelial TRPV4 channels induced vasodilation predominantly via activation of IK/SK channels in small MAs constricted by intravascular pressure²². Presence of U46619 in the superfusate did not alter the IK/SK channel-dependent nature of TRPV4 channel-induced vasodilation in MAs (Figure 6C, 6D). We, therefore, tested the effect of IK and SK channel inhibitors, Tram-34 (1 μmol/L) and apamin (300 nmol/L), respectively, on TRPV4-vasodilation in small PAs. While NS309-induced vasodilation was reduced by 70.0 ± 10.6% (n=5 PAs) in the presence of Tram-34

and apamin, TRPV4 channel-induced vasodilation was not affected by IK/SK channel inhibitors (Figures 6A, 6B), raising an interesting possibility that a distinct local Ca^{2+} signaling network mediated TRPV4-induced vasodilation in small PAs. Although the activation of eNOS by localized Ca^{2+} signals has not been described, global increase in Ca^{2+} is known to activate eNOS¹⁶⁴. We, therefore, tested the possibility that TRPV4 sparklets activated eNOS to cause vasodilation in small PAs. Inhibition of NOS with L-NNA (L-N^G-Nitroarginine; 100 $\mu\text{mol/L}$) constricted PAs by approximately $13 \pm 1\%$ ($n=12$ PAs), indicating a tonic influence of NO on basal diameter of PAs. In the presence of L-NNA, GSK101-induced vasodilation was abolished (Figures 6A, 6B). However, L-NNA is a non-selective inhibitor of eNOS, inducible NOS (iNOS) and neuronal NOS (nNOS). To determine the relative contribution from each NOS isoform to TRPV4-vasodilation, we used a selective iNOS inhibitor 1400W¹⁶⁵ (1 $\mu\text{mol/L}$) or a selective nNOS inhibitor N ω -Propyl-L-arginine hydrochloride¹⁶⁶ (NPLA, 300 nmol/L). In the presence of either of these inhibitors, the TRPV4-vasodilation was not altered (Figures 6A, 6B), pointing to a TRPV4-eNOS signaling network in PAs. The role of eNOS in TRPV4-induced vasodilation was verified by studying TRPV4 dilations in eNOS^{-/-} mice in the presence of 1400W (iNOS inhibitor)¹⁶⁵ to account for a possible compensation by iNOS¹⁶⁷. In the PAs from eNOS^{-/-} mice, TRPV4 dilations were absent (Figures 6A, 6B), confirming that TRPV4-vasodilation in PAs was being mediated by eNOS activation.

FIGURE 6. TRPV4 CHANNEL ACTIVATION DILATES CANNULATED, PRESSURIZED SMALL PAS THROUGH ENDOTHELIAL NITRIC OXIDE SYNTHASE (eNOS) ACTIVATION, AND SMALL MAS THROUGH IK/SK CHANNEL ACTIVATION.

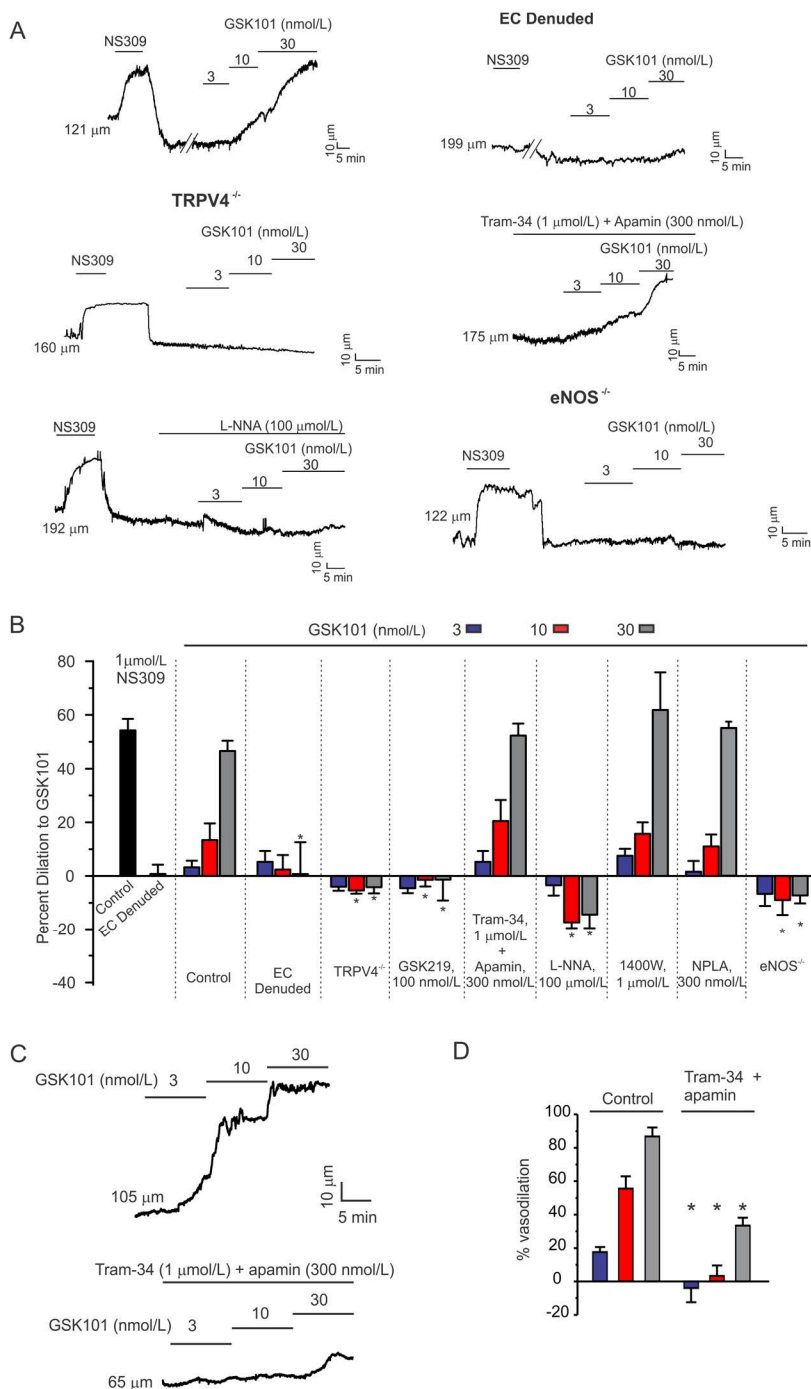


Figure 6. TRPV4 channel activation dilates cannulated, pressurized small PAs through endothelial nitric oxide synthase (eNOS) activation, and small MAs through IK/SK channel activation. Fourth-order PAs from left lung were cannulated and pressurized to 15 mmHg and third-order MAs were pressurized to 80 mmHg to record the changes in internal diameter. Both PAs and MAs were pre-constricted with thromboxane analog U46619 (100 nmol/L). Dilation to NS309 (1 μ mol/L), an activator of endothelial IK and SK channels, was used as a criterion to confirm functional viability of the endothelium. **A.** Representative traces for GSK101-induced vasodilation under control conditions, in the endothelium-denuded PAs, in the PAs from TRPV4^{-/-} mice, in the presence of IK and SK channel inhibitors (Tram-34 and Apamin, respectively), NOS inhibitor L-NNA, and in PAs from eNOS^{-/-} mice. Experiments in eNOS^{-/-} mice were performed in the presence of iNOS inhibitor 1400W to account for a possible compensation by iNOS¹⁶⁷. **B.** (*left to right*) Averaged diameter responses to NS309 in control (n=37 arteries) and endothelium-denuded (n=5 arteries) PAs, GSK101 in control PAs (n=8 arteries), in endothelium-denuded PAs (n=5 arteries), in PAs from TRPV4^{-/-} mice (n=9 arteries), in the presence of GSK219 (n=4 arteries), Tram-34 + apamin (n=9 arteries), L-NNA (n=11 arteries), 1400W (n=5 arteries), NPLA (nNOS inhibitor, n=8 arteries), and in PAs from eNOS^{-/-} mice (n=5 arteries,. Data are mean \pm SEM; P<0.0001 using two-way ANOVA and *post hoc* Tukey test; *P<0.05 versus corresponding concentration under control conditions. **C.** Representative diameter traces for the effect of GSK101 on MA diameter in the absence (*left*) or presence (*right*) of the IK and SK channel inhibitors Tram-34 and apamin, respectively. **D.** Averaged diameter data for GSK101-induced dilations in

the absence or presence of Tram-34 and apamin (n= 4 arteries; * P<0.05 using two-way ANOVA and *post hoc* Tukey test).

TRPV4 sparklets regulate NO release from the endothelium in PAs but not in MAs

The eNOS-dependent nature of TRPV4 sparklet-induced vasodilation suggested a local TRPV4-eNOS coupling in small PAs. Because NO generated in ECs can passively diffuse to the SMCs, we postulated that NO levels are increased in both EC and SMC layers following TRPV4 channel activation. NO levels in ECs and SMCs were assessed by recording 4-Amino-5-Methylamino-2',7'-Difluorofluorescein Diacetate (DAF-FM) fluorescence. Spermine NONOate (NONOate, 3-30 $\mu\text{mol/L}$), a NO donor, caused a concentration dependent increase in DAF-FM fluorescence in both EC and SMC layers (Figure 7A and B), demonstrating that an increase in NO level could be detected with DAF-FM. Both ECs and SMCs showed a low level of basal DAF-FM fluorescence (Figures 8A, 8B). Activation of TRPV4 channels with GSK101 (30 nmol/L) increased DAF-FM fluorescence in EC and SMC layers in small PAs (Figures 8A, 8B). Consistent with the NOS-independent nature of TRPV4-vasodilation in small mesenteric arteries²² (Figures 4C, 4D), TRPV4 channel activation failed to increase NO levels in ECs and SMCs from MAs (Figure 8C). In PAs, GSK101 produced a 1.8-fold increase in DAF-FM fluorescence in ECs and a 2-fold increase in SMCs (Figure 8C). Pretreatment with L-NNA inhibited the GSK101-induced increases in DAF-FM fluorescence in both ECs and SMCs (Figures 8A, 8B, and 8C). Moreover, in PAs from eNOS^{-/-} mice, GSK101 was unable to increase DAF-FM fluorescence in ECs or SMCs (Figure 8B). These results support the concept that local TRPV4-eNOS signaling regulates NO levels and endothelium-dependent vasodilation in small PAs.

To test the possibility that TRPV4 sparklets regulate NO release under basal conditions (without TRPV4 agonist) in small PAs, we studied the effect of GSK219 on NO levels. The basal DAF-FM fluorescence in both ECs and SMCs was reduced by around 30% (Figure 8D, *left*) in the presence of GSK219 supporting TRPV4 regulation of basal eNOS activity in PAs. TRPV4 channels are Ca²⁺-selective channels, but they can also conduct other ions including Na⁺ and K⁺¹⁶¹. To determine whether Ca²⁺ influx through TRPV4 channels is solely responsible for the regulation of eNOS activity by TRPV4 channels, we studied the effect of TRPV4 activation on NO levels in the presence of 0 mmol/L extracellular Ca²⁺. TRPV4 agonist GSK101 was unable to increase NO levels under these conditions (Figure 8D, *right*), confirming that Ca²⁺ influx through TRPV4 channels activated eNOS in small PAs.

To determine whether TRPV4 sparklets potentiate Ca²⁺ release from the ER in PAs, Ca²⁺ signals were recorded in PAs from mice that express the Ca²⁺ biosensor GCaMP2 selectively in ECs^{129,130}. The effect of GSK101 on the activity of Ca²⁺ release events and TRPV4 Ca²⁺ sparklets was studied by utilizing the differences in kinetics between Ca²⁺ release signals from the ER (Ca²⁺ pulsars^{22,138}, spikes with duration < 300 ms, Figure 9A, B)²² and TRPV4 Ca²⁺ sparklets (discrete, square amplitudes, duration > 300 ms, Figure 9A, B). Ca²⁺ release signals were unaffected by 0 mM extracellular Ca²⁺ and TRPV4 inhibitor, but were inhibited by CPA (Figure 9C). TRPV4 sparklet activity was unaffected by CPA, but was inhibited by 0 mM extracellular Ca²⁺ and TRPV4 inhibitor. GSK101 stimulated Ca²⁺ sparklet activity, but had no effect on the frequency of Ca²⁺ release events

(Figure 9B, C), suggesting that Ca^{2+} release from the ER did not contribute to eNOS activation by TRPV4 sparklets.

FIGURE 7. SPERMINE NONOATE, A NO DONOR, INCREASES DAF-FM FLUORESCENCE IN ECS AND SMCS FROM SMALL PAS AND CAUSES VASODILATION IN A CONCENTRATION-DEPENDENT MANNER.

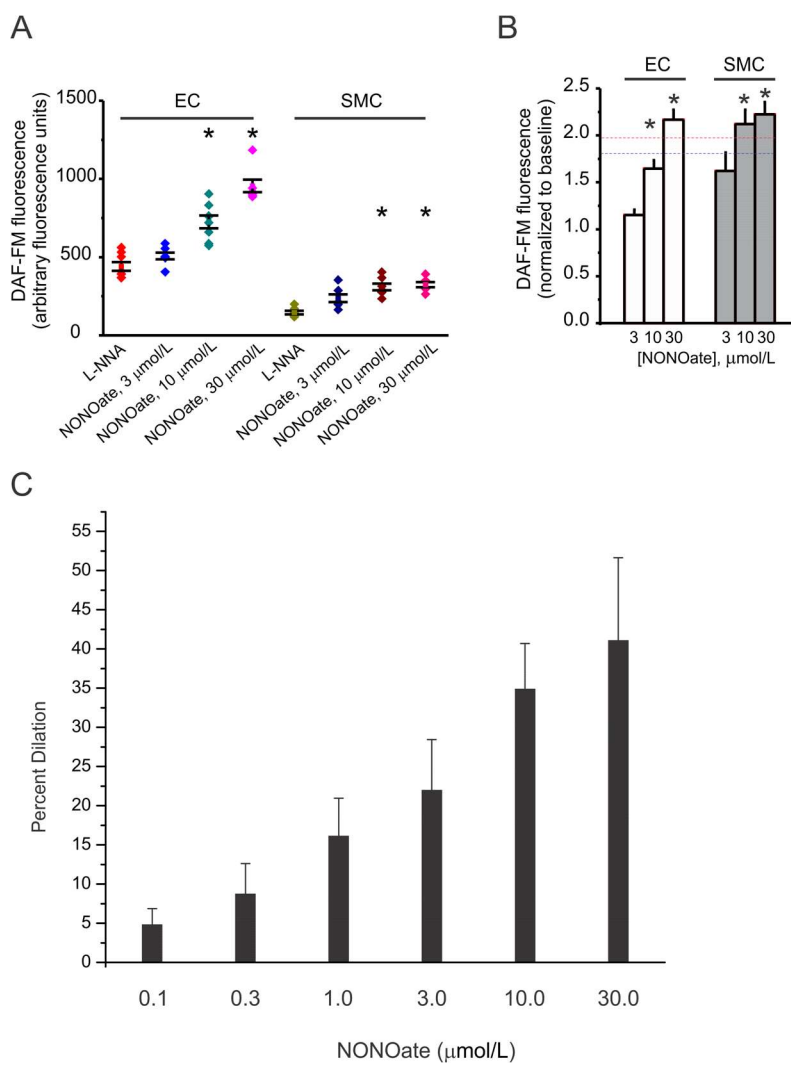


Figure 7. Spermine NONOate, a NO donor, increases DAF-FM fluorescence in ECs and SMCs from small PAs and causes vasodilation in a concentration-dependent manner. Nitric oxide (NO) fluorescence was recorded in *en face* fourth-order PAs using DAF-FM (fluorescent NO indicator; 5 $\mu\text{mol/L}$). The diameter studies were carried out in cannulated fourth-order PAs pressurized to 15 mmHg. **A.** Averaged DAF-FM fluorescence (arbitrary fluorescence units) in ECs and SMCs from PAs treated with L-NNA (100 $\mu\text{mol/L}$) alone and a combination of L-NNA and NONOate (3–30 $\mu\text{mol/L}$). Data are mean \pm SEM; individual data points represent averaged fluorescence of all the ECs or SMCs in a field of view (n=8, 6, 8, 6, 6, 6, 7, 6 fields from left to right; $P<0.0001$ using one-way ANOVA; * $P<0.05$ versus L-NNA). **B.** Averaged NONOate-dependent change in DAF-FM fluorescence in ECs and SMCs from PAs relative to the fluorescence in the presence of L-NNA (baseline). Data are mean \pm SEM (n=6, 8, 6, 6, 8, 6 fields from left to right; $P<0.0001$ using one-way ANOVA; * $P<0.05$ versus 3 $\mu\text{mol/L}$ NONOate). The dotted blue line indicates GSK101-induced increase in DAF fluorescence in ECs, whereas dotted red line indicates GSK101-induced increase in DAF fluorescence in SMCs. **C.** Averaged percent dilations of PAs to NONOate (1-30 $\mu\text{mol/L}$; n=7, 9, 9, 9, 9, 6 PAs from left to right; $P=0.0077$ using one-way ANOVA).

FIGURE 8. TRPV4-eNOS Ca^{2+} SIGNALING MECHANISM REGULATES NITRIC OXIDE LEVELS IN SMALL PAS.

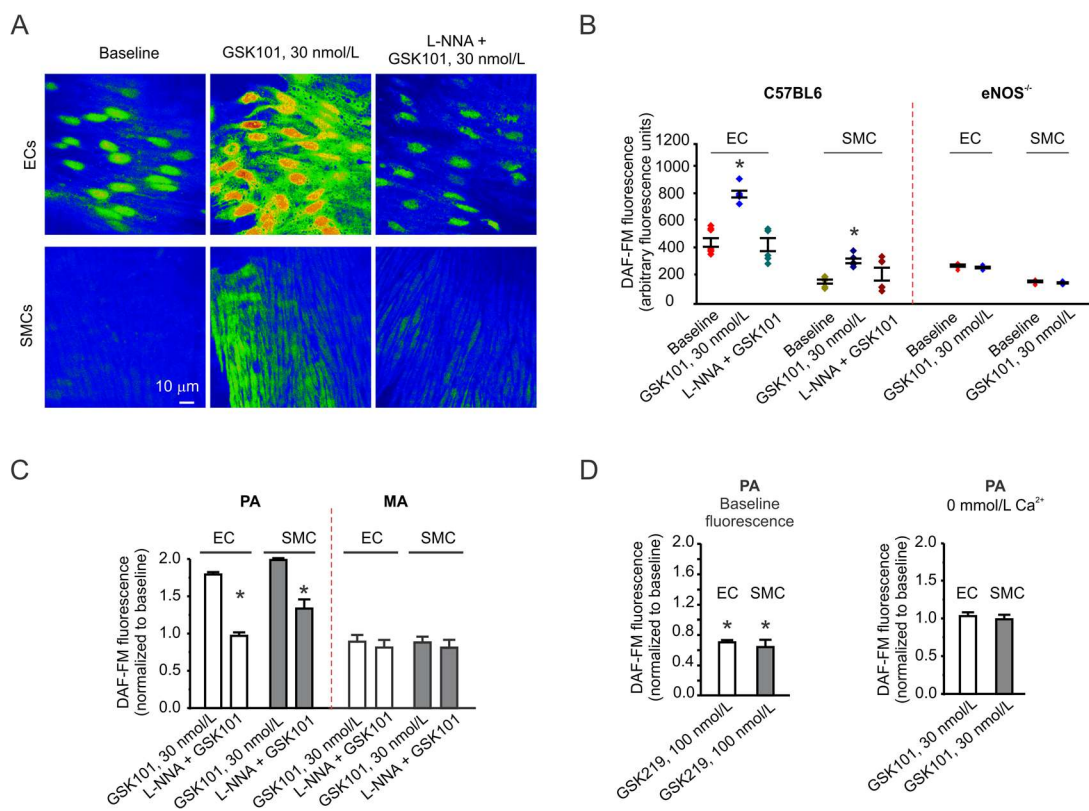


Figure 8. TRPV4-eNOS Ca^{2+} signaling mechanism regulates nitric oxide levels in small PAs. Nitric oxide (NO) levels were recorded in *en face* fourth-order PAs and third-order MAs loaded with DAF-FM (fluorescent NO indicator; 5 $\mu\text{mol/L}$). Images were acquired along the z-axis using a spinning disk confocal microscope. **A.** Representative images for DAF-FM fluorescence in ECs (*top*) and SMCs (*bottom*) of small PAs under basal conditions (*left*), and in the presence of GSK101 (*middle*) alone or with L-NNA (200 $\mu\text{mol/L}$, *right*). **B.** Averaged raw fluorescence in ECs and SMCs from PAs of control (*left*) and eNOS^{-/-} mice (*right*); data are mean \pm SEM; individual data points represent averaged fluorescence of all ECs or SMCs in a field of view (n=6 fields; P<0.0001 using one-way ANOVA and *post hoc* Dunnett test; *P<0.05 versus the baseline). **C.** Averaged DAF-FM fluorescence in ECs and SMCs from PAs and MAs relative to the baseline fluorescence (n=6 fields; *P<0.0001 versus GSK101 for PAs using one-way ANOVA and *post hoc* Tukey test). **D. Left**, the effect of TRPV4 channel inhibition (GSK219) on baseline DAF-FM fluorescence in both ECs and SMCs from small PAs (n=6 fields; *P<0.0001 versus baseline with independent t-test); *right*, the increase in DAF-FM fluorescence induced by GSK101 was abolished in the presence of 0 mmol/L extracellular Ca^{2+} (n=6 fields, P=0.9793 for ECs and 0.8087 for SMCs using independent t-test).

FIGURE 9. Ca^{2+} INFLUX VIA ENDOTHELIAL TRPV4 CHANNELS DOES NOT INCREASE Ca^{2+} RELEASE FROM THE ENDOPLASMIC RETICULUM (ER) IN PAS.

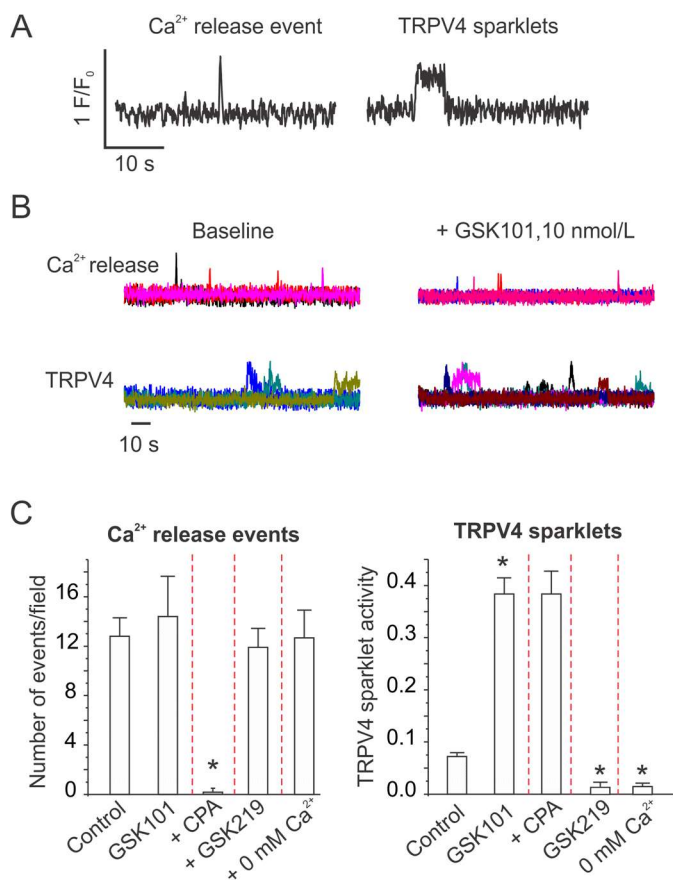


Figure 9. Ca²⁺ influx via endothelial TRPV4 channels does not increase Ca²⁺ release from the endoplasmic reticulum (ER) in PAs. Ca²⁺ events were simultaneously recorded in *en face* fourth-order PAs from GCaMP2^{Cx40} mice. **A.** Representative fractional fluorescence (F/F₀) traces illustrating the differences in kinetics of Ca²⁺ release from the ER (spike shape; less than 300 ms duration, left) and unitary Ca²⁺ influx through TRPV4 channels (Ca²⁺ sparklets; square event; greater than 300 ms duration, right). **B.** Representative F/F₀ traces of Ca²⁺ pulsars (top) and Ca²⁺ sparklets (bottom) under baseline condition and in the presence of GSK101 (10 nM). **C.** Averaged number of Ca²⁺ pulsars per field in the absence (Control) and presence of GSK101 (10 nM), CPA (20 μM), TRPV4 inhibitor GSK219 (100 nM), and 0 mM extracellular Ca²⁺ (left; n=5 fields; *P<0.05 versus control one-way ANOVA). Averaged NP_O per field for TRPV4 sparklets (right; n=5 fields; *P<0.05 versus control one-way ANOVA) in the absence (Control) and presence of GSK101 (10 nM), CPA (20 μM), TRPV4 inhibitor GSK219 (100 nM), and 0 mM extracellular Ca²⁺. Data are mean ± SEM; the TRPV4 sparklet activity is expressed as NP_O where N represents the number of channels and P_O is the open state probability of the channels).

NO-dependent negative feedback loop limits Ca^{2+} influx through TRPV4 channels in PAs.

Studies in expression systems reveal an increase in the activity of TRPV4 channels by S-nitrosylation¹⁵¹ and a decrease by GC-PKG signaling¹⁵², and NO can activate both these mechanisms. We hypothesized that NO released by TRPV4-eNOS signaling serves as an immediate feedback regulator of TRPV4 channel activity in small PAs. To determine the effect of NO on baseline TRPV4 sparklet activity, PAs were treated with L-NNA (100 μ mol/L) in the absence of GSK101. L-NNA produced a 3-fold increase in TRPV4 sparklet activity (Figure 10A), revealing TRPV4 channel inhibition by NO. TRPV4 inhibitor GSK219 completely blocked the L-NNA-induced increase in sparklet activity confirming the specific inhibition of TRPV4 sparklets by NO (Figure 10A). Consistent with the NOS-independent nature of vasodilation in small MAs, L-NNA did not increase baseline sparklet activity in small MAs (Figure 10A, *right*). For a more detailed analysis of the effect of NO on TRPV4 sparklets in PAs, we increased the open state probability of TRPV4 channels by using a small concentration of GSK101 (6 nmol/L). L-NNA also increased sparklet activity in the presence of GSK101 (Figure 10B). To further assess the inhibitory effect of NO on TRPV4 channel function, we examined the effect of NONOate on TRPV4 sparklet activity. At 10 and 30 μ mol/L, NONOate increased DAF-FM fluorescence in ECs and SMCs to levels similar to GSK101 (30 nM; Figure 7B). Moreover, PA dilation caused by 30 nmol/L GSK101 was similar to that caused by 10 and 30 μ mol/L NONOate (Figure 7C). We therefore used both 10 and 30 μ mol/L NONOate for determining the effect of NO on TRPV4 sparklet activity. In the presence of L-NNA, the activity of TRPV4 sparklets was inhibited by approximately 2-fold with 10 μ mol/L NONOate and by 3-fold with 30

$\mu\text{mol/L}$ NONOate (Figure 10B, *right*) confirming that NO limits Ca^{2+} influx through TRPV4 channels in the endothelium from PAs.

We recently demonstrated that Ca^{2+} -dependent cooperative openings of TRPV4 channels amplify Ca^{2+} influx through the channels by 2-3 fold in MAs^{22,23}. The F/F_0 traces for TRPV4 sparklets in PAs in the presence of L-NNA displayed simultaneous openings of multiple channels at a site under control conditions, but a lesser number of channels opened simultaneously in the presence of NONOate (Figure 10B), implying that NO may interfere with cooperative openings of TRPV4 channels at a site. Using a coupled Markov chain model in Matlab, we determined coupling coefficients (κ) as an indicator of coupling strength among TRPV4 channels, as we have done previously²³. The κ values range between 0, which indicates no coupling, and 1, which indicates maximum coupling. Addition of L-NNA increased the coupling strength among TRPV4 channels at a site, and NONOate reduced the coupling strength (Figure 10C). Using an arbitrary cutoff of $\kappa=0.1$, around 50% of the sparklet sites showed coupled openings under control conditions, a number that was increased to 95% in the presence of L-NNA and reduced to 35% by NONOate. These results confirmed that NO disrupted the functional coupling among TRPV4 channels at a site, thereby reducing Ca^{2+} influx in ECs.

FIGURE 10. NITRIC OXIDE DISRUPTS COOPERATIVE OPENINGS OF TRPV4 CHANNELS AND LOWERS CHANNEL ACTIVITY IN SMALL PAS.

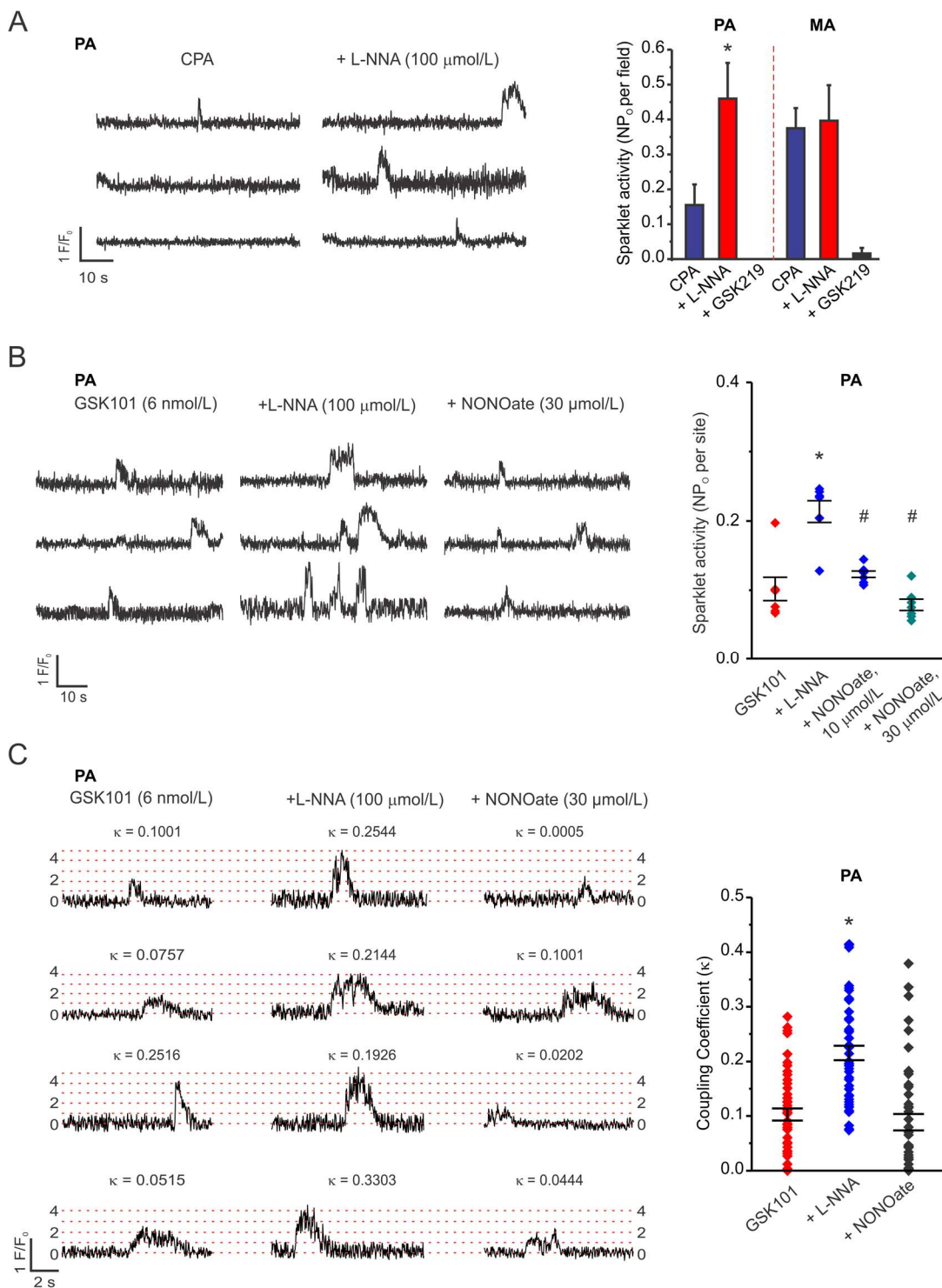


Figure 10. Nitric oxide disrupts cooperative openings of TRPV4 channels and lowers channel activity in small PAs. TRPV4 sparklets were recorded in *en face* fourth-order PAs or third-order MAs loaded with fluo-4AM (10 $\mu\text{mol/L}$). Cyclopiazonic acid (CPA, 20 $\mu\text{mol/L}$) was used in order to eliminate the interference from Ca^{2+} release from intracellular stores. L-NNA (100 $\mu\text{mol/L}$) was used as an inhibitor of NOS and spermine NONOate (NONOate, 10-30 $\mu\text{mol/L}$) was used as a NO donor. **A.** Representative F/F_0 traces of three distinct sparklet sites in a field of view under basal conditions (CPA) and in the presence of L-NNA (*left*) in small PAs. Averaged TRPV4 sparklet activity expressed as NP_O per field, which is a summation of NP_O per site for all the sparklet sites in a field of view. N is the number of channels at a site and P_O is the probability of finding the channel in an open state (n=6 fields; $P < 0.05$ using two-way ANOVA *post hoc* Tukey test; * $P < 0.05$ versus CPA) (*right*). **B.** Representative F/F_0 traces from three distinct sparklet sites in a field of view in the presence of GSK101, after the addition of L-NNA, and NONOate in the presence of L-NNA (*left*). Averaged TRPV4 sparklet activity (NP_O) per site; each data point represents the averaged sparklet activity per site for a field (n=7 fields; $P < 0.0001$ using one-way ANOVA and *post hoc* Tukey test; * $P < 0.05$ versus GSK101; # $P < 0.05$ versus L-NNA) (*right*). **C.** To estimate the coupling strength of TRPV4 channels at a sparklet site, we determined coupling coefficients, or κ values, using coupled Markov Chain model in Matlab. Representative F/F_0 traces with corresponding κ values for four distinct sparklet sites under control conditions (GSK101), in the presence of L-NNA and in the presence of L-NNA and 30 $\mu\text{mol/L}$ NONOate (*left*). Dotted lines represent the quantal levels derived

from all-points histograms. Averaged κ values, data are mean \pm SEM (n=47 sites; P<0.0001 using one-way ANOVA and *post hoc* Tukey test; *P<0.05 versus GSK101) (*right*).

NO limits Ca²⁺-dependent cooperativity of TRPV4 channels via GC-PKG signaling

The commonly used inhibitors of S-nitrosylation (N-acetyl cysteine, dithiothreitol, and ultraviolet light¹⁶⁸) did not affect the NO-inhibition of TRPV4 channels (Figure 11A), suggesting that S-nitrosylation does not play a major role in the NO-inhibition of TRPV4 channels in small PAs. GC-PKG signaling has been shown to inhibit TRPV4 channels in expression systems¹⁵². We therefore tested the hypothesis that NO activates endothelial GC-PKG signaling to limit Ca²⁺ influx through TRPV4 channels. Both ECs and SMCs from PAs showed a strong expression of PKG (Figure 11B). Similar to L-NNA, GC inhibitor ODQ (3 $\mu\text{mol/L}$)¹⁶⁹ and PKG inhibitor Rp-8-Br-PET-CGMPS (PET; 30 $\mu\text{mol/L}$)¹⁷⁰ increased the baseline sparklet activity by ~ 2 -fold (Figure 11C), confirming that GC-PKG signaling constitutively inhibits TRPV4 channels in PA endothelium. In the presence of GC or PKG inhibitor, L-NNA was unable to further increase the activity of TRPV4 sparklets (Figure 11C, *left*). Moreover, NONOate did not attenuate TRPV4 sparklet activity in the presence of GC or PKG inhibitor (Figure 11C, *right*). GC or PKG inhibitor also enhanced the coupling strength among TRPV4 channels (Figure 11D) by ~ 2 -fold. In the presence of GC or PKG inhibitors, neither L-NNA nor NONOate (10 and 30 $\mu\text{mol/L}$) was able to alter the coupling strength among TRPV4 channels at a site (Figure 11D). These results supported the novel concept that in small PAs, NO limits TRPV4 channel activity through GC-PKG signaling in the native endothelium.

Ca²⁺-dependent cooperativity of TRPV4 channels is a key endogenous regulatory mechanism for TRPV4 channel activity^{22,23,153,154}. Using EGTA to chelate local Ca²⁺, we previously demonstrated that coupled openings of channels in a cluster were dependent on

local increases in Ca^{2+} ²³. To determine whether NO-GC-PKG signaling disrupts the functional coupling between the channels by interfering with Ca^{2+} -dependent cooperativity, we studied the effect of NONOate on sparklet activity in the presence of EGTA-AM, a cell permeable form of EGTA. EGTA lowered the sparklet activity and coupling strength among TRPV4 channels in PAs in the presence of L-NNA (Figures 12A, 12B). Moreover, NONOate was unable to further reduce the activity of sparklets and coupling strength among TRPV4 channels in the presence of EGTA (Figures 12A, 12B). Whereas 43% of the total sparklet sites showed cooperative openings ($\kappa > 0.1$) in the presence of EGTA alone, 41% of the sparklet sites showed cooperative openings after the addition of NONOate in the presence of EGTA, suggesting that NO did not further reduce the cooperativity of TRPV4 sparklets in the presence of EGTA. GSK219, however, was able to cause a further decrease in sparklet activity in the presence of EGTA (n=4 PAs). These results suggest that NO interferes with Ca^{2+} -dependent activation of TRPV4 channels, thereby limiting cooperative channel openings.

Based on the NO-GC-PKG negative feedback mechanism for regulating TRPV4 channel activity, we postulated that removing this inhibition would augment TRPV4-vasodilation in PAs. In the presence of GC inhibitor ODQ, the dilation to GSK101 was markedly increased at each concentration (3-30 nmol/L) when compared to vasodilation in the absence of ODQ (Figures 12C, 12D), further supporting the role of NO-GC-PKG negative feedback mechanism as a “limiter” of Ca^{2+} influx through TRPV4 channels and TRPV4-vasodilation in PAs.

FIGURE 11. ENDOTHELIAL NO-GUANYLYL CYCLASE (GC)-PROTEIN KINASE G (PKG) SIGNALING DISRUPTS COOPERATIVE OPENINGS OF TRPV4 CHANNELS IN SMALL PAS.

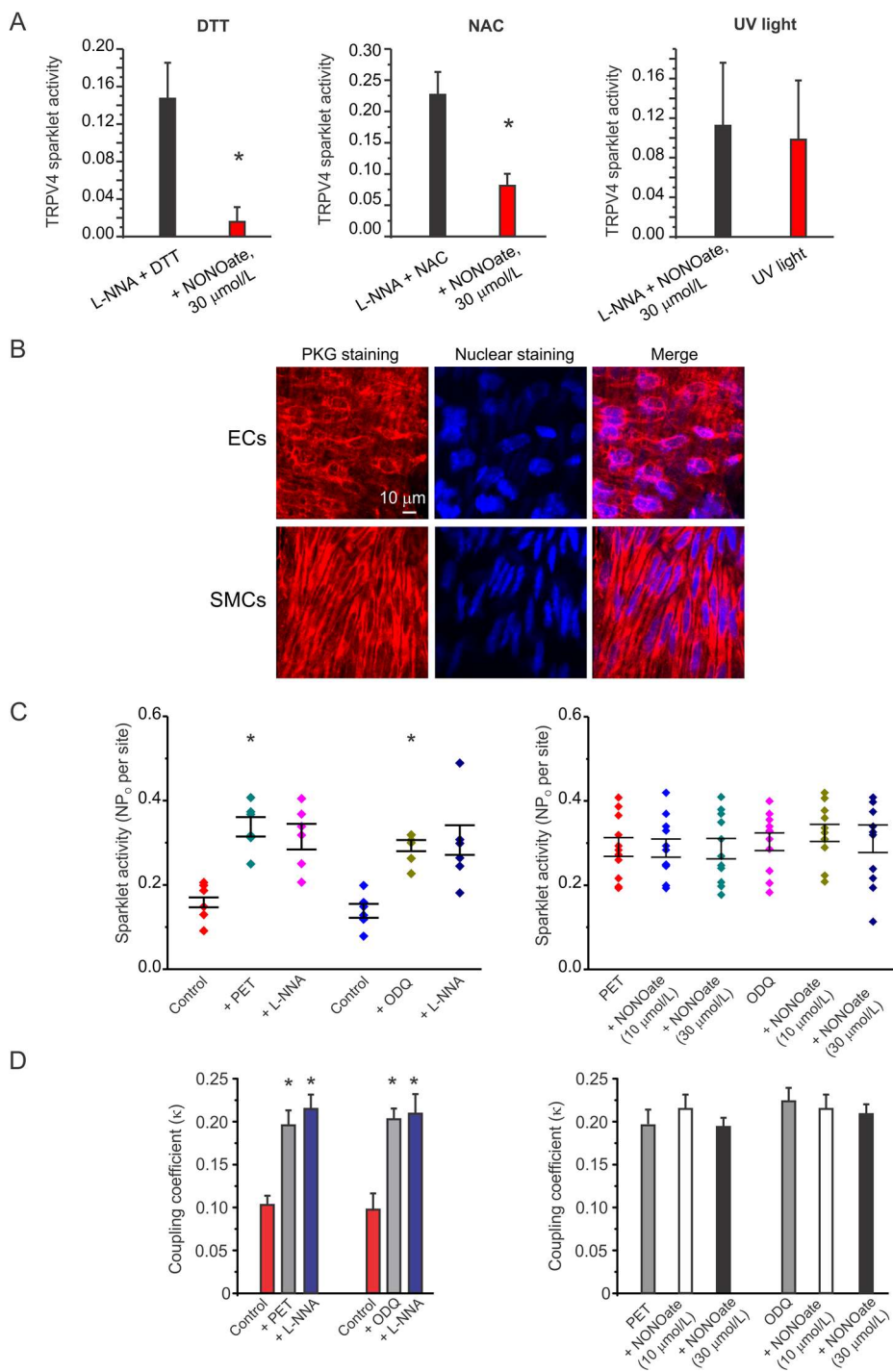


Figure 11. Endothelial NO-guanylyl cyclase (GC)-protein kinase G (PKG) signaling disrupts cooperative openings of TRPV4 channels in small PAs. NONOate (30 $\mu\text{mol/L}$)-induced suppression of TRPV4 sparklet activity was assessed after pharmacological inhibition of S-nitrosylation with dithiothreitol (DTT, 1 mmol/L) or N-acetyl cysteine (NAC, 5 mmol/L). In addition, ultraviolet (UV) light was applied to physically disrupt serine (S)-NO covalent bonds formed by NO on EC TRPV4 channels. PKG expression and Ca^{2+} signals were recorded in *en face* fourth-order PAs. TRPV4 sparklets were recorded in small PAs loaded with fluo-4AM (10 $\mu\text{mol/L}$). The experiments were performed in the presence of CPA (20 $\mu\text{mol/L}$) to eliminate the interference from Ca^{2+} release from intracellular stores. L-NNA (100 $\mu\text{mol/L}$) was used as an inhibitor of NOS and spermine NONOate (NONOate, 10-30 $\mu\text{mol/L}$) was used as a NO donor. To estimate the coupling strength among TRPV4 channels at a sparklet site, we determined coupling coefficients, or κ values, using a coupled Markov Chain model in Matlab. Cyclopiazonic acid (CPA, 20 $\mu\text{mol/L}$) was used throughout the experiments to eliminate intracellular Ca^{2+} signaling and exclusively assess Ca^{2+} influx through TRPV4 channels.

A. Averaged TRPV4 sparklet activity (NP_0 per site) and the effect of NONOate (30 $\mu\text{mol/L}$) in the presence of DTT (*left*; $n=3$ fields; $*P=0.0083$ using paired t-test), NAC (*middle*; $n=3$ fields; $*P=0.0190$ using paired t-test), and after UV exposure (*right*; $n=3$ fields; $P=0.8576$ using paired t-test). Data are mean \pm SEM. **B.** Representative images for PKG immunostaining (*left*), nuclear staining with DAPI (*middle*) and a merged image (*right*) in the ECs (*top*) and SMCs (*bottom*) from a small PA. The experiments were repeated in four small PAs. **C.** Averaged data indicating the effect of the PKG inhibitor

(Rp-8-Br-PET-cGMPS, PET, 30 $\mu\text{mol/L}$) and the GC inhibitor (ODQ, 3 $\mu\text{mol/L}$) on TRPV4 sparklet activity, and on L-NNA (100 $\mu\text{mol/L}$) activation of TRPV4 sparklets (n=6 fields; $P<0.001$ using one-way ANOVA and *post hoc* Dunnett test; * $P<0.05$ versus control) (*left*). Averaged TRPV4 sparklet activity indicating the effect of NONOate in the presence of PKG (PET) and GC (ODQ) inhibitors (n=10 fields; $P=0.4708$ versus PET or ODQ using one-way ANOVA and *post hoc* Dunnett test) (*right*). PET or ODQ were added in the presence of L-NNA (*right* panel), and did not cause a further increase in sparklet activity in the presence of L-NNA. **D.** Averaged κ values under control conditions (GSK101, 6 nmol/L) and with PET or ODQ before or after the addition of L-NNA (100 $\mu\text{mol/L}$). Data are mean \pm SEM (n=47 sites; $P<0.0001$ using one-way ANOVA and *post hoc* Dunnett test; * $P<0.05$ versus control) (*left*). Averaged κ values in the presence of PET or ODQ before or after the addition of NONOate. Data are mean \pm SEM (n=47 sites; $P=0.2315$ versus PET or ODQ using one-way ANOVA and *post hoc* Dunnett test) (*right*).

FIGURE 12. NO-GC-PKG SIGNALING IMPAIRS Ca^{2+} -DEPENDENT COOPERATIVE OPENINGS OF TRPV4 CHANNELS IN SMALL PAS.

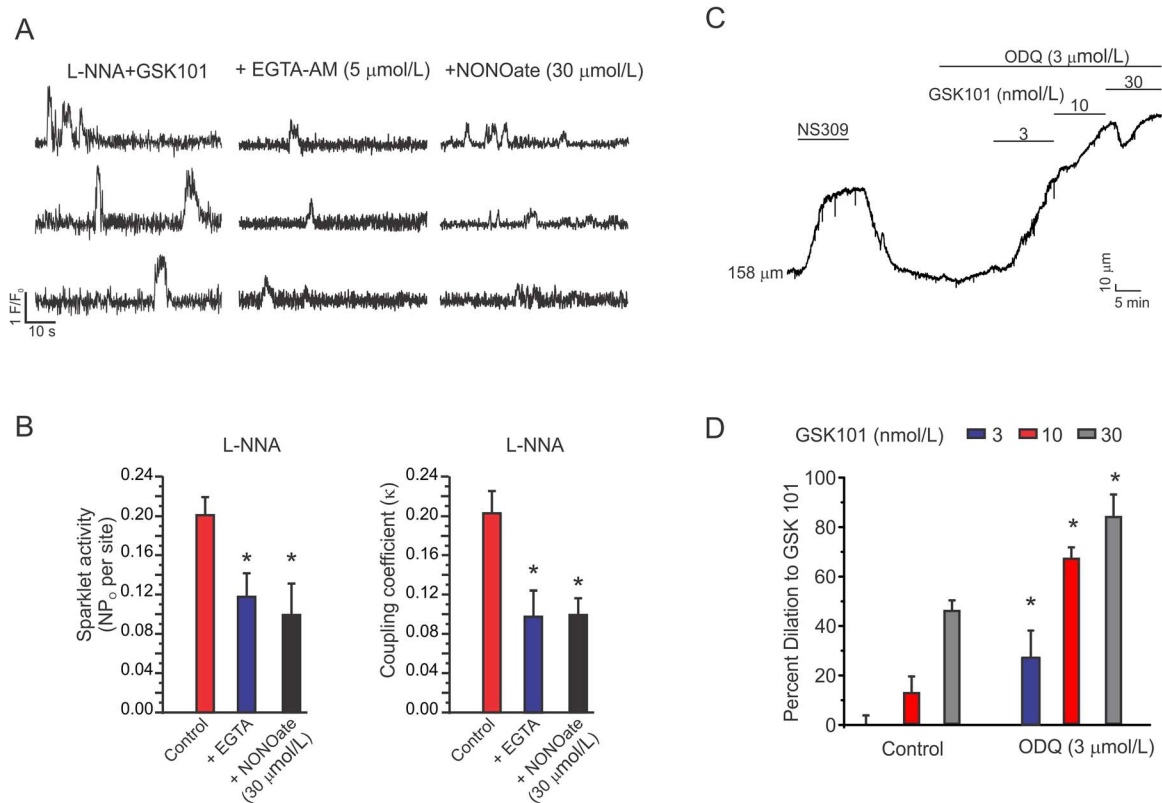


Figure 12. NO-GC-PKG signaling impairs Ca²⁺-dependent cooperative openings of TRPV4 channels in small PAs. TRPV4 sparklets were recorded in PAs loaded with fluo-4AM (10 μmol/L). The experiments were performed in the presence of CPA (20 μmol/L) to eliminate the interference from Ca²⁺ release from intracellular stores. L-NNA (100 μmol/L) was used as an inhibitor of NOS and spermine NONOate (NONOate, 10-30 μmol/L) was used as a NO donor. Coupling coefficients, or κ values, for coupling among TRPV4 channels were determined using a coupled Markov Chain model in Matlab. Changes in internal diameter were recorded in cannulated fourth-order PAs pressurized to 15 mmHg. **A.** Experiments were performed in the presence of GSK101 (6 nmol/L) and L-NNA (100 μmol/L). Representative F/F₀ traces indicate the effect of membrane permeable Ca²⁺ chelator EGTA-AM and NONOate in the presence of EGTA-AM on TRPV4 sparklet activity. **B.** Averaged TRPV4 sparklet activity per site indicating a decrease in sparklet activity with EGTA-AM and lack of effect of NONOate on TRPV4 sparklet activity in the presence of EGTA-AM (n=24 sites; P<0.0001 using one-way ANOVA and *post hoc* Dunnett test; *P<0.05 versus GSK101 control) (*left*). Averaged κ values, data are mean ± SEM (n= 24 sites; P<0.0001 using one-way ANOVA; *P<0.05 versus GSK101 control) (*right*). **C.** A representative diameter trace for GSK101-induced vasodilations in small PAs pretreated with GC inhibitor ODQ (3 μmol/L). **D.** Averaged percent dilation to GSK101 (3-30 nmol/L) in PAs treated with ODQ (3 μmol/L) compared to control PAs. Data are mean ± SEM (n=8 and 4 arteries for control and ODQ, respectively; P<0.0001 using one-way ANOVA and *post hoc* Tukey test; *P< 0.05 versus control).

ATP is an endogenous activator of TRPV4 sparklets in endothelium from small PAs.

In small mesenteric and cremaster arteries, physiological muscarinic receptor agonist acetylcholine caused vasodilation predominantly through activation of endothelial TRPV4 sparklets^{1,22,23}. In small PAs, however, neither muscarinic receptor agonist (carbachol or CCh) nor bradykinin receptor agonist (bradykinin) was able to activate TRPV4 sparklets (Figure 13). CCh dilated large PAs (> 400 μm), but was unable to evoke dilation in small PAs (Figure 14A), underscoring functional differences in the endothelium from large and small PAs. We, therefore, postulated that TRPV4 channels in ECs from small PAs couple to novel physiological activators. Previous studies in large PAs revealed that endogenous purinergic receptor activator ATP increases endothelial Ca^{2+} and causes endothelium-dependent vasorelaxation^{155-157,171,172}. We, therefore, hypothesized that ATP dilates small PAs via activation of TRPV4 sparklets. ATP (10 $\mu\text{mol/L}$) induced a 8-fold increase in TRPV4 sparklet activity in PAs, an effect that was inhibited by a general P2 purinergic receptor inhibitor suramin and TRPV4 inhibitor GSK219, and was absent in PAs from TRPV4^{-/-} mice (Figure 14B), suggesting P2 purinergic receptor-dependent activation of TRPV4 channels by ATP. In cannulated, pressurized small PAs, ATP (1-10 $\mu\text{mol/L}$) induced a concentration dependent dilation, which was inhibited by GSK219 and L-NNA, and was absent in endothelium-denuded PAs and PAs from TRPV4^{-/-} mice (Figures 14C). It is possible that catabolism of ATP to adenosine diphosphate (ADP) and/or adenosine may activate TRPV4 channels through P2Y1¹⁷³ and adenosine receptors, respectively. ADP itself did not induce dilation in PAs (Figure 14D). Adenosine dilated PAs, but this effect was not inhibited by TRPV4 inhibitor, thus ruling out a role for

adenosine in ATP-induced vasodilation of PAs (Figure 14E). Taken together, these results reveal that ATP is a novel endogenous activator of local TRPV4-eNOS signaling in small PAs.

FIGURE 13. CLASSICAL ACTIVATORS OF ENDOTHELIAL G_q PROTEIN-COUPLED RECEPTORS, CARBACHOL (CCh) AND BRADYKININ, DO NOT INCREASE EC TRPV4 CA²⁺ SPARKLET ACTIVITY IN SMALL PAS.

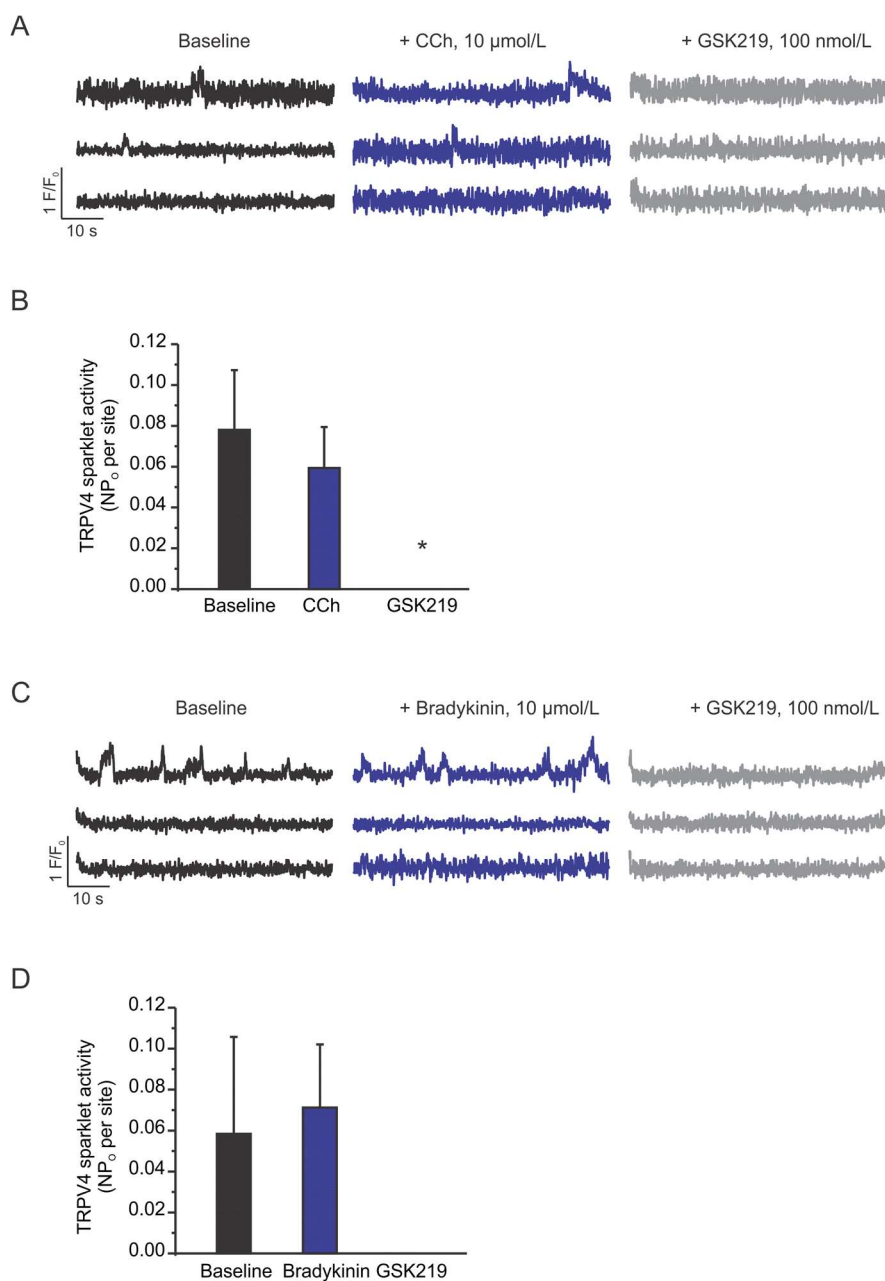


Figure 13. Classical activators of endothelial G_q protein-coupled receptors, carbachol (CCh) and bradykinin, do not increase EC TRPV4 Ca²⁺ sparklet activity in small PAs. EC TRPV4 sparklet activity was examined in *en face* fourth-order PAs loaded with fluo-4AM (10 μmol/L) in the absence or presence of muscarinic (CCh) and bradykinin receptor (bradykinin) activators. Cyclopiazonic acid (CPA, 20 μmol/L) was used throughout the Ca²⁺ imaging experiments in order to eliminate the interference from Ca²⁺ release from internal stores. **A.** Representative fractional fluorescence (F/F₀) traces of TRPV4 sparklets under baseline conditions (CPA, *left*), in the presence of the muscarinic receptor agonist (CCh, 10 μM, *middle*) and with the addition of TRPV4 inhibitor GSK219 (100 nmol/L, *right*). **B.** Averaged TRPV4 sparklet activity (NP₀ per site); data are mean ± SEM (n=4 fields; P=0.0105 using one-way ANOVA; *P<0.05 versus baseline). **C.** Three representative F/F₀ traces of TRPV4 sparklets under baseline conditions (CPA, *left*) or in the presence of bradykinin (10 μmol/L; *middle*), and with the addition of GSK219 (100 nmol/L; *right*). **D.** Averaged TRPV4 sparklet activity (NP₀ per site). Data are mean ± SEM (n=5, 8, 5 fields from left to right; P=0.1517 using one-way ANOVA).

FIGURE 14. ATP IS AN ENDOGENOUS ACTIVATOR OF LOCAL TRPV4-eNOS SIGNALING IN SMALL PAS.

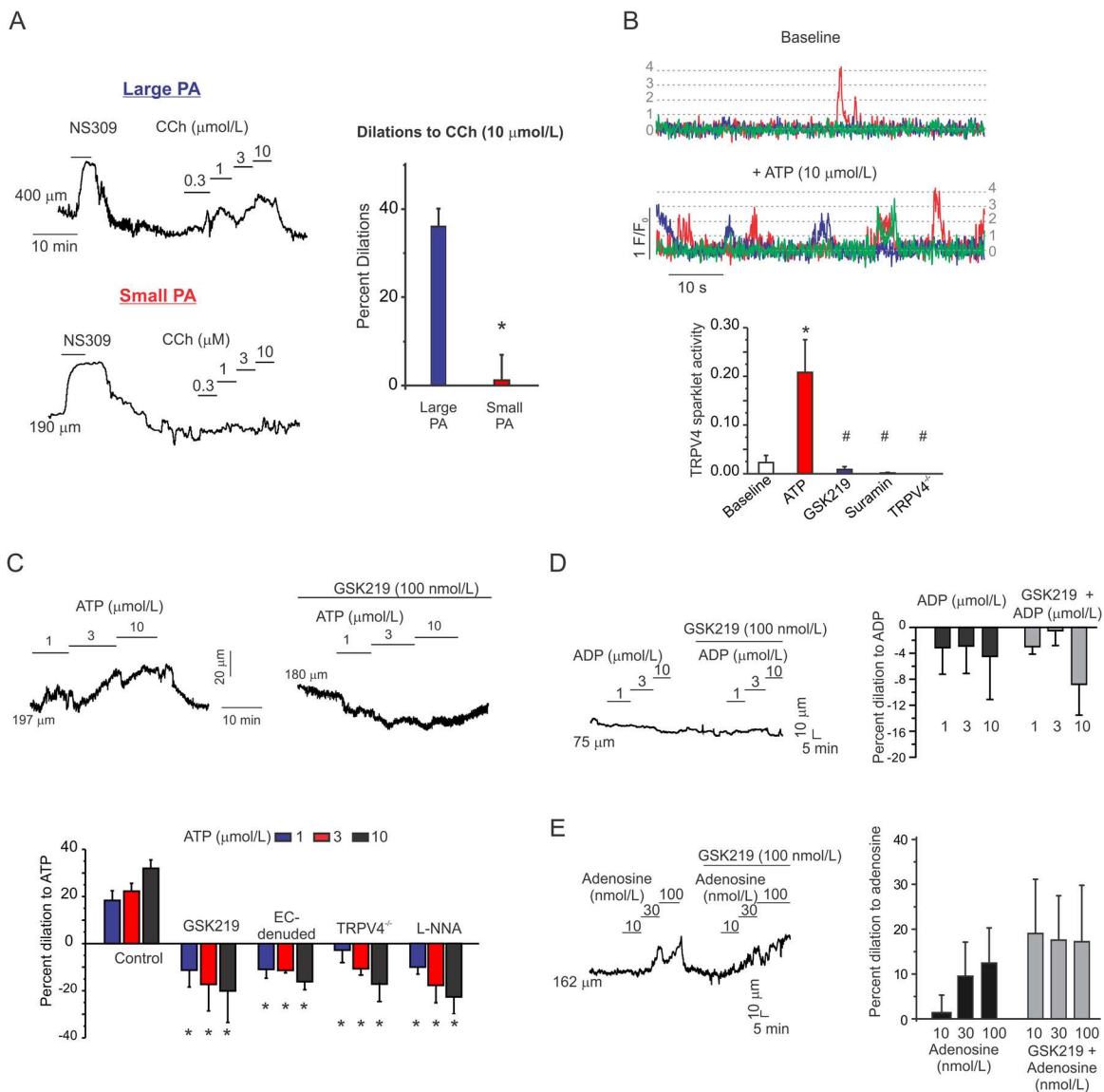


Figure 14. ATP is an endogenous activator of local TRPV4-eNOS signaling in small PAs. Changes in internal diameter were recorded in cannulated large PAs and small fourth-order PAs pressurized to 15 mmHg. TRPV4 sparklets were recorded in *en face* fourth-order PAs loaded with fluo-4AM (10 $\mu\text{mol/L}$). CPA (20 $\mu\text{mol/L}$) was used in order to eliminate the interference from Ca^{2+} release from intracellular stores. **A.** Representative diameter traces for acetylcholine analog carbachol (CCh)-induced vasodilation in large second-order PAs ($\sim 400 \mu\text{m}$, *top left*) and small fourth-order PAs (100-200 μm , *bottom left*). Averaged diameter responses to CCh; data are mean \pm SEM; (n= 5 large PAs, 9 small PAs; *P< 0.01 using independent t-test) (*right*). **B.** Representative F/F₀ traces of TRPV4 sparklets under baseline conditions (CPA) and with the addition of ATP (10 $\mu\text{mol/L}$) (*left*). Averaged TRPV4 sparklet activity (NP₀) per field of view under basal condition (CPA), in the presence of ATP, ATP in the presence of TRPV4 inhibitor GSK219 (100 nmol/L), P2 purinergic receptor inhibitor suramin (500 $\mu\text{mol/L}$), or in the PAs from TRPV4^{-/-} mice (n=10 fields; P<0.0004 using one-way ANOVA and *post hoc* Tukey test; *P<0.05 versus baseline; #P<0.05 versus ATP) (*right*). **C.** Representative diameter traces for ATP-induced dilation in fourth-order PAs before (*top left*) and after (*top right*) addition of TRPV4 inhibitor GSK219 (100 nmol/L). (*Bottom*) Averaged percent dilation to ATP (1-10 $\mu\text{mol/L}$, n=7 arteries) in control PAs, in the presence of GSK219 (n=5 arteries), in EC-denuded PAs (n=5 arteries), in the presence of L-NNA (100 $\mu\text{mol/L}$, n=6 arteries), and in the PAs from TRPV4^{-/-} mice (n=5 arteries); data are mean \pm SEM; (P<0.0001 using two-way ANOVA and *post hoc* Tukey test; *P< 0.05 versus control). **D.** Representative diameter trace (*left*) and averaged data (*right*) for the effect of adenosine diphosphate (ADP) on PA diameter

in the absence or presence of TRPV4 inhibitor GSK219 (100 nmol/L; grey; n=5 PAs; P=0.8284 using one-way ANOVA and *post hoc* Tukey test). **E.** Representative diameter trace (*left*) and averaged diameter data (*right*) for adenosine-induced dilations in the absence or presence of GSK219 (100 nmol/L; grey; n=4 arteries; P=0.8337 using two-way ANOVA and *post hoc* Tukey test).

FIGURE 15. LOCAL TRPV4 CHANNEL-DEPENDENT Ca^{2+} SIGNALING REGULATES ENDOTHELIUM-DEPENDENT VASODILATION IN RESISTANCE-SIZED PAS.

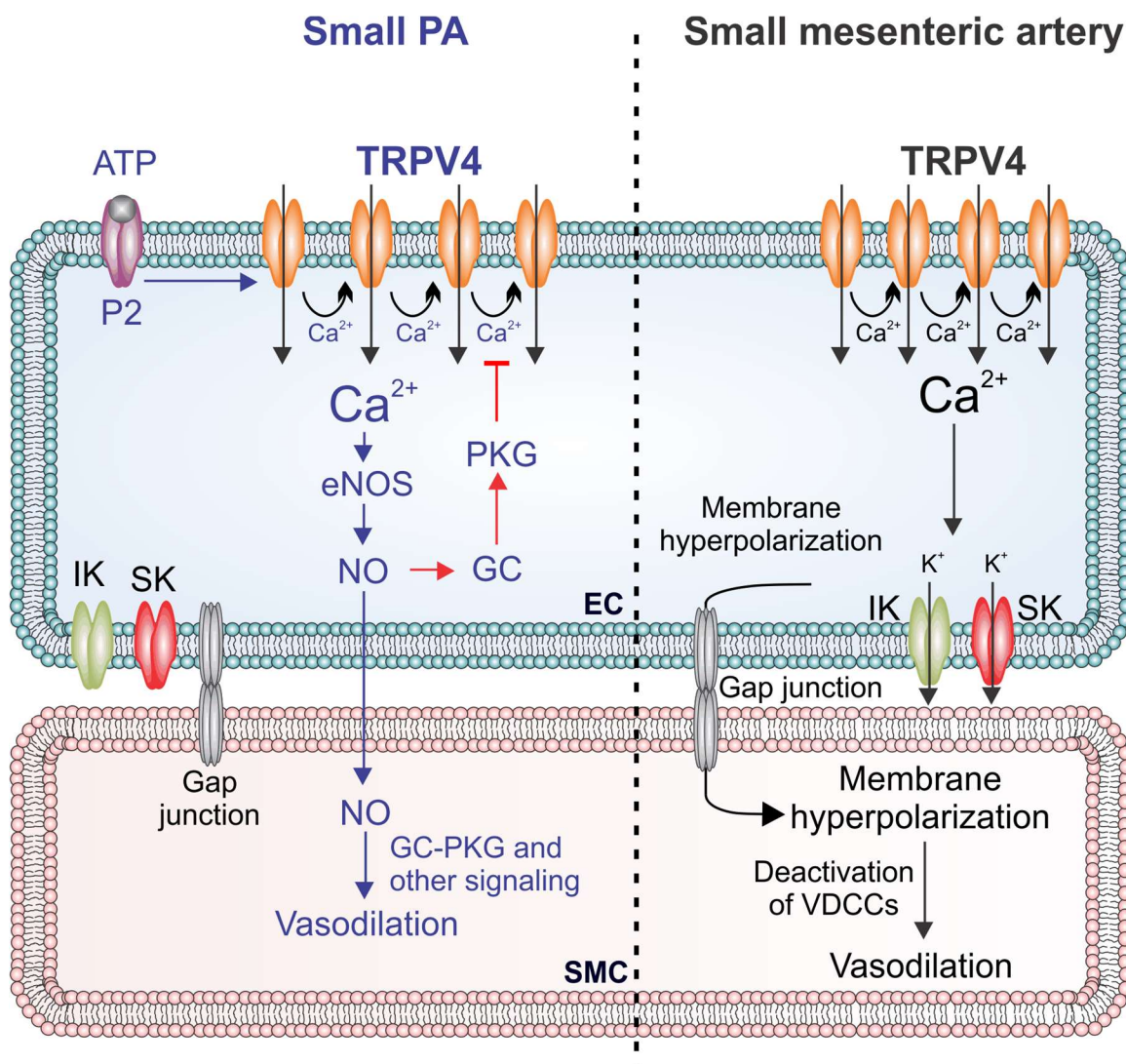


Figure 15. Local TRPV4 channel-dependent Ca^{2+} signaling regulates endothelium-dependent vasodilation in resistance-sized PAs. The cartoon depicts TRPV4 channel-dependent endothelial Ca^{2+} signaling mechanisms in small PAs and small mesenteric arteries^{22,132,141}. In small PAs, TRPV4 sparklets promote eNOS activity and NO release. P2 purinergic receptor agonist ATP is an endogenous activator of the TRPV4-eNOS signaling in PAs. Endothelium-derived NO then causes vasodilation through the activation of SMC guanylyl cyclase (GC)-protein kinase G (PKG) signaling and a GC-PKG-independent mechanism. Blue arrows indicate this pathway. NO also induces activation of endothelial GC-PKG signaling, which lowers Ca^{2+} -dependent cooperative opening of TRPV4 channels and limits TRPV4-mediated vasodilations. This pathway is indicated by red arrows. In small mesenteric arteries, TRPV4 Ca^{2+} sparklets selectively activate endothelial IK and SK channels, which hyperpolarize EC and SMC membranes. SMC membrane hyperpolarization deactivates voltage-dependent Ca^{2+} channels (VDCCs), which results in vasodilation, as described earlier²².

3.4 Discussion

Despite the functional differences between systemic and pulmonary circulations, the identity of local Ca^{2+} signals that regulate vascular function in small PAs remains entirely unknown. Our discoveries of spatially distinct TRPV4 sparklets in small PAs and local TRPV4-eNOS signaling network not only support a novel paradigm that eNOS can be activated by spatially restricted Ca^{2+} signals, but also identifies TRPV4 channels as a key regulator of basal and induced eNOS activity in pulmonary microcirculation. Moreover, inhibition of TRPV4 channel cooperativity by NO through GC-PKG signaling represents a novel endogenous mechanism for the regulation of TRPV4 channel function. Although endothelial TRPV4 channels have been studied for several years, their physiological roles remain unclear. Our findings of ATP as a novel endogenous activator of TRPV4 channels may prove crucial for deciphering the physiological roles of TRPV4 channels. Because small PAs regulate vascular resistance, TRPV4 channel-induced vasodilation of small PAs may be important for the regulation of PVR under normal and disease conditions. Pulmonary vascular disorders, including PAH are associated with reduced NO bioavailability and loss of endothelial function¹⁷⁴⁻¹⁷⁶. It is plausible that an impairment in the TRPV4-eNOS signaling results in endothelial dysfunction in these disorders. Inhaled NO represents a major advancement in acute treatment of PAH, but sustained improvements in the clinical outcomes have not been achieved in adult patients¹⁷⁷. Inhibition of endothelial TRPV4 channels by inhaled NO may contribute to the negative outcome in PAH. Inhibition of TRPV4 channel activity by NO-GC-PKG

signaling will also have implications in the diseases characterized by excessive activation of TRPV4 channels, such as pulmonary edema and lung injury¹⁷⁸⁻¹⁸⁰.

Previous studies of endothelial Ca²⁺ signals have demonstrated that localized Ca²⁺ signals predominantly activate IK and SK channels to cause vasodilation in small systemic arteries including mesenteric, cremaster and cerebral arteries^{22,132,138,139,181}. In small PAs, TRPV4 sparklets preferentially activated eNOS to cause vasodilation. Activation of eNOS by TRPV4 channels was absent in PAs from eNOS^{-/-} mice (Figure 8B), was inhibited by TRPV4 channel inhibitor (Figure 8D, *left*), and required influx of extracellular Ca²⁺ (Figure 8, *right*). TRPV4 sparklets did not activate Ca²⁺ release from intracellular stores (Figure 9C). Additionally, all the Ca²⁺ influx signals in response to TRPV4 channel agonist were inhibited by TRPV4 channel inhibitor and were absent in PAs from TRPV4^{-/-} mice (Figure 2A). These results, in combination with the local nature of TRPV4 sparklets, support a direct activation of eNOS by TRPV4 sparklets.

Selective coupling of TRPV4 sparklets with eNOS for vasodilation in small PAs supports differential Ca²⁺ signaling networks in small PAs and mesenteric/cremaster/cerebral arteries. Our data suggest that the presence of U46619 alone (Figure 6C, 6D) does not alter the IK/SK channel-dependent nature of TRPV4-vasodilation in MAs. The differences in signaling pathways may arise from drastic physiological differences in intravascular pressures in pulmonary and systemic circulations. The pressures used in this study mimicked the physiological intravascular pressures of the two vascular beds. Localization of Ca²⁺ signals and IK/SK channels at myoendothelial projections (MEPs) has been proposed as a mechanism for preferential activation of IK/SK

channels by TRPV4 sparklets in small MAs and cremaster arterioles^{132,138}. The non-MEP localization of sparklets in small PAs is consistent with IK/SK channel-independent nature of TRPV4-vasodilation in small PAs, however, the molecular mechanism underlying preferential TRPV4-eNOS coupling in PAs is not clear. In MAs, the MEP-localization of TRPV4 sparklet activity is attributed to A-kinase anchoring protein 150 (AKAP150)-mediated cooperative opening of TRPV4 channels at the MEPs²³. Surprisingly, AKAP150 staining was not observed at the MEPs in PAs (Figure 2E), and only a small fraction of TRPV4 sparklets occurred at the MEPs (Figure 2D). Caveolin, a major structural protein of caveolae, directly interacts with and inhibits eNOS activity¹⁸². Endothelial hemoglobin- α (Hb α) and cytochrome b5 reductase 3 (CytB5R3) have also been shown to regulate the effects of NO on vascular reactivity¹⁸³. It is, therefore, conceivable that differential expression of caveolin, Hb α and CytB5R3, along with the absence of AKAP150, is responsible for selective activation of eNOS over IK/SK channels in small PAs. Additionally, differences in the aforementioned mechanisms could be responsible for species-, vessel size-, and vascular bed-specific coupling of TRPV4 sparklets with their signaling targets.

Although TRPV4 channels have been proposed as a key Ca²⁺ influx pathway in vascular endothelium, their endogenous activators remain elusive. The discovery of ATP as an endogenous activator of TRPV4-eNOS signaling may be a crucial step towards deciphering the physiological and pathological roles of TRPV4 channels in the pulmonary circulation. Purinergic signaling is an essential component to the pulmonary vasculature^{30,184-187}, and ATP activation of TRPV4 channels represents a mechanism that

may link physiological stimuli to the regulation of pulmonary vascular function. ATP can be released from sympathetic nerves during synaptic transmission, or can be released into the circulation by ECs, SMCs, or erythrocytes^{158,159,188,189}. Shear stress, which is a well-known activator of endothelial TRPV4 channels¹⁹⁰⁻¹⁹², also induces the release ATP¹⁸⁹, suggesting a possible involvement of P2 purinergic receptor-TRPV4 signaling in flow-induced vasodilation. Endothelial Gq-protein coupled receptor agonists CCh and bradykinin activated TRPV4 channels through a phospholipase C-diacylglycerol-protein kinase C (PKC) mechanism in MAs²³. ATP may also activate endothelial TRPV4 channels through Gq-coupled P2 purinergic receptors, a possibility that will be explored in future studies.

While TRPV4 channels play a physiologically important role at a low level of activation, excessive TRPV4 channel activity can cause Ca²⁺ overload and EC death²². In this context, a dual role for NO—as a mediator of TRPV4-vasodilation and as a limiter of TRPV4 channel activity—provides a more precise control over channel activation and vasodilation. Prior studies in the expression systems reveal two possibilities for the modulation of TRPV4 channel function by NO: an increase in channel activity by S-nitrosylation¹⁵¹, and a decrease in channel activity by GC-PKG signaling¹⁵². Although S-nitrosylation and activation of TRPV4 channels by NO cannot be ruled out, our results suggest that NO-induced TRPV4 channel inhibition via GC-PKG pathway predominates in intact PAs. Unlike PKG, protein kinase A (PKA) and PKC activation potentiates TRPV4 channel function via channel phosphorylation³⁹. These findings point to an interesting possibility that PKG phosphorylates the channel at a site that is different from PKC or PKA

phosphorylation, and results in channel inhibition. Previous studies by Yin et al.¹⁵⁰ using Fura-2 indicated that NO-cGMP signaling lowers TRPV4-induced increases in global Ca^{2+} levels in lung venular capillary endothelium. Whether this effect of NO is due to a direct effect on single channel function of TRPV4 channels remains unknown. Moreover, a functional effect of NO on TRPV4 channel-induced vasodilation of small PAs is not known. The effect of NO-GC-PKG signaling on Ca^{2+} -dependent cooperative openings of TRPV4 channels represents a novel mechanism to control the diameter of small PAs in response to TRPV4 channel activation. How PKG phosphorylation of TRPV4 channel inhibits the coupling among TRPV4 channels is not known but one possible mechanism could be inhibition of Ca^{2+} -potentiation of the channel, thereby limiting the effect of Ca^{2+} on channel cooperativity. In support of this claim, our results demonstrate that in the presence of Ca^{2+} chelator EGTA, which limits TRPV4 channel cooperativity²³, NO had no effect on channel activity (Figure 12).

Our results also point to distinct functional roles of GC-cGMP-PKG signaling pathways from ECs and SMCs (Figure 15). Activation of the canonical GC-PKG pathway in SMCs leads to vasodilation¹⁹³. Indeed, SMC GC has been targeted to dilate PAs and reduce pulmonary vascular resistance in PAH¹⁹⁴. Interestingly, the finding that endothelial GC-PKG pathway has an inhibitory effect on vasodilation suggests that EC and SMC pathways work in opposite directions, and excessive activation of endothelial GC-PKG signaling could lead to increased vasoconstriction and vascular resistance under pathological conditions. Moreover, the finding that GC inhibitor did not inhibit the vasodilation caused by EC-derived NO (Figures 12C, 12D) suggests that in small PAs there

is a vasodilatory component that is activated by NO and that acts independently of the SMC GC-PKG signaling.

In conclusion, our results represent the first direct evidence that localized Ca^{2+} signals regulate NO release in small PAs. Reduced NO bioavailability is a major contributor to endothelial dysfunction in many pulmonary vascular disorders including PAH. The perturbations of TRPV4-eNOS pathway may provide a mechanistic explanation for reduced NO levels and endothelial dysfunction in these disorders. Our results also reveal a potent inhibitory role of NO on TRPV4 channel function, defining it as a novel physiological regulator (limiter) of TRPV4 channels (Figure 15). TRPV4 channels are Ca^{2+} -selective cation channels with a large single channel conductance; the amount of Ca^{2+} entering through one TRPV4 channels is ~ 100 times higher than an L-type Ca^{2+} channel¹⁴⁹. A slight overactivation of TRPV4 channels could lead to Ca^{2+} overload. It is, therefore, critical to tightly control the activity of these channels without inhibiting their physiological effect. The TRPV4-eNOS signaling achieves this feat by mediating the functional effect of TRPV4 channels, and by limiting the channel function through endothelial GC-PKG signaling. While some pulmonary vascular disorders show reduced NO levels^{70,101,175,176}, others show excessive TRPV4 channel activity^{178-180,195,196}. Thus, we propose that abnormalities in NO-PKG-TRPV4 feedback mechanism may be involved in both the types of pulmonary dysfunctions.

**CHAPTER 4. IMPAIRED ENDOTHELIAL CAVEOLIN-1-TRPV4 CHANNEL
SIGNALING CONTRIBUTES TO ENDOTHELIAL DYSFUNCTION IN
PULMONARY HYPERTENSION**

4.1 Abstract

Endothelial dysfunction is a hallmark of pulmonary hypertension (PH) contributing to impaired endothelium-dependent vasodilation and increased pulmonary arterial pressure (PAP). However, the mechanisms regulating endothelial dysfunction in the pathogenesis of PH remains poorly understood. Recently, endothelial TRPV4 (TRPV4_{EC}) channels have been identified as key regulators of endothelium-dependent vasodilation in resistance PAs. The purpose of this study was to determine the physiological role of TRPV4_{EC} channel activity in the maintenance of resting PAP and its contribution to the development of PH. Novel endothelium-specific TRPV4_{EC}^{-/-} mice showed elevated PAP revealing the crucial role of TRPV4_{EC} channel activity in the maintenance of resting PAP. Caveolin-1 (Cav-1_{EC}) is an important structural protein in the pulmonary endothelium which is known to associate with TRPV4_{EC} channels in cultured endothelial cells. We hypothesized that Cav-1_{EC} regulates TRPV4_{EC} channel activity and that Cav-1_{EC}-TRPV4_{EC} channel regulation is impaired in PH. PH was induced in mice using a three-week chronic hypoxia (CH) model. In normal mice, protein kinase C (PKC) anchoring to Cav-1_{EC} potentiated TRPV4_{EC} channel activity. However, in CH mice loss of Cav-1_{EC}-PKC anchoring attenuated TRPV4_{EC} channel activity resulting in impaired vasodilation and elevation in PAP. Impairment in Cav-1_{EC}-PKC-TRPV4_{EC} channel signaling was a result of elevated peroxynitrite production (PN). Scavenging PN rescued TRPV4_{EC} channel activity, endothelium-dependent vasodilation, and lowered resting PAP in CH mice. Together, our data reveal a novel Cav-1_{EC}-dependent regulation of TRPV4_{EC} channel activity which is disrupted in PH resulting in endothelial dysfunction and increased PAP.

4.2 Introduction

Pulmonary hypertension (PH) is a vascular disorder characterized by impaired vasodilation, excessive vasoconstriction, and vascular remodeling of the small, resistance-sized pulmonary arteries (PAs) that regulate pulmonary arterial pressure (PAP)¹⁹⁷. The higher vascular resistance, caused by impaired vasodilation in small PAs, increases PAP and ultimately leads to right ventricular failure⁹⁰. While the association between vascular dysfunction and elevated PAP in PH is well-known, the mechanisms contributing to impaired vascular function remain poorly understood. Current therapies for the treatment of PH include administration of vasodilators to help lower vascular resistance in small PAs¹⁹⁸. However, therapeutic interventions have a poor long-term efficacy, with PH patients continuing to have a 5-year mortality rate of approximately 30%⁸⁹. To develop more effective therapeutic treatments, it is imperative to understand the mechanisms underlying vascular dysfunction in PH.

Impaired vasodilation in PH is caused by dysregulation of endothelial Ca^{2+} signaling leading to endothelial dysfunction and elevated PAP^{92,101}. TRPV4 (transient receptor potential vanilloid 4), a cell membrane cation channel, has recently emerged as an important regulator of vascular function both in resistance PAs²⁹. Spatially localized Ca^{2+} influx through endothelial TRPV4 (TRPV4_{EC}) channels promotes vasodilation through the activation of endothelial nitric oxide synthase (eNOS) and subsequent release of nitric oxide (NO)²⁹. TRPV4_{EC} channels can be activated by a multitude of physiological stimuli, including ATP, which potentiate TRPV4 channel activity through Gq-protein coupled receptors (GPCR) signaling^{22,29}. Although the importance of TRPV4_{EC} channel-mediated

vasodilation is well appreciated, the mechanisms that regulate TRPV4_{EC} channel activity remain to be elucidated. Caveolin-1 (Cav-1), the main structural component of caveolae, has emerged as an important structural protein for GPCR signaling in the pulmonary circulation and has been associated with the development of primary PH⁸². Furthermore, Cav-1 and TRPV4 channels have been shown to colocalize in cultured endothelial cells (EC)^{199,200}. However, the potential role of endothelial Cav-1 (Cav-1_{EC}) as a regulator of TRPV4_{EC} channel function, and its contributions to the development of PH remain to be discovered.

Endothelial dysfunction caused by increased oxidative stress has been implicated in the pathogenesis of PH^{92,101}. PH patients have elevated levels of peroxynitrite (PN), a reactive nitrogen product of the reaction between superoxide (O₂⁻) and NO²⁰¹. Oxidative stress has also been shown to alter Ca²⁺ signaling in cultured pulmonary microvascular ECs^{58,202}. However, the mechanisms by which oxidative stress causes endothelial dysfunction in resistance PAs, remains unknown. Therefore, we hypothesize that Cav-1_{EC} regulation of TRPV4_{EC} channel activity maintains a low resting PAP under normal conditions and that elevated PN formation in PH inhibits TRPV4_{EC} channel activity resulting in endothelial dysfunction, impaired vasodilation, and ultimately elevation of PAP.

To test our hypothesis, we developed novel inducible endothelium-specific TRPV4_{EC}^{-/-} and Cav-1_{EC}^{-/-} mouse models. Our data demonstrate that both TRPV4_{EC}^{-/-} and Cav-1_{EC}^{-/-} mice have impaired TRPV4_{EC} channel activity, reduced endothelium-dependent vasodilation, and elevated resting PAP. Furthermore, we show that Cav-1_{EC}-TRPV4_{EC}

channel signaling is impaired in a chronic hypoxia model of PH due to increased PN production. Scavenging PN rescued TRPV4_{EC} channel activity and restored resting PAP. Our results provide novel insights into the mechanisms underlying endothelial dysfunction and reveals novel therapeutic targets for the treatment of PH.

4.3 Results

TRPV4_{EC} channel activity lowers resting PAP.

To identify the role of TRPV4_{EC} channel activity on resting PAP, we generated tamoxifen-inducible endothelium-specific TRPV4 knockout (TRPV4_{EC}^{-/-}) mice, where TRPV4 channels are exclusively knocked out in endothelial cells (ECs). Endothelial knockout of TRPV4 channels was confirmed at the protein level using immunofluorescence on *en face* resistance PAs (Figure 16A) and at the mRNA level on freshly isolated ECs (Figure 16 B). Localized, unitary Ca²⁺ influx events through TRPV4_{EC} channels – termed TRPV4_{EC} sparklets – were recorded on *en face* PAs. TRPV4_{EC} sparklet activity induced by the specific TRPV4 channel agonist, GSK1016790A (GSK101; 3-10 nM), was significantly reduced in TRPV4_{EC}^{-/-} PAs compared to wild-type (WT) PAs (Figure 16C). Resistance PA from TRPV4_{EC}^{-/-} mice also had impaired endothelium-dependent vasodilation to GSK101 (3-30 nM) (Figure 16D). Importantly, TRPV4_{EC}^{-/-} mice had elevated right ventricular systolic pressure (RVSP), which is used as a standard indirect measurement of PAP (Figure 16E). However, TRPV4_{EC}^{-/-} mice did not develop right ventricular hypertrophy measured by the Fulton index, a ratio of the right ventricular (RV) weight over the left ventricle and septal (LV +S) weight (Figure 16E). Together, these data

are the first to show that TRPV₄^{EC} channel activity regulates vasodilation in resistance PAs thereby maintaining normal resting PAP.

FIGURE 16. ENDOTHELIUM-SPECIFIC TRPV4 KNOCKOUT (TRPV4_{EC}^{-/-}) MICE HAVE ELEVATED PAP.

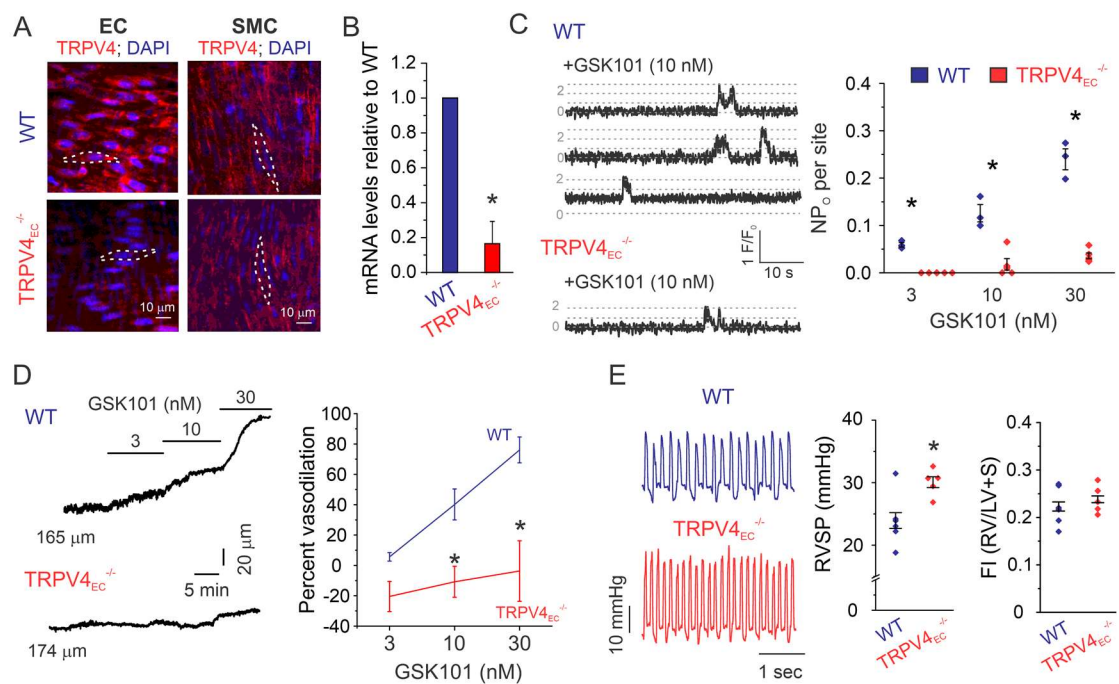


Figure 16. Endothelium-specific TRPV4 knockout (TRPV4_{EC}^{-/-}) mice have elevated PAP. **A.** Representative image of an *en face*, fourth-order resistance PAs from WT (top) and TRPV4_{EC}^{-/-} (bottom) mice showing immunofluorescence for TRPV4 (red) and DAPI (blue) in ECs (left) and SMCs (right). **B.** Relative TRPV4 mRNA expression in freshly isolated ECs from WT and TRPV4_{EC}^{-/-} mice. n=3 mice, *p< 0.05 for TRPV4_{EC} mice relative to WT, t-test. **C.** *Left*, representative fractional fluorescence (F/F₀) traces of TRPV4_{EC} sparklet sites after treatment with GSK101 (10 nM) in *en face* PAs from WT and TRPV4_{EC}^{-/-} mice. Dotted lines indicate quantal levels for TRPV4_{EC} channel activation previously derived from an all points histogram²⁹. *Right*, average TRPV4_{EC} sparklet activity (NP_O per site) following treatment with GSK101 (3-30 nM) in PAs from WT and TRPV4_{EC}^{-/-} mice. n=3-5 fields, *p<0.05 for WT vs. TRPV4_{EC}^{-/-}, two-way ANOVA. **D.** *Left*, representative diameter traces of pressurized PAs from WT and TRPV4_{EC}^{-/-} mice treated with GSK101 (3-30 nM). *Right*, average percent vasodilation following treatment with GSK101 (3-30 nM) in WT and TRPV4_{EC}^{-/-} PAs. n=3 PAs, *p<0.05 for WT vs. TRPV4_{EC}^{-/-}, two-way ANOVA. **E.** *Left*, representative RVSP traces of WT and TRPV4_{EC}^{-/-} mice. *Right*, average RVSP in WT and TRPV4_{EC}^{-/-} mice and average Fulton index (RV weight/LV+S weight) for WT and TRPV4_{EC}^{-/-} mice. n=5-6 mice, *p<0.05 for WT vs. TRPV4_{EC}^{-/-} mice, t-test. All data are represented as mean ± SEM.

TRPV4_{EC} channel activity is impaired in PH and contributes to elevated PAP.

Since TRPV4_{EC} channel activity regulates resting PAP, we examined whether impaired TRPV4_{EC} channel activity contributes to endothelial dysfunction in PH. TRPV4_{EC} channel activity was analyzed in a chronic hypoxia (CH) mouse model of PH, where mice are housed in a hyperbaric chamber and exposed to 10% O₂ for three weeks, while the normoxic (N) controls are exposed to room air (20% O₂). Consistent with previous studies, CH mice had elevated RVSP accompanied by right ventricular hypertrophy (Figure 17A), indicative of a robust development of PH. Interestingly, vasodilation in response to GSK101 (3-30 nM), was impaired in PAs from CH mice (Figure 17B). To confirm that the impaired vasodilation observed in CH mice was due to TRPV4_{EC} channel dysfunction rather than a complete loss of endothelium-dependent vasodilatory capacity, PAs were treated with NS309 (1 μM), a specific agonist for intermediate and small conductance K⁺ channel (IK and SK channels respectively). Opening of IK and SK channels generates a hyperpolarizing current that is transmitted from the ECs to the SMCs to dilate PAs²⁰³. IK and SK channels are not coupled to TRPV4_{EC} channels in resistance PAs and are therefore a good indicator of endothelial health independent of TRPV4_{EC} channel activity. In PAs from CH mice, addition of NS309 (1 μM) caused a similar vasodilation compared to PAs from N mice (Figure 17C), demonstrating that endothelium-dependent vasodilatory capacity is intact in CH mice. TRPV4_{EC} channel dysfunction was confirmed by decreased TRPV4_{EC} sparklet activity in response to GSK101 (3-30 nM) in PAs from CH mice (Figure 17D). Importantly, TRPV4 mRNA levels did not differ in PAs from N and CH mice (Figure 17E), suggesting that altered TRPV4_{EC} sparklet activity in

CH mice is caused by changes in TRPV₄EC channel regulation rather than changes in channel expression.

TRPV₄EC channels activate eNOS-NO signaling to dilate resistance PAs, therefore uncoupling of eNOS could contribute to the impaired endothelium-dependent vasodilation observed in CH mice. To test whether eNOS downstream of TRPV₄EC channels was uncoupled in the ECs of CH mice, TRPV₄EC-dependent release of NO was measured using the fluorescent indicator 4-amino-5 methylamino-2',7'difluorofluorescein diacetate (DAF-FM, 5 μ M). Equal activation of TRPV₄EC sparklets in PAs from N and CH mice by GSK101 (10 nM and 30 nM respectively) caused a similar increase in DAF-FM fluorescence (Figure 18A), indicating that eNOS downstream of TRPV₄EC channels was still able to be activated by TRPV₄EC channel signaling. Furthermore, addition of the NO donor, NONOate (0.1-10 μ M), dilated PAs from CH and N mice to the same extent, indicating that the signaling targets downstream of NO were not affected in PH (Figure 18B), further supporting an impairment in TRPV₄EC channel regulation, not expression, as the main insult causing endothelial dysfunction in PH.

FIGURE 17. TRPV4_{EC} CHANNEL ACTIVITY IS IMPAIRED IN PH CONTRIBUTING TO ELEVATED PAP.

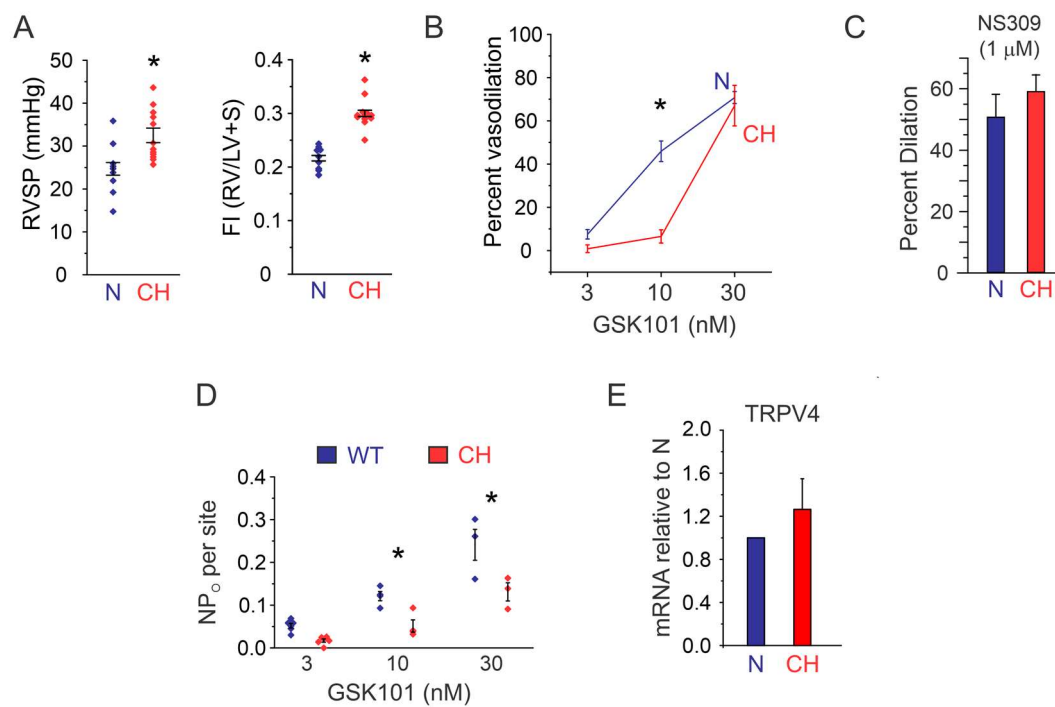


Figure 17. TRPV4_{EC} channel activity is impaired in PH contributing to elevated PAP.

A. Averaged RVSP (*left*) and Fulton index (*right*) for normoxic (N) and chronic hypoxic (CH) mice. n=9-12 mice, *p<0.05 for N vs. CH mice, t-test. **B.** Average percent vasodilation following treatment with GSK101 (3-30 nM) in N and CH PAs. n=9-10 PAs, *p<0.05 for N vs. CH, two-way ANOVA. **C.** Percent vasodilation following treatment with NS309 (1 μ M) in N and CH PAs. n=5 PAs. **D.** Average NP_O per site following treatment with GSK101 (3-30 nM) in PAs from N and CH mice. n=3-6 fields, *p<0.05 for N vs. CH, two-way ANOVA. **E.** Relative TRPV4 mRNA expression from isolated PAs from N and CH mice. n=3 mice. All data are represented as mean \pm SEM.

FIGURE 18. NO SIGNALING DOWNSTREAM OF TRPV4_{EC} CHANNEL ACTIVATION IS UNAFFECTED IN CH MICE.

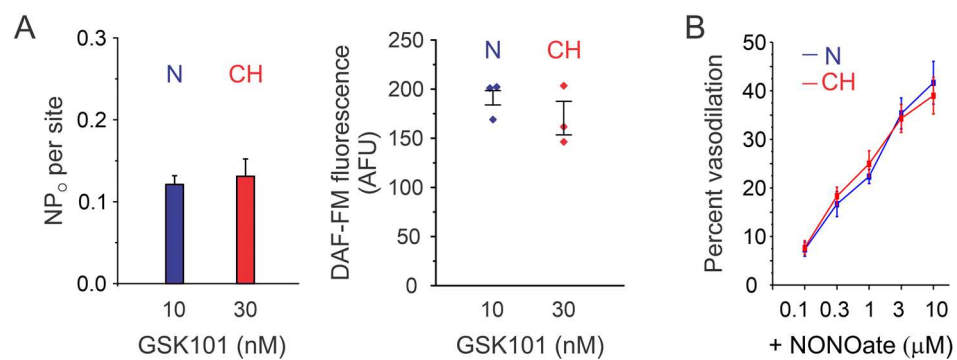


Figure 18. NO signaling downstream of TRPV4_{EC} channel activation is unaffected in CH mice. **A.** *Left*, averaged NP_O per site of N and CH mice treated with 10 nM and 30 nM GSK101, respectively. n= 3-4 fields. *Right*, averaged DAF-FM fluorescence of PAs from N and CH mice treated with 10 nM and 30 nM GSK101, respectively. n= 3 PAs. **B.** Average percent vasodilation following treatment with NONOate (0.1-10 μ M) in N and CH PAs. n=5 PAs. All data are represented as mean \pm SEM.

Cav-1_{EC}-dependent potentiation of TRPV4_{EC} channels is impaired in PH

TRPV4_{EC} channels require an anchoring protein to facilitate channel activation by physiological agonists^{39,49,203}. Cav-1 has been suggested to interact with TRPV4 channels in cultured ECs and has emerged as an important structural protein in the pulmonary endothelium^{199,200}. To determine the role of Cav-1_{EC} on TRPV4_{EC} channel activation, we developed a novel, tamoxifen-inducible, endothelium-specific, Cav-1^{-/-} mouse (Cav-1_{EC}^{-/-}). Endothelium-specific knockout of Cav-1 was confirmed by a decrease in immunofluorescence of Cav-1_{EC} in *en face* PAs and by a decrease in Cav-1_{EC} mRNA expression on freshly isolated ECs (Figure 19A and B). Loss of Cav-1_{EC} resulted in elevated RVSP without right ventricular hypertrophy (Figure 19C). TRPV4_{EC} sparklet activity was decreased in PAs from Cav-1_{EC}^{-/-} mice (Figure 19D). Furthermore, PAs from Cav-1_{EC}^{-/-} mice had impaired vasodilation in response to GSK101 (3-10 nM) (Figure 19E). These data are the first to show that Cav-1_{EC} is an important structural protein regulating TRPV4_{EC} channel activity.

Cav-1 can facilitate TRPV4 channel opening by localizing physiological activators, such as protein kinase C (PKC), by anchoring at the caveolin scaffold domain (CSD) in close proximity to the channel^{204,205}. We examined whether PKC anchoring to Cav-1_{EC} potentiates TRPV4_{EC} activity in resistance PAs. Addition of the PKC activator, phorbol 12-myristate 13-acetate (PMA, 10 nM), increased TRPV4_{EC} sparklet activity in WT PAs but had no effect on Cav-1_{EC}^{-/-} PAs (Figure 19F). Blocking PKC anchoring to Cav-1 using CSD competing peptide^{205,206} (10 μM) attenuated PKC-dependent potentiation of TRPV4_{EC} channels in control PAs (Figure 19G). Together, these data reveal that PKC

anchoring to Cav-1_{EC} at the CSD is required for the PKC-dependent potentiation of TRPV4_{EC} channels. Next, we examined if TRPV4_{EC} channel dysfunction in PH is due to the dysregulation of Cav-1_{EC}-PKC signaling. Addition of PMA (10 nM) did not increase TRPV4_{EC} sparklet activity in CH PAs supporting an impaired Cav-1_{EC}-PKC signaling in PH (Figure 19H). This was further confirmed by decreased Cav-1_{EC}-PKC, colocalization in CH mice (Figure 19I). However, Cav-1_{EC}:TRPV4_{EC} colocalization was not altered in CH (Figure 19I). Together, these data are the first to demonstrate that Cav-1_{EC}-PKC signaling potentiates TRPV4_{EC} channel activity and that loss of PKC anchoring to Cav-1_{EC} in PH contributes to TRPV4_{EC} channel dysfunction.

FIGURE 19. CAV-1_{EC}-DEPENDENT POTENTIATION OF TRPV4_{EC} CHANNELS IS IMPAIRED IN PH.

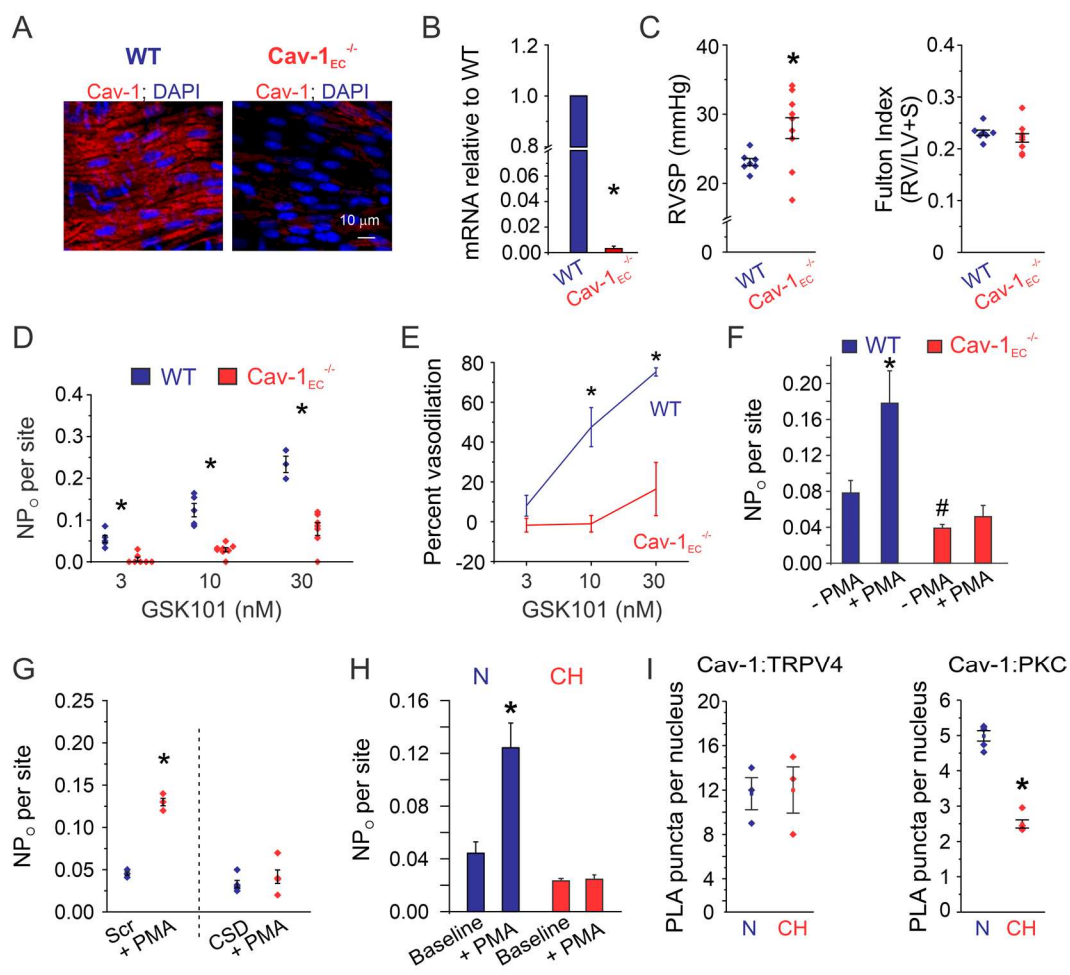


Figure 19. Cav-1_{EC}-dependent potentiation of TRPV4_{EC} channels is impaired in PH.

A. Representative image of an *en face*, fourth-order resistance PAs from WT (left) and Cav-1_{EC}^{-/-} (right) mice showing immunofluorescence for Cav-1 (red) and DAPI (blue) in ECs. **B.** Relative Cav-1 mRNA expression in ECs from WT and Cav-1_{EC}^{-/-} mice. n=4 mice, *p< 0.05 for TRPV4_{EC} mice relative to WT, t-test. **C.** Averaged RVSP (*left*) and Fulton index (*right*) for WT and Cav-1_{EC}^{-/-} mice. n=7-9 mice, *p<0.05 for WT vs. Cav-1_{EC}^{-/-} mice, t-test. **D.** Average NP_O per site at following treatment with GSK101 (3-30 nM) in PAs from WT and Cav-1_{EC}^{-/-} mice. n=3-8 fields, *p<0.05 for WT vs Cav-1_{EC}^{-/-}, two-way ANOVA. **E.** Average percent vasodilation following treatment with GSK101 (3-30 nM) in WT and Cav-1_{EC}^{-/-} PAs. n=3-6 PAs, *p<0.05 for WT vs Cav-1_{EC}^{-/-}, two-way ANOVA. **F.** Average NP_O per site in WT and Cav-1_{EC}^{-/-} PAs treated with 3 nM GSK101 in the absence or presence of PMA (10 nM). n=5 fields, *,#p<0.05 WT before PMA vs. WT plus PMA and WT vs Cav-1_{EC}^{-/-} before PMA respectively, t-test. **G.** Average NP_O per site to PMA (10 nM) in the absence or presence of the caveolin-1 scaffolding domain peptide (CSD, 2 μM) or scramble peptide (Scr, 2 μM). n=3 PAs, *p<0.05, t-test. **H.** Average NP_O per site following treatment with PMA (10 nM) in N and CH PAs. n=5 fields, *p<0.05, t-test vs. baseline. **I.** Average proximity ligation assay (PLA) puncta per cell for Cav-1:TRPV4 (*left*) or Cav-1:PKC (*right*) in N and CH PAs. n=3 PAs, *p<0.05, t-test. All data are represented as mean ± SEM.

Peroxynitrite (PN) impairs Cav-1_{EC}-PKC-TRPV4_{EC} channel signaling in PH.

Elevated production of the nitrative species peroxynitrite (PN) has been implicated in the pathogenesis of PH²⁰⁷. Inhibiting PN production with uric acid (UA; 200 μ M; PN scavenger), Fe^{III}-tetra-(4-sulfonatophenyl)-porphyrin (FeTTPS; 1 μ M; PN decomposer), or Tempol (200 μ M; a superoxide dismutase (SOD) mimetic that reduces O₂⁻) rescued TRPV4_{EC} sparklet activity in response to GSK101 (3 nM) in CH PAs (Figure 20A). Increased TRPV4_{EC} sparklet activity in the presence of UA was mirrored by improved endothelium-dependent vasodilation in response to GSK101 (10 nM) (Figure 20B). Strikingly, an acute injection of FeTTPs (30 mg/ kg body weight, i.p.) reduced the RVSP of CH mice back to normal levels but had no effect on N mice (Figure 20C), demonstrating that PN-dependent impairment of TRPV4_{EC} channel activity attenuates endothelium-dependent vasodilation and elevates RVSP in CH mice.

To confirm the specific role of PN on TRPV4_{EC} channel activity, *en face* PAs from N mice were incubated with exogenous PN (5 μ M). Treatment with exogenous PN decreased TRPV4_{EC} sparklet activity, an effect that could be reversed by washing out PN (Figure 21A). Inhibition of TRPV4_{EC} sparklets by exogenous PN was attenuated in the presence of UA (Figure 21B). Addition of PN donor, SIN-1 (100 μ M), which decomposes into O₂⁻ and NO to form PN, also decreased TRPV4_{EC} sparklet activity (Figure 21C). Selective scavenging NO with carboxy-PTIO potassium salt (CPTIO; 50 μ M) rescued TRPV4_{EC} sparklets, indicating that the effect of SIN-1 on TRPV4_{EC} channel activity was specific to PN (Figure 21C). As such, PN impaired TRPV4_{EC}-dependent vasodilation but did not affect IK/SK-dependent vasodilation, demonstrating that PN was not altering

endothelium-dependent vasodilatory capacity (Figure 21D and E). Interestingly, PN had no effect on TRPV4_{EC} sparklet activity in PAs obtained from Cav-1_{EC}^{-/-} mice suggesting that PN specifically targets Cav-1_{EC} to inhibit TRPV4_{EC} channel activity (Figure 21F). This was confirmed using HEK293 cells transfected with TRPV4 channels alone or TRPV4 channels and Cav-1. Exogenous PN had no effect on TRPV4 currents when the cells were transfected with TRPV4 channels alone (Figure 21G). However, when cells were co-transfected with TRPV4 channels and Cav-1, addition of PN attenuated TRPV4 channel currents (Figure 21G), supporting the specificity effect of PN on Cav-1_{EC}.

FIGURE 20. PN IMPAIRS TRPV4_{EC} CHANNEL ACTIVITY IN PH.

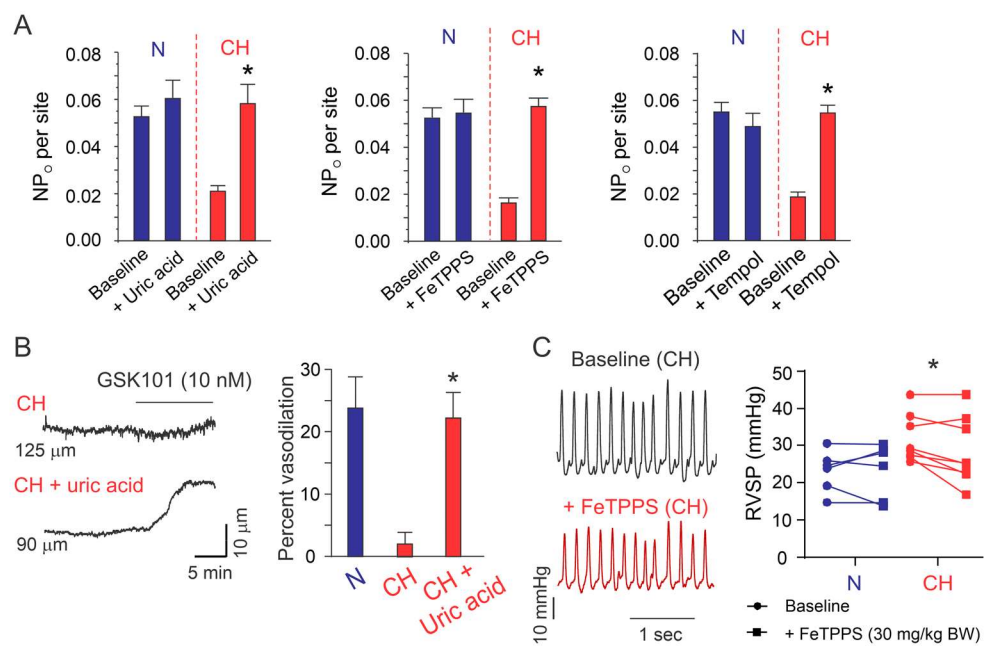


Figure 20. PN impairs TRPV4_{EC} channel activity in PH. **A.** Average NP_O per site in N and CH PAs in the absence or presence of uric acid (200 μ M, *left*), FeTPPs (1 mM, *middle*), or tempol (200 mM, *right*). n=3-5 PAs, *p<0.05 using one-way ANOVA. **B.** *Left*, representative diameter traces of pressurized PAs from CH mice treated with GSK101 (10 nM) in the absence or presence of uric acid (200 μ M). *Right*, average percent vasodilation in N and CH mice following treatment with GSK101 (10 nM) in the absence or presence of uric acid (200 μ M). n=5 PAs, *p<0.05 for CH vs. CH plus UA, one-way ANOVA. **C.** *Left*, representative RVSP traces of CH mice at baseline and after acute injection of FeTPPs (30 mg/kg BW, i.p.). *Right*, average RVSP in N and CH mice before and after treatment with FeTPPs. n=6-8 mice, *p<0.05 for baseline vs. FeTPPs, paired t-test. All data are represented as mean \pm SEM.

FIGURE 21. EXOGENOUS PN ATTENUATES TRPV4_{EC} SPARKLET ACTIVITY IN NORMAL MICE.

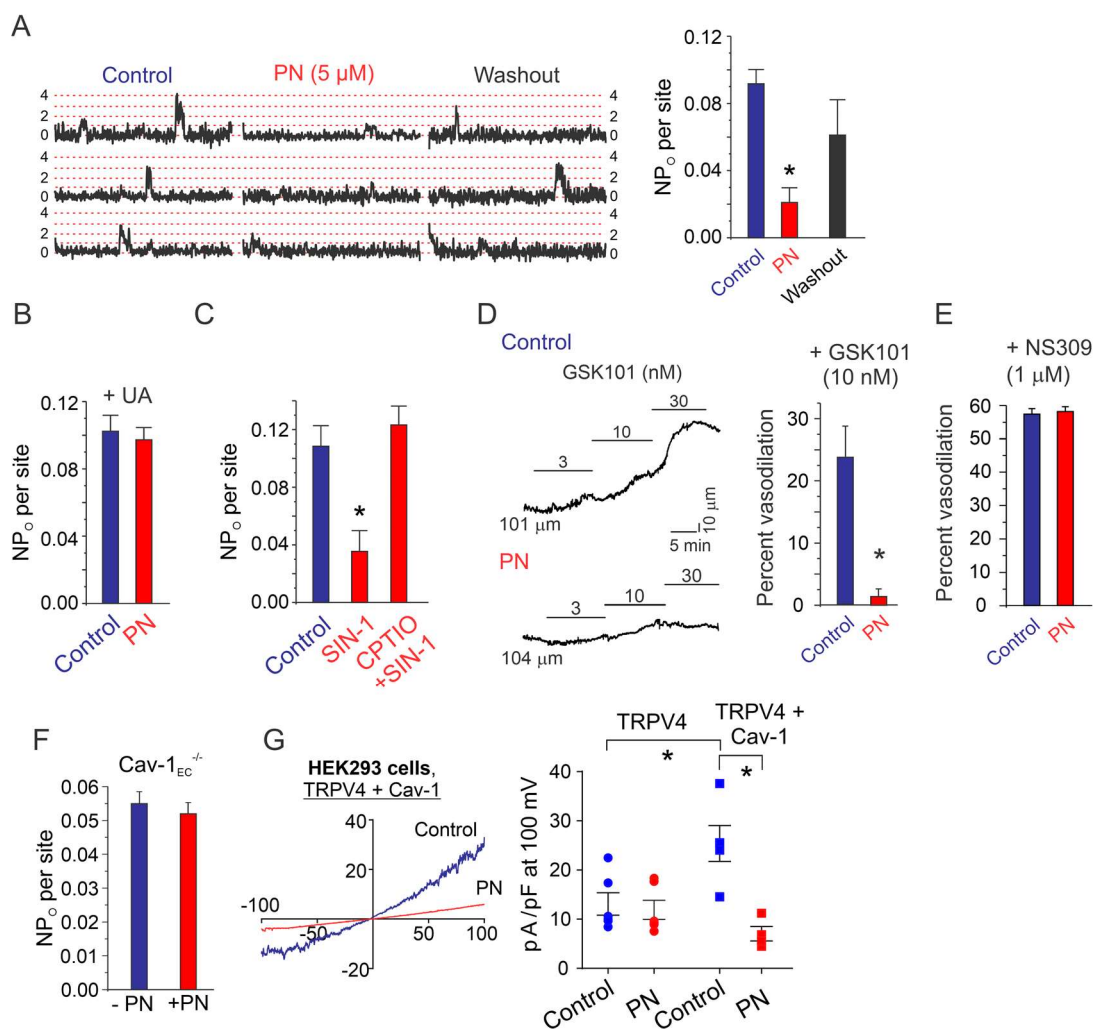


Figure 21. Exogenous PN attenuates TRPV4_{EC} sparklet activity in normal mice. **A.** *Left*, representative F/F₀ traces of TRPV4_{EC} sparklet sites in WT mice to GSK101 (10 nM), after exogenous addition of PN (5 μM), and after washout. *Right*, average NP_O per site treated with GSK101 (10 nM) and after addition of PN (5 μM), and after washout. n=5 PAs, *p<0.05 using one-way ANOVA. **B.** Average NP_O per site with GSK101 (10 nM) and after addition of PN (5 μM) in the presence of uric acid (200 μM, UA). n=3 PAs. **C.** Average NP_O per site PAs with GSK101 (10 nM), after addition of SIN-1 (100 μM), and after addition of CPTIO (50 μM). n=3 PAs, *p<0.05 using one-way ANOVA. **D.** *Left*, representative diameter traces of pressurized PAs from N mice treated with GSK101 (3-10 nM) in the absence or presence of PN (5 μM). *Right*, average percent vasodilation to GSK101 (10 nM) in the absence or presence of PN (5 μM). n=5 PAs, *p<0.05 using t-test. **E.** Average percent vasodilation to NS309 (1 μM) in N mice in the absence or presence of PN (5 μM). n=5 PAs. **F.** Average NP_O per site in WT and Cav-1_{EC}^{-/-} mice treated with GSK101 (3 nM) in the absence or presence of PN (5 μM). n=3 PAs. **G.** *Left*, representative TRPV4 current traces in HEK293 cells transfected with TRPV4 channels and Cav-1 in the presence or absence of PN (5 μM). *Right*, averaged TRPV4 current density in HEK293 cells transfected with TRPV4 channels alone or in conjunction with Cav-1. n=5-6 cells, *p<0.05 using one-way ANOVA. All data are represented as mean ± SEM.

NOX1, mitochondria, and iNOS are sources of ROS in PH.

NADPH oxidases (NOXs) and the mitochondria are a main source of $O_2^{\cdot-}$ production which have been associated with the development of PH¹⁰². However, the specific sources of $O_2^{\cdot-}$ production contributing to the formation of PN in the endothelium of resistance PAs has not been elucidated. NOX1 expression was increased in PAs from CH mice, identifying NOX1 as the possible source of $O_2^{\cdot-}$ production in PH (Figure 22A). Inhibition of NOX1 activity with ML171 (1 μ M) or selectively scavenging mitochondrial-derived ROS using the mitochondrial targeted antioxidant MitoQ (1 μ M) rescued TRPV4_{EC} sparklet activity in CH mice (Figure 22A and B). Both $O_2^{\cdot-}$ and NO production are required for the formation of PN. Increased expression of inducible nitric oxide synthase (iNOS), resulting in NO production, has been associated with the development of PH^{208,209}. Although iNOS mRNA expression was not different between N and CH PAs, specific inhibition of iNOS with 1400W (1 μ M) rescued TRPV4_{EC} sparklet activity in CH PAs (Figure 22C), suggesting that iNOS activity is increased in CH. Together, these data suggest that NOX1 and the mitochondria are the main sources of $O_2^{\cdot-}$ and iNOS is the source of NO which generate PN and inhibit TRPV4_{EC} channel activity in PH.

FIGURE 22. NOX1-, MITOCHONDRIA-, AND INOS-DEPENDENT SIGNALING IMPAIRS TRPV4_{EC} SPARKLET ACTIVITY IN CH MICE.

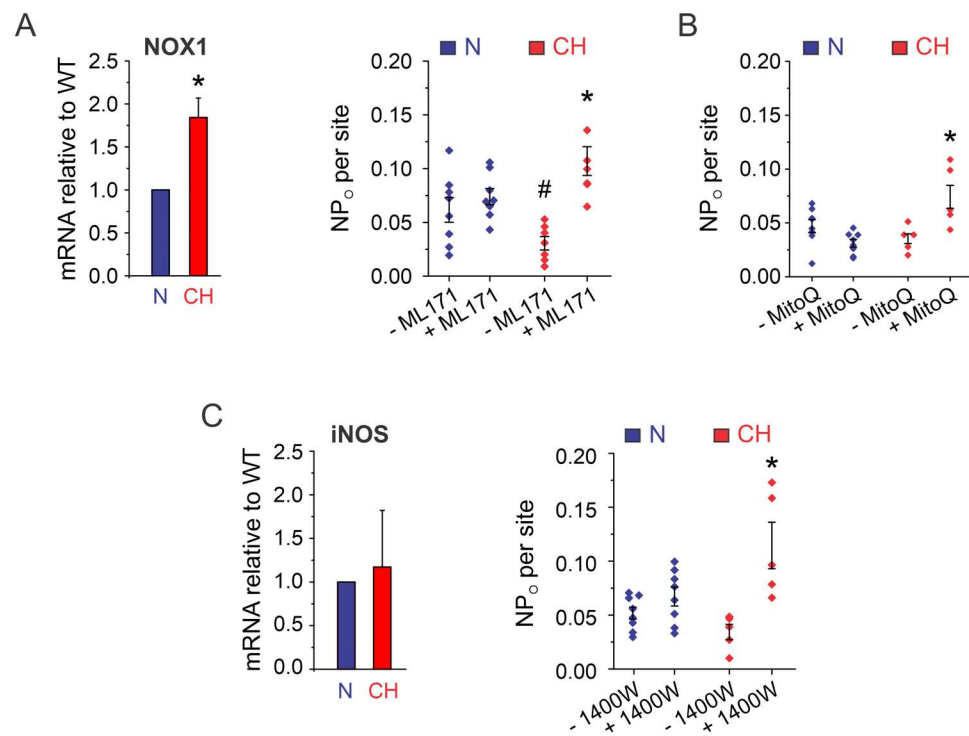


Figure 22. NOX1-, mitochondria-, and iNOS- dependent signaling impairs TRPV4_{EC} sparklet activity in CH mice. **A.** *Left*, Relative NOX1 mRNA expression in whole PAs from N and CH mice. n=5 mice, *p< 0.05 for NOX1 expression in CH mice relative to N, t-test. *Right*, Average NP_O per site in N and CH mice treated with GSK101 (3 nM) in the absence or presence of ML171 (1 μM). n=7-8 fields, *,#p<0.05 using paired t-test vs. CH baseline and independent t-test vs. N baseline, respectively. **B.** Average NP_O per site in N and CH mice treated with GSK101 (3 nM) in the absence or presence of MitoQ (1 μM). n=5-8 fields, *p<0.05 using paired t-test vs. CH baseline. **C.** *Left*, Relative iNOS mRNA expression in whole PAs from N and CH mice. n=5 mice. *Right*, Average NP_O per site in N and CH mice treated with GSK101 (3 nM) in the absence or presence of 1400W (1 μM). n=5-8 fields, *p<0.05 using paired t-test vs. CH baseline. All data are represented as mean ± SEM.

FIGURE 23. PEROXYNITRITE INHIBITS CAV-1_{EC}-PKC-TRPV4_{EC} SIGNALING IN PULMONARY HYPERTENSION.

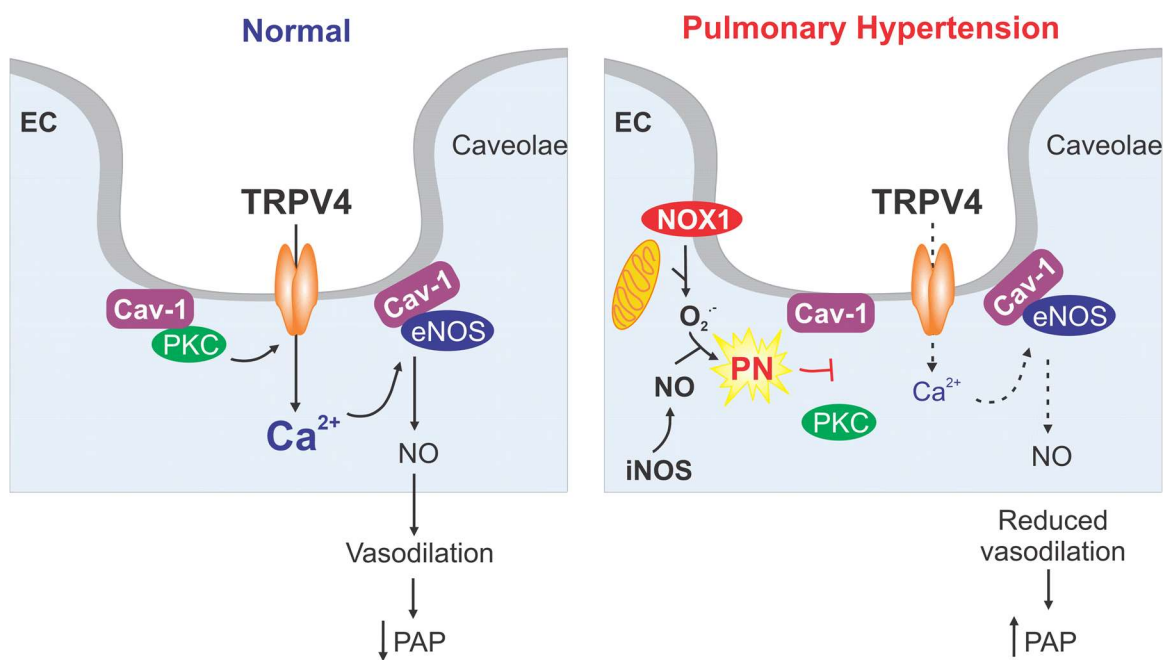


Figure 23. Peroxynitrite inhibits Cav-1_{EC}-PKC-TRPV4_{EC} signaling in pulmonary hypertension. Schematic represents changes regulation of TRPV4_{EC} channel activity in normal PAs and in pulmonary hypertension. In normal PAs anchoring of protein kinase C (PKC) to caveolin-1 (Cav-1) potentiates TRPV4_{EC} channel activity. Ca²⁺ influx through TRPV4_{EC} channels activates endothelial nitric oxide synthase (eNOS) causing the release of nitric oxide (NO) leading to vasodilation and overall decrease in pulmonary arterial pressure (PAP). In pulmonary hypertension, release of superoxide (O₂⁻) from NADPH oxidase 1 (NOX1) and mitochondria and NO release from inducible NOS (iNOS) leads to the formation of peroxynitrite (PN). Increased production of PN blocks Cav-1-PKC anchoring resulting in reduced TRPV4_{EC} channel activity, attenuated vasodilation, and ultimately increase in PAP.

4.4 Discussion

Impaired endothelium-dependent vasodilation in PAs is associated with increased PAP leading to PH^{92,101}. Localized Ca²⁺ influx through TRPV4_{EC} channels promotes endothelium-dependent vasodilation of small resistance PAs whose vasoreactivity affects PAP²⁹. Prior to this study, the contribution of TRPV4_{EC} channel activity on resting PAP had been difficult to elucidate due to the lack of an EC-specific knockout models. By generating inducible, endothelium-specific TRPV4_{EC}^{-/-} mice, we were able to show for the first time that TRPV4_{EC} channel activity can lower resting PAP. We demonstrate that Cav-1_{EC}-PKC signaling potentiates TRPV4_{EC} channel activity and is impaired in PH, leading to elevated RVSP. Increased production of PN in PH inhibits Cav-1_{EC}-PKC-TRPV4_{EC} channel signaling by blocking the anchoring of PKC to Cav-1_{EC}, resulting in endothelial dysfunction. PN is formed from O₂⁻ generated by NOX1 and the mitochondria and NO produced by iNOS. Taken together these data support a novel Cav-1_{EC}-PKC-TRPV4_{EC} channel-dependent signaling pathway that lowers resting PAP which is impaired in PH through elevated production of PN (Figure 23). Results from these studies reveal important potential therapeutic targets for the treatment of PH.

TRPV4 channels are expressed in both pulmonary ECs and SMCs but have opposing effects on vascular tone. Global TRPV4^{-/-} mice have normal PAP making the precise contribution of EC and SMC TRPV4 channel signaling on resting PAP difficult to determine^{210,211}. Furthermore, compensatory signaling mechanisms in global knockout mice may also help maintain normal pulmonary blood pressure. Using inducible endothelium-specific TRPV4_{EC}^{-/-} mice revealed, for the first time, that TRPV4_{EC} channel

activity is a crucial for maintaining a low resting PAP. Elevated PAP and impaired endothelial function in the CH model of PH was caused, in part, by reduced TRPV4_{EC} channel activity. It is possible that increased SMC TRPV4 channel expression or activity contributed to elevated PAP in PH²¹⁰. However, rescuing TRPV4_{EC} channel activity alone was sufficient to restore endothelium-dependent vasodilation and resting PAP in PH mice, emphasizing the importance of TRPV4_{EC} channel signaling in maintaining resting PAP. Further studies are necessary to understand the SMC-specific effect of TRPV4 channels in both health and disease conditions.

TRPV4_{EC} channel activity is potentiated by anchoring proteins that localize physiological activators within close proximity to the channel^{39,49,203}. Cav-1_{EC} is a prominent structural protein in the pulmonary circulation and can regulate Ca²⁺ signaling in pulmonary ECs²¹². Furthermore, Cav-1 and TRPV4 channels colocalize in cultured EC^{199,200}, but the possible role of Cav-1_{EC}-dependent regulation of TRPV4_{EC} activity in intact resistance PAs had not been investigated. Impaired TRPV4_{EC} activity and elevated RVSP in Cav-1_{EC}^{-/-} mice are the first evidence of a Cav-1_{EC}-dependent regulation of TRPV4_{EC} channel activity in resistance PAs. Cav-1_{EC} anchors PKC, a known potentiator of TRPV4_{EC} channels, at the CSD^{204,205}. PKC-dependent potentiation of TRPV4_{EC} channels requires PKC to be within close proximity to the channel for efficient signaling. Our data demonstrating loss of PKC-dependent activation of TRPV4_{EC} channels in the presence of the CSD competing peptide supported a role for Cav-1_{EC}-PKC dependent signaling mechanism potentiating TRPV4_{EC} channels signaling in resistance PAs and lowering PAP.

Previous reports have associated changes in Cav-1 expression with the development of PH^{78,213}. Our data show that Cav-1_{EC}-dependent regulation of TRPV4_{EC} channels, not changes in Cav-1_{EC} expression, contributes to endothelial dysfunction in PH. PN inhibited Cav-1_{EC}-PKC anchoring thereby decreasing TRPV4_{EC} channel activity in CH PAs. Scavenging endogenous PN production quickly rescued TRPV4_{EC} channel activity and Cav-1_{EC}-PKC localization. Interestingly, exogenous PN had no effect on TRPV4_{EC} channel activity in Cav-1_{EC}^{-/-} mice indicating that PN affects Cav-1_{EC}-dependent regulation of TRPV4_{EC} channel activity. Further studies are necessary to investigate the specific mechanism by which PN affect Cav-1_{EC}.

Increased levels of PN, formed by the reaction of O₂⁻ and NO, are linked to endothelial dysfunction in multiple vascular pathologies, including PH^{92,101}. O₂⁻ is released by NOX enzymes which have been shown to colocalize with Cav-1 on cell membranes²¹⁴. Our data demonstrate that NOX1 is a source of O₂⁻ in pulmonary ECs from CH mice. Mitochondrial-derived ROS has also been implicated in the pathogenesis of PH. Selectively scavenging mitochondrial-derived ROS rescued TRPV4 sparklet activity in CH mice suggesting that the mitochondria may be another source of O₂⁻ production in PH. Increased expression of iNOS and release of NO also contribute to the formation of PN in CH mice. Previous reports have attributed eNOS uncoupling as a source of O₂⁻ in PH. However, our data indicate that the pool of eNOS localized downstream of TRPV4_{EC} activity is not affected in CH mice. TRPV4_{EC} channel activation to normal levels was still able to increase eNOS-dependent NO release in CH mice. Thus, low baseline NO production observed in CH mice can be attributed to impaired TRPV4_{EC} channel activity

rather than impairments in eNOS function. Together, these data demonstrate that endothelial dysfunction in PH is not caused by eNOS uncoupling, but rather changes in TRPV_{4EC} channel regulation.

Recently, a NOS-independent pathway of NO production has emerged as an important source of NO. Nitrite, derived from NO oxidation, is an inert product that is stored in red blood cells²¹⁵. Under hypoxia, nitrite is converted to NO which diffuses out of the red blood cells promoting vasodilation²¹⁶. However, the role of nitrite-derived NO on resistance PAs and its contribution to resting PAP under normal conditions and in PH remain unknown. It is possible that nitrite-derived NO exerts a small but constant vasodilatory effect on resistance PAs and that TRPV_{4EC} channels activate in response to neurohumoral signaling to dynamically regulate arterial vasodilation. Although nitrite levels have not been directly studied in PH, it is plausible that reduced nitrite levels would further contribute to lower NO production and increased PAP.

In summary, TRPV_{4EC} channel activity is necessary for maintaining low resting PAP in the pulmonary circulation. Cav-1_{EC}-PKC signaling potentiates TRPV_{4EC} channel activity in normal resistance PAs. Impaired Cav-1_{EC}-PKC-TRPV_{4EC} channel signaling by PN contributes to endothelial dysfunction and elevated PAP in PH. Scavenging PN rescued Cav-1_{EC}-PKC-TRPV_{4EC} channel signaling, improved endothelial function, and lowered PAP. These results identify a novel mechanism that can be exploited for the development of therapeutic interventions to treat PH.

CHAPTER 5. FUTURE DIRECTIONS

5.1 Chapter 3 Future Directions.

Our work identified ATP, a novel physiological activator of TRPV_{4EC} channels, as being unique to the pulmonary circulation. We show that ATP signals through P2 purinergic receptors to potentiate TRPV_{4EC} sparklet activity (Figure 14). However, the identity of the specific P2 receptor involved in ATP-TRPV_{4EC} signaling remains unknown. There are two major classes of P2 receptors; G-protein coupled P2Y receptors and ionotropic P2X receptors. P2Y1, P2Y2, and P2Y4 receptors are expressed in normal lung tissue homogenates, but only P2Y2 receptors (P2Y2R) preferentially bind ATP and therefore are most likely contributing to ATP-TRPV_{4EC} channel signaling in resistance PAs¹⁷¹. To this point, deletion of P2Y2R impairs Ca²⁺ signaling in cultured ECs and blocks ATP-dependent vasodilation in systemic arteries^{217,218}. Preliminary data of *en face* PAs treated with P2Y2R inhibitor, AR-C118925XX (AR-C, 10 μM), show attenuated ATP-dependent increase in TRPV_{4EC} sparklet activity (Figure 24), revealing an ATP-P2Y2R-dependent mechanism for potentiating TRPV_{4EC} channel activity in resistance PAs. Future studies are needed to test whether loss of P2Y2R signaling impairs endothelium-dependent vasodilation, resulting in elevation of PAP. Pressure myography studies of resistance PAs incubated with P2Y2R antagonist should show attenuated ATP-dependent vasodilations. These data can be further confirmed by using PAs from tamoxifen inducible endothelium-specific P2Y2R^{-/-} (P2Y2R_{EC}^{-/-}) mice driven by a Cdh5 ERT2 Cre. PAs from P2Y2R_{EC}^{-/-} mice are expected to have lower baseline and ATP-dependent TRPV_{4EC} sparklet activity along with impaired ATP-dependent vasodilation. Loss of TRPV_{4EC} channel activity may

elevate RVSP in these mice, suggesting that ATP-P2Y₂R-TRPV₄_{EC} channel signaling regulates resting PAP.

P2X receptor signaling may also contribute to TRPV₄_{EC} channel activation in resistance PAs. P2X₄ receptors (P2X₄R), contribute to flow mediated increases in Ca²⁺ in cultured human pulmonary ECs³⁰. P2X₄R are expressed in SMCs of rat PAs and cultured human ECs, however their expression and functional role in the intact endothelium of resistance PAs remain unknown^{31,219}. Expression of P2X₄R must first be confirmed by immunofluorescence in *en face* resistance PAs. ATP-dependent increase in TRPV₄_{EC} sparklet activity can then be tested in the presence of specific P2X₄R inhibitors. Influx of Ca²⁺ through P2X receptors may potentiate TRPV₄ sparklet activity via Ca²⁺-CaM interactions²²⁰. To test the Ca²⁺-dependence of P2XR signaling, ATP-induced increase in TRPV₄_{EC} sparklet activity can be measured in the presence of the Ca²⁺ chelator, EGTA. Attenuation of ATP-dependent increase of TRPV₄_{EC} sparklet activity in the presence of EGTA would confirm that Ca²⁺ influx through P2XR potentiates TRPV₄_{EC} channel activity.

FIGURE 24. ATP INCREASES TRPV4_{EC} SPARKLETS IN A P2Y2R-DEPENDENT MANNER.

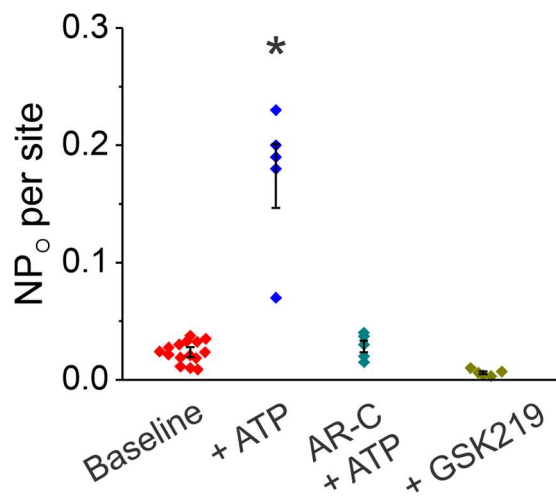


Figure 24. ATP increases TRPV4_{EC} sparklets in a P2Y2R-dependent manner.

Baseline and ATP-induced TRPV4 sparklet activity (NP₀ per site) in the presence of the P2Y2R inhibitor (AR-C; 10 μM) and TRPV4_{EC} channel inhibitor (GSK219; 100 nM). Data are represented as mean ± SEM, n=5 PAs, * P < 0.05, t-test versus baseline.

Pannexin 1 (Panx1) channels are ATP-release channels found on ECs membranes and may be an upstream regulator of ATP-P2R-TRPV4_{EC} channel signaling in resistance PAs²²¹. To determine whether Panx1 is the ATP-release channel contributing to ATP-TRPV4_{EC} channel signaling, baseline TRPV4_{EC} sparklet activity should be measured in PAs from WT and endothelium-specific Panx1^{-/-} (Panx1_{EC}^{-/-}) mice. Decreased baseline TRPV4_{EC} sparklet activity would be predicted in PAs from Panx1_{EC}^{-/-} mice due to attenuated ATP-release compared to WT mice. However, addition of exogenous ATP should rescue TRPV4_{EC} sparklet activity in Panx1_{EC}^{-/-} mice to normal levels. High shear stress in resistance PAs may be the physiological activator of the mechanosensitive Panx1 channel²²¹. Shear stress-induced ATP release and activation of TRPV4_{EC} sparklets can be measured in Panx1_{EC}^{-/-} and WT mice to confirm whether Panx1 channels are the main ATP-release channels which activate TRPV4_{EC} channels in resistance PAs. Reduced TRPV4_{EC} sparklet activity in Panx1_{EC}^{-/-} mice is predicted to impair vasodilation and result in elevated of PAP. However, preliminary data show no difference in RVSP between Panx1_{EC}^{-/-} and WT mice suggesting that there are compensatory ATP-release mechanisms which maintain normal resting PAP (Figure 25). Additional studies are needed in order to confirm these results.

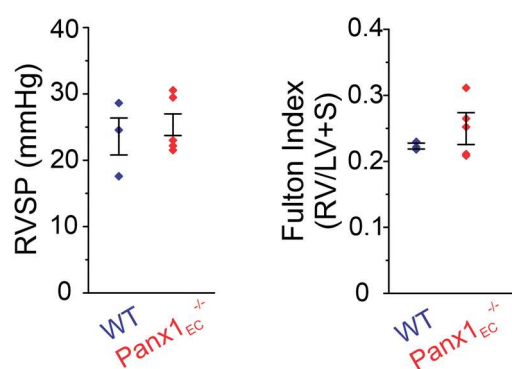
FIGURE 25. RVSP OF PANX1_{EC}^{-/-} MICE

Figure 25. RVSP of Panx1_{EC}^{-/-} mice. Average RVSP (*left*) and Fulton index (*right*) from WT control and Panx1_{EC}^{-/-} mice. Data are represented as mean ± SEM, n = 3-5 mice.

Localization of signaling components in close proximity to one another is essential for efficient signal transduction. Our work has shown that TRPV4_{EC} and PKC localization with Cav-1_{EC} is necessary for potentiation of TRPV4_{EC} channel activity. What remains to be confirmed is whether P2Y2R, and potentially Panx1 channels, also colocalize with Cav-1_{EC} to form a specialized micro-signaling domain. Colocalization of P2Y2R and Panx1 with Cav-1_{EC} can be tested in *en face* PAs using proximity ligation assay (PLA). However, PLA only tests the colocalization of two individual proteins and cannot verify that all signaling components colocalize with one another. Using cell fractioning techniques, the caveolar rich fraction from cell membranes can be isolated from pulmonary ECs and probed for the proteins of interest (Panx1, P2Y2R, Cav-1_{EC}, and TRPV4_{EC}) using western blot to confirm that all signaling components localize to caveolae. Alternatively, imaging of all the proteins of interest in intact pulmonary ECs can be achieved using immunostaining techniques on *en face* PAs, however this would require the availability of antibodies that fluoresce at different wavelengths.

5.2 Chapter 4 future directions

The importance of Cav-1_{EC}-TRPV4_{EC} channel signaling as a regulator of resting PAP was evident by the increased RVSP in Cav-1_{EC}^{-/-} and TRPV4_{EC}^{-/-} mice. However, RVSP recordings are only an indirect measurement of PAP. Further pressure studies should be conducted with isolated perfused lung system to directly measure PAP in lungs from Cav-1_{EC}^{-/-} and TRPV4_{EC}^{-/-} mice in an *ex vivo* preparation. This technique could elucidate even greater differences in PAP in knockout mice versus WT. Also of interest would be to

challenge these mice with CH and study how loss of Cav-1_{EC}-TRPV4_{EC} signaling impacts the development of PH. Normoxic knockout mice already have characteristics of PH (endothelial dysfunction and elevated RVSP), and therefore would be more susceptible to developing severe PH when exposed to CH. In these mice, addition of PN scavengers would not be sufficient to restore endothelial function and reduce PAP, since the mice already had impaired TRPV4_{EC} sparklet activity under normoxic conditions.

It would also be interesting to investigate the effects of CH on available global NOX1^{-/-} and iNOS^{-/-} mice^{222,223}. Lack of NOX1 or iNOS expression would attenuate PN formation, thereby protecting mice from developing severe PH with exposure to CH. Other compensatory pathways, such as NOX2 signaling or eNOS uncoupling, could be upregulated in global NOX1^{-/-} or iNOS^{-/-} mice. If that occurs, the mice might not show any differences in RVSP and TRPV4_{EC} sparklet activity compared to WT mice. The best way to test the possible protective effects of disrupted NOX1 or iNOS signaling would be to generate tamoxifen-inducible endothelium-specific knockout mice. However, these animals must first be developed and characterized before using them in these experiments.

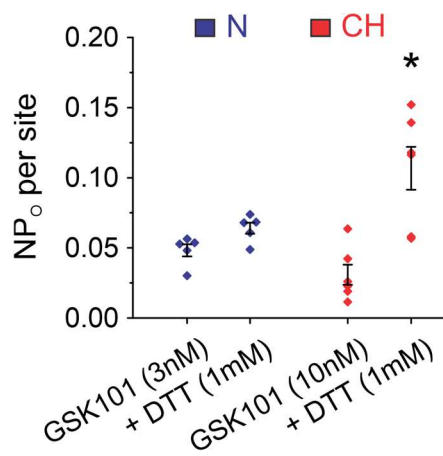
Another area of future studies should focus on the possibility of increased NO signaling in Cav-1_{EC}^{-/-} mice. Although our studies show that loss of PKC-dependent activation is the main contributor to TRPV4_{EC} channel dysfunction in Cav-1_{EC}^{-/-} mice, other mechanisms may also be affecting TRPV4_{EC} sparklet activity. Anchoring of eNOS to Cav-1_{EC} inhibits enzyme activity, therefore it is possible that Cav-1_{EC}^{-/-} mice have elevated NO production, which is known to act as a negative feedback signaling molecule inhibiting TRPV4_{EC} channel coupling^{29,76}. Measurements of baseline NO production using the NO

indicator, DAF-FM, in *en face* PAs from WT and Cav-1_{EC}^{-/-} mice would directly reveal whether NO production is elevated by the loss of Cav-1_{EC}. Early studies show that scavenging NO with carboxy-PTIO potassium salt (C-PTIO, 50 μM) had no effect on TRPV4_{EC} sparklet activity, suggesting that NO does not impair TRPV4_{EC} channel activity in Cav-1_{EC}^{-/-} mice. Furthermore, elevated NO signaling would be predicted to lower PAP, however, elevated RVSP in Cav-1_{EC}^{-/-} mice suggest that there is not an increase in NO production and NO-dependent vasodilation.

Cav-1 anchoring of eNOS also functions to localize the co-factors necessary for eNOS coupling and activation⁷⁶. Loss of Cav-1_{EC} could result in inability of cofactor binding and eNOS uncoupling resulting in production of O₂⁻. It would be interesting to see whether O₂⁻ or PN are elevated in Cav-1_{EC}^{-/-} mice contributing to the TRPV4_{EC} channel dysfunction observed. Estimating O₂⁻ and PN formation using dihydroethidium and coumarin boronic acid (CBA), respectively, would determine whether oxidative stress is higher in Cav-1_{EC}^{-/-} mice. Since NO scavengers did not rescue TRPV4_{EC} activity, PN is most likely not contributing to endothelial dysfunction in Cav-1_{EC}^{-/-} mice. Selective scavenging of O₂⁻ would test whether the effect on TRPV4_{EC} channels is in part due to O₂⁻-dependent signaling. It should be noted that PN levels have been shown to be elevated in global Cav-1^{-/-} mice^{98,224}. However, our studies using inducible Cav-1_{EC}^{-/-} mice, approximately one month following induction, are more physiological and are expected to be different from global knockout mice.

Future studies are also needed to understand the mechanisms by which PN impairs Cav-1_{EC}-PKC-TRPV4_{EC} channel signaling in PH. PN modifies signal transduction

pathways by directly oxidizing proteins and altering their function. Two of the main oxidizing reactions induced by PN are cystine oxidation and tyrosine nitrosylation²²⁵. Our data show that the PN specifically inhibits Cav-1_{EC} dependent potentiation of TRPV4_{EC} channel activity. However, the exact modification induced by PN on Cav-1_{EC} remains unknown. The CSD on Cav-1 is an important site for PKC anchoring which allows for the PKC dependent potentiation of TRPV4_{EC} channel activity²⁰⁵. Addition of either exogenous PN or the CSD competing peptide alone attenuated TRPV4_{EC} sparklet activity. However, early studies show that administration of PN followed by CSD peptide did not further decrease TRPV4_{EC} sparklet activity, suggesting that PN is modifying the CSD region of Cav-1_{EC} to inhibit TRPV4_{EC} channel potentiation. The CSD contains two tyrosine residues (Y97, Y100) that are potential nitration sites⁸². It's important to note that there are no cysteine residues on the CSD, the only three cysteines in the protein are located within the C-terminus (C133, C143, C156)⁸². Administration of the reducing agent dithiothreitol (DTT, 1mM) in CH mice rescued TRPV4_{EC} sparklet activity, suggesting that PN is oxidizing cysteine residues on Cav-1_{EC} impairing TRPV4_{EC} channel activity (Figure 26). Future studies should focus on identifying whether PN is modifying the tyrosine residues on the CSD or the cysteine residues which may allosterically attenuate PKC binding to the CSD domain. Mass spectrometry on purified Cav-1_{EC} protein could be used to identify all the individual residues that are oxidized after exposure to PN. Generation of Cav-1_{EC} with point-mutations on the oxidized residues could be used to confirm the specificity of PN inhibition of Cav-1_{EC}-TRPV4_{EC} signaling.

FIGURE 26. CYSTEINE OXIDATION INHIBITS TRPV4_{EC} SPARKLET ACTIVITY IN CH MICE.**Figure 26. Cysteine oxidation inhibits TRPV4_{EC} sparklet activity in CH mice.**

Averaged TRPV4_{EC} sparklet activity (NP₀ per field) from N and CH in the presence of GSK101 (3 and 10 nM respectively) followed by the addition of DTT (1 mM). Data are mean \pm SEM, n = 5-6 fields from 3 PAs, *P<0.05, paired t-test versus CH treated with GSK101 alone.

Although the CH mouse model is a well-established murine model of PH, it does not recapitulate all aspects of human PH pathology. Specifically, mice challenged with CH lack formation of plexiform lesion in resistance PAs. Results from CH models must be confirmed with a second model of PH to make the findings more translatable to the human disease. The Su + CH mouse model develops endothelial dysfunction and SMC remodeling observed in CH alone, but also promotes the formation of plexiform lesions. Key results from our study must be verified in a Su + CH model of PH. Preliminary data show that TRPV4_{EC} sparklet activity and TRPV4_{EC}-dependent vasodilation was impaired in Su + CH mice (Figure 27). Future studies should investigate whether Cav-1_{EC}-PKC-TRPV4_{EC} signaling is also impaired in Su + CH mice and the possibility of PN as the inhibitory signaling molecule in this pathway.

FIGURE 27. TRPV4_{EC} SPARKLET ACTIVITY AND TRPV4_{EC} CHANNEL-DEPENDENT VASODILATION IS IMPAIRED IN SU + CH MICE.

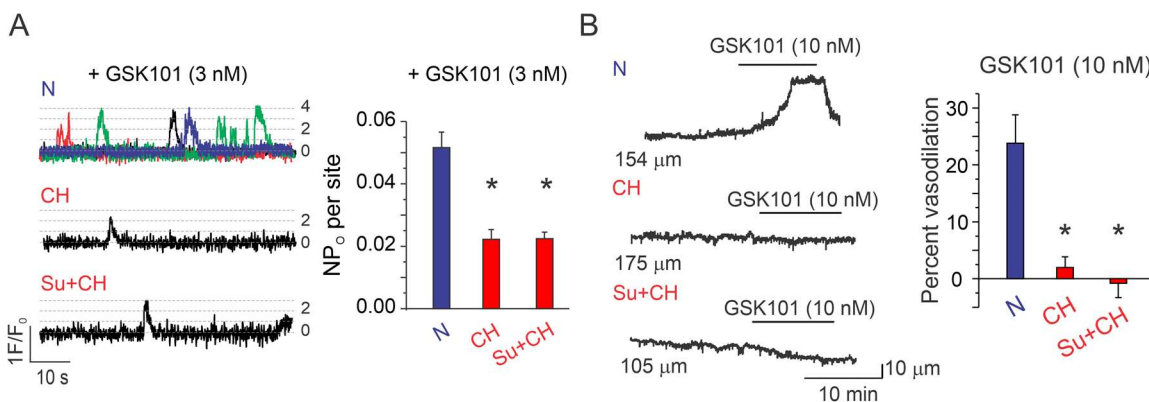


Figure 27. TRPV4_{EC} sparklet activity and TRPV4_{EC} channel-dependent vasodilation is impaired in SU + CH mice. **A. Left,** representative fractional fluorescence traces (F/F_0) traces of TRPV4 sparklet sites to GSK101 (3 nM) in PAs from normoxic (N) or hypertensive (CH and Su + CH) mice; dotted lines indicate quantal amplitudes. **Right,** average NP₀ per site in PAs obtained from control or hypertensive mice in the presence of the GSK101 (3 nM). n=5 PAs, *p<0.05, one-way ANOVA versus normoxic. **B. Left,** representative diameter traces following GSK101 (10 nM) treatment in PAs obtained from control or hypertensive mice. **Right,** averaged percent dilation to GSK101 (10 nM). n=5 PAs, *p<0.05, one-way ANOVA versus normoxic. All data are represented as mean \pm SEM.

Finally, mouse studies must be followed up with experiments using human PAs from PH patients, as it is the most direct way of testing whether the mechanisms we have observed are translatable into the human disease. Resistance PAs isolated from lung wedge samples obtained from PH patients have lower TRPV₄_{EC} sparklet activity compared to control PAs (Figure 28). This was the first ever recording of functional TRPV₄_{EC} channels in freshly isolated human PAs. Impaired TRPV₄_{EC} sparklet activity was also observed in cultured human pulmonary ECs, supporting a role for TRPV₄_{EC} channel dysfunction in PH. However, whether Cav-1_{EC}-PKC signaling regulates TRPV₄_{EC} channels in human PAs, and whether PN production contributes to lower TRPV₄_{EC} channel activity remains to be tested.

FIGURE 28. TRPV4_{EC} SPARKLET ACTIVITY IS IMPAIRED IN PAS FROM PH PATIENTS.

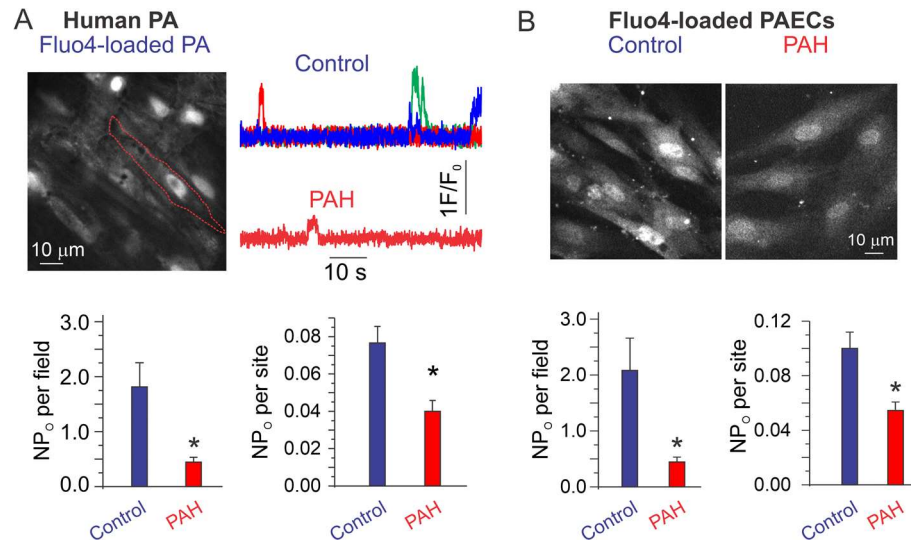


Figure 28. TRPV4_{EC} sparklet activity is impaired in PAs from PH patients. **A.** *Top*, grayscale field of view of *en face* human PA (one EC outlined in red) and representative F/F₀ traces of TRPV4 sparklet sites in PAs from control or PH human lungs. *Bottom*, averaged TRPV4 sparklet activity (NP₀ per field and NP₀ per site) in PAs obtained from control and PH human lungs in the presence of GSK101 (10 nM). n=3 PAs from 2 samples, *P<0.05, t-test. **B.** *Top*, grayscale field of view of fluo-4 loaded pulmonary artery ECs (PAECs) obtained from control and PH patients. *Bottom*, averaged TRPV4 sparklet activity (NP₀ per field and NP₀ per site) in PAECs in the presence of GSK101 (10 nM). n=3 patients, *P<0.05, t-test. All data are represented as mean \pm SEM.

CHAPTER 6. ACKNOWLEDGEMENTS

6.1 Acknowledgements for Chapter 3: We would like to acknowledge GlaxoSmithKline for providing TRPV4^{-/-} breeder mice, Dr Adrian Bonev (University of Vermont) for SparkAn, Dr Luis F. Santana (University of California, Davis) for providing the software program for determining coupling coefficients, and Dr Avril Somlyo for her comments on the manuscript.

6.2 Acknowledgements for Chapter 4: I would like to acknowledge Drs. Kwangseok Hong and Swapnil Sonkusare for Ca²⁺ imaging studies, Eric Cope for diameter studies, and Matteo Ottolini for help with patch clamp and qPCR studies. I would also like to thank Drs. Wolfgang Liedtke (Duke University) for TRPV4^{fl/fl} mice, Richard Minshall (University of Illinois, Chicago) for Cav-1^{fl/fl} mice, and Gary Owens (University of Virginia) for the Cdh5 ERT2 Cre mice. I would like to thank Drs. Bruce Freeman and Mark Gladwin (both University of Pittsburgh) for their advice on peroxynitrite signaling. Finally, I would like to thank Dr. Lisa Palmer for training on the RVSP experiments.

CHAPTER 7. REFERENCES

- 1 Bayliss, W. M. On the local reactions of the arterial wall to changes of internal pressure. *J Physiol* **28**, 220-231, doi:10.1113/jphysiol.1902.sp000911 (1902).
- 2 Michel, R. P. Arteries and veins of the normal dog lung: qualitative and quantitative structural differences. *Am J Anat* **164**, 227-241, doi:10.1002/aja.1001640304 (1982).
- 3 Townsley, M. I. Structure and composition of pulmonary arteries, capillaries, and veins. *Compr Physiol* **2**, 675-709, doi:10.1002/cphy.c100081 (2012).
- 4 Heath, D., Wood, E. H., Dushane, J. W. & Edwards, J. E. The structure of the pulmonary trunk at different ages and in cases of pulmonary hypertension and pulmonary stenosis. *J Pathol Bacteriol* **77**, 443-456 (1959).
- 5 Harris, P., Heath, D. & Apostolopoulos, A. Extensibility of the human pulmonary trunk. *Br Heart J* **27**, 651-659, doi:10.1136/hrt.27.5.651 (1965).
- 6 Hislop, A. & Reid, L. Normal structure and dimensions of the pulmonary arteries in the rat. *J Anat* **125**, 71-83 (1978).
- 7 Reid, L. The angiogram and pulmonary artery structure and branching (in the normal and with reference to disease). *Proc R Soc Med* **58**, 681-684 (1965).
- 8 Tabuchi, A. *et al.* Precapillary oxygenation contributes relevantly to gas exchange in the intact lung. *Am J Respir Crit Care Med* **188**, 474-481, doi:10.1164/rccm.201212-2177OC (2013).
- 9 Mackay, E. H., Banks, J., Sykes, B. & Lee, G. Structural basis for the changing physical properties of human pulmonary vessels with age. *Thorax* **33**, 335-344, doi:10.1136/thx.33.3.335 (1978).
- 10 Suresh, K. & Shimoda, L. A. Lung Circulation. *Compr Physiol* **6**, 897-943, doi:10.1002/cphy.c140049 (2016).
- 11 Wandall-Frostholm, C. *et al.* Genetic deficit of KCa 3.1 channels protects against pulmonary circulatory collapse induced by TRPV4 channel activation. *Br J Pharmacol* **172**, 4493-4505, doi:10.1111/bph.13234 (2015).
- 12 de Jesus Perez, V. A. Molecular pathogenesis and current pathology of pulmonary hypertension. *Heart Fail Rev* **21**, 239-257, doi:10.1007/s10741-015-9519-2 (2016).
- 13 Sylvester, J. T., Shimoda, L. A., Aaronson, P. I. & Ward, J. P. Hypoxic pulmonary vasoconstriction. *Physiol Rev* **92**, 367-520, doi:10.1152/physrev.00041.2010 (2012).
- 14 Dunham-Snary, K. J. *et al.* Hypoxic Pulmonary Vasoconstriction: From Molecular Mechanisms to Medicine. *Chest* **151**, 181-192, doi:10.1016/j.chest.2016.09.001 (2017).
- 15 Hall, J. E. & Guyton, A. C. *Guyton and Hall Textbook of Medical Physiology*. 13th edn, 509 (Elsevier, 2016).
- 16 Davies, P. F. Hemodynamic shear stress and the endothelium in cardiovascular pathophysiology. *Nat Clin Pract Cardiovasc Med* **6**, 16-26, doi:10.1038/ncpcardio1397 (2009).

- 17 Erkens, R. *et al.* Modulation of Local and Systemic Heterocellular Communication by Mechanical Forces: A Role of Endothelial Nitric Oxide Synthase. *Antioxid Redox Signal* **26**, 917-935, doi:10.1089/ars.2016.6904 (2017).
- 18 Helmke, B. P. & Davies, P. F. The cytoskeleton under external fluid mechanical forces: hemodynamic forces acting on the endothelium. *Ann Biomed Eng* **30**, 284-296 (2002).
- 19 Busse, R. & Fleming, I. Regulation of endothelium-derived vasoactive autacoid production by hemodynamic forces. *Trends Pharmacol Sci* **24**, 24-29 (2003).
- 20 Faraci, F. M. & Heistad, D. D. Regulation of cerebral blood vessels by humoral and endothelium-dependent mechanisms. Update on humoral regulation of vascular tone. *Hypertension* **17**, 917-922 (1991).
- 21 Nausch, L. W. *et al.* Sympathetic nerve stimulation induces local endothelial Ca²⁺ signals to oppose vasoconstriction of mouse mesenteric arteries. *Am J Physiol Heart Circ Physiol* **302**, H594-602, doi:10.1152/ajpheart.00773.2011 (2012).
- 22 Sonkusare, S. K. *et al.* Elementary Ca²⁺ signals through endothelial TRPV4 channels regulate vascular function. *Science* **336**, 597-601, doi:10.1126/science.1216283 (2012).
- 23 Sonkusare, S. K. *et al.* AKAP150-dependent cooperative TRPV4 channel gating is central to endothelium-dependent vasodilation and is disrupted in hypertension. *Sci Signal* **7**, ra66, doi:10.1126/scisignal.2005052 (2014).
- 24 Stevens, T. Functional and molecular heterogeneity of pulmonary endothelial cells. *Proc Am Thorac Soc* **8**, 453-457, doi:10.1513/pats.201101-004MW (2011).
- 25 Kelly, J. J. *et al.* Pulmonary microvascular and macrovascular endothelial cells: differential regulation of Ca²⁺ and permeability. *Am J Physiol* **274**, L810-819, doi:10.1152/ajplung.1998.274.5.L810 (1998).
- 26 Taylor, C. W. & Tovey, S. C. IP(3) receptors: toward understanding their activation. *Cold Spring Harb Perspect Biol* **2**, a004010, doi:10.1101/cshperspect.a004010 (2010).
- 27 Suematsu, E., Hirata, M., Hashimoto, T. & Kuriyama, H. Inositol 1,4,5-trisphosphate releases Ca²⁺ from intracellular store sites in skinned single cells of porcine coronary artery. *Biochem Biophys Res Commun* **120**, 481-485, doi:10.1016/0006-291x(84)91279-8 (1984).
- 28 Marshall, I. C. & Taylor, C. W. Biphasic effects of cytosolic Ca²⁺ on Ins(1,4,5)P₃-stimulated Ca²⁺ mobilization in hepatocytes. *J Biol Chem* **268**, 13214-13220 (1993).
- 29 Marziano, C. *et al.* Nitric Oxide-Dependent Feedback Loop Regulates Transient Receptor Potential Vanilloid 4 (TRPV4) Channel Cooperativity and Endothelial Function in Small Pulmonary Arteries. *J Am Heart Assoc* **6**, doi:10.1161/jaha.117.007157 (2017).
- 30 Yamamoto, K. *et al.* Endogenously released ATP mediates shear stress-induced Ca²⁺ influx into pulmonary artery endothelial cells. *Am J Physiol Heart Circ Physiol* **285**, H793-803, doi:10.1152/ajpheart.01155.2002 (2003).

- 31 Yamamoto, K. *et al.* P2X(4) receptors mediate ATP-induced calcium influx in human vascular endothelial cells. *Am J Physiol Heart Circ Physiol* **279**, H285-292, doi:10.1152/ajpheart.2000.279.1.H285 (2000).
- 32 Coste, B. *et al.* Piezo1 and Piezo2 are essential components of distinct mechanically activated cation channels. *Science* **330**, 55-60, doi:10.1126/science.1193270 (2010).
- 33 Zhong, M., Komarova, Y., Rehman, J. & Malik, A. B. Mechanosensing Piezo channels in tissue homeostasis including their role in lungs. *Pulm Circ* **8**, 2045894018767393, doi:10.1177/2045894018767393 (2018).
- 34 Friedrich, E. E. *et al.* Endothelial cell Piezo1 mediates pressure-induced lung vascular hyperpermeability via disruption of adherens junctions. *Proc Natl Acad Sci U S A* **116**, 12980-12985, doi:10.1073/pnas.1902165116 (2019).
- 35 Heller, S. & O'Neil, R. G. in *TRP Ion Channel Function in Sensory Transduction and Cellular Signaling Cascades* (eds W. B. Liedtke & S. Heller) (CRC Press/Taylor & Francis Taylor & Francis Group, LLC., 2007).
- 36 Liedtke, W. *et al.* Vanilloid receptor-related osmotically activated channel (VR-OAC), a candidate vertebrate osmoreceptor. *Cell* **103**, 525-535, doi:10.1016/s0092-8674(00)00143-4 (2000).
- 37 Strotmann, R., Harteneck, C., Nunnenmacher, K., Schultz, G. & Plant, T. D. OTRPC4, a nonselective cation channel that confers sensitivity to extracellular osmolarity. *Nat Cell Biol* **2**, 695-702, doi:10.1038/35036318 (2000).
- 38 Wissenbach, U., Boddling, M., Freichel, M. & Flockerzi, V. Trp12, a novel Trp related protein from kidney. *FEBS Lett* **485**, 127-134, doi:10.1016/s0014-5793(00)02212-2 (2000).
- 39 Fan, H. C., Zhang, X. & McNaughton, P. A. Activation of the TRPV4 ion channel is enhanced by phosphorylation. *J Biol Chem* **284**, 27884-27891, doi:10.1074/jbc.M109.028803 (2009).
- 40 Strotmann, R., Schultz, G. & Plant, T. D. Ca²⁺-dependent potentiation of the nonselective cation channel TRPV4 is mediated by a C-terminal calmodulin binding site. *J Biol Chem* **278**, 26541-26549, doi:10.1074/jbc.M302590200 (2003).
- 41 Watanabe, H. *et al.* Activation of TRPV4 channels (hVRL-2/mTRP12) by phorbol derivatives. *J Biol Chem* **277**, 13569-13577, doi:10.1074/jbc.M200062200 (2002).
- 42 Watanabe, H. *et al.* Modulation of TRPV4 gating by intra- and extracellular Ca²⁺. *Cell Calcium* **33**, 489-495 (2003).
- 43 Nilius, B., Prenen, J., Wissenbach, U., Boddling, M. & Droogmans, G. Differential activation of the volume-sensitive cation channel TRP12 (OTRPC4) and volume-regulated anion currents in HEK-293 cells. *Pflugers Arch* **443**, 227-233, doi:10.1007/s004240100676 (2001).
- 44 Voets, T. *et al.* Molecular determinants of permeation through the cation channel TRPV4. *J Biol Chem* **277**, 33704-33710, doi:10.1074/jbc.M204828200 (2002).

- 45 Doyle, D. A. *et al.* The structure of the potassium channel: molecular basis of K⁺ conduction and selectivity. *Science* **280**, 69-77, doi:10.1126/science.280.5360.69 (1998).
- 46 Zhou, Y., Morais-Cabral, J. H., Kaufman, A. & MacKinnon, R. Chemistry of ion coordination and hydration revealed by a K⁺ channel-Fab complex at 2.0 Å resolution. *Nature* **414**, 43-48, doi:10.1038/35102009 (2001).
- 47 Watanabe, H. *et al.* Anandamide and arachidonic acid use epoxyeicosatrienoic acids to activate TRPV4 channels. *Nature* **424**, 434-438, doi:10.1038/nature01807 (2003).
- 48 Watanabe, H. *et al.* Heat-evoked activation of TRPV4 channels in a HEK293 cell expression system and in native mouse aorta endothelial cells. *J Biol Chem* **277**, 47044-47051, doi:10.1074/jbc.M208277200 (2002).
- 49 Mercado, J. *et al.* Local control of TRPV4 channels by AKAP150-targeted PKC in arterial smooth muscle. *J Gen Physiol* **143**, 559-575, doi:10.1085/jgp.201311050 (2014).
- 50 Guler, A. D. *et al.* Heat-evoked activation of the ion channel, TRPV4. *J Neurosci* **22**, 6408-6414, doi:20026679 (2002).
- 51 Chung, M. K., Lee, H. & Caterina, M. J. Warm temperatures activate TRPV4 in mouse 308 keratinocytes. *J Biol Chem* **278**, 32037-32046, doi:10.1074/jbc.M303251200 (2003).
- 52 Voets, T. *et al.* The principle of temperature-dependent gating in cold- and heat-sensitive TRP channels. *Nature* **430**, 748-754, doi:10.1038/nature02732 (2004).
- 53 Gao, X., Wu, L. & O'Neil, R. G. Temperature-modulated diversity of TRPV4 channel gating: activation by physical stresses and phorbol ester derivatives through protein kinase C-dependent and -independent pathways. *J Biol Chem* **278**, 27129-27137, doi:10.1074/jbc.M302517200 (2003).
- 54 Cao, S. *et al.* Transient receptor potential vanilloid 4 (TRPV4) activation by arachidonic acid requires protein kinase A-mediated phosphorylation. *J Biol Chem* **293**, 5307-5322, doi:10.1074/jbc.M117.811075 (2018).
- 55 Alvarez, D. F. *et al.* Transient receptor potential vanilloid 4-mediated disruption of the alveolar septal barrier: a novel mechanism of acute lung injury. *Circ Res* **99**, 988-995, doi:10.1161/01.Res.0000247065.11756.19 (2006).
- 56 Fernandez-Fernandez, J. M. *et al.* Functional coupling of TRPV4 cationic channel and large conductance, calcium-dependent potassium channel in human bronchial epithelial cell lines. *Pflugers Arch* **457**, 149-159, doi:10.1007/s00424-008-0516-3 (2008).
- 57 Sukumaran, S. V. *et al.* TRPV4 channel activation leads to endothelium-dependent relaxation mediated by nitric oxide and endothelium-derived hyperpolarizing factor in rat pulmonary artery. *Pharmacol Res* **78**, 18-27, doi:10.1016/j.phrs.2013.09.005 (2013).
- 58 Suresh, K. *et al.* Reactive oxygen species induced Ca²⁺ influx via TRPV4 and microvascular endothelial dysfunction in the SU5416/hypoxia model of pulmonary arterial hypertension. *Am J Physiol Lung Cell Mol Physiol* **314**, L893-1907, doi:10.1152/ajplung.00430.2017 (2018).

- 59 Simonsen, U., Wandall-Frosthalm, C., Olivan-Viguera, A. & Kohler, R. Emerging roles of calcium-activated K channels and TRPV4 channels in lung oedema and pulmonary circulatory collapse. *Acta Physiol (Oxf)* **219**, 176-187, doi:10.1111/apha.12768 (2017).
- 60 Forstermann, U. & Sessa, W. C. Nitric oxide synthases: regulation and function. *Eur Heart J* **33**, 829-837, 837a-837d, doi:10.1093/eurheartj/ehr304 (2012).
- 61 Forstermann, U. *et al.* Nitric oxide synthase isozymes. Characterization, purification, molecular cloning, and functions. *Hypertension* **23**, 1121-1131, doi:10.1161/01.hyp.23.6.1121 (1994).
- 62 Gunnett, C. A., Lund, D. D., McDowell, A. K., Faraci, F. M. & Heistad, D. D. Mechanisms of inducible nitric oxide synthase-mediated vascular dysfunction. *Arterioscler Thromb Vasc Biol* **25**, 1617-1622, doi:10.1161/01.ATV.0000172626.00296.ba (2005).
- 63 Crabtree, M. J. & Channon, K. M. Synthesis and recycling of tetrahydrobiopterin in endothelial function and vascular disease. *Nitric Oxide* **25**, 81-88, doi:10.1016/j.niox.2011.04.004 (2011).
- 64 Noble, M. A. *et al.* Potentiometric analysis of the flavin cofactors of neuronal nitric oxide synthase. *Biochemistry* **38**, 16413-16418, doi:10.1021/bi992150w (1999).
- 65 Stuehr, D., Pou, S. & Rosen, G. M. Oxygen reduction by nitric-oxide synthases. *J Biol Chem* **276**, 14533-14536, doi:10.1074/jbc.R100011200 (2001).
- 66 Hemmens, B. & Mayer, B. Enzymology of nitric oxide synthases. *Methods Mol Biol* **100**, 1-32 (1998).
- 67 Cho, H. J. *et al.* Calmodulin is a subunit of nitric oxide synthase from macrophages. *J Exp Med* **176**, 599-604, doi:10.1084/jem.176.2.599 (1992).
- 68 Kobzik, L. *et al.* Nitric oxide synthase in human and rat lung: immunocytochemical and histochemical localization. *Am J Respir Cell Mol Biol* **9**, 371-377, doi:10.1165/ajrcmb/9.4.371 (1993).
- 69 Xue, C. & Johns, R. A. Endothelial nitric oxide synthase in the lungs of patients with pulmonary hypertension. *N Engl J Med* **333**, 1642-1644, doi:10.1056/nejm199512143332416 (1995).
- 70 Giaid, A. & Saleh, D. Reduced expression of endothelial nitric oxide synthase in the lungs of patients with pulmonary hypertension. *N Engl J Med* **333**, 214-221, doi:10.1056/NEJM199507273330403 (1995).
- 71 Abman, S. H., Chatfield, B. A., Hall, S. L. & McMurtry, I. F. Role of endothelium-derived relaxing factor during transition of pulmonary circulation at birth. *Am J Physiol* **259**, H1921-1927, doi:10.1152/ajpheart.1990.259.6.H1921 (1990).
- 72 Fineman, J. R., Heymann, M. A. & Soifer, S. J. N omega-nitro-L-arginine attenuates endothelium-dependent pulmonary vasodilation in lambs. *Am J Physiol* **260**, H1299-1306, doi:10.1152/ajpheart.1991.260.4.H1299 (1991).
- 73 North, A. J. *et al.* Pulmonary endothelial nitric oxide synthase gene expression is decreased in a rat model of congenital diaphragmatic hernia. *Am J Respir Cell Mol Biol* **13**, 676-682, doi:10.1165/ajrcmb.13.6.7576705 (1995).

- 74 Villamor, E. *et al.* Chronic intrauterine pulmonary hypertension impairs endothelial nitric oxide synthase in the ovine fetus. *Am J Physiol* **272**, L1013-1020, doi:10.1152/ajplung.1997.272.5.L1013 (1997).
- 75 Steudel, W. *et al.* Pulmonary vasoconstriction and hypertension in mice with targeted disruption of the endothelial nitric oxide synthase (NOS 3) gene. *Circ Res* **81**, 34-41 (1997).
- 76 Oliveira, S. D. S. & Minshall, R. D. Caveolin and Endothelial NO Signaling. *Curr Top Membr* **82**, 257-279, doi:10.1016/bs.ctm.2018.09.004 (2018).
- 77 Oliveira, S. D. S. *et al.* Inflammation-induced caveolin-1 and BMPRII depletion promotes endothelial dysfunction and TGF-beta-driven pulmonary vascular remodeling. *Am J Physiol Lung Cell Mol Physiol* **312**, L760-1771, doi:10.1152/ajplung.00484.2016 (2017).
- 78 Achcar, R. O. *et al.* Loss of caveolin and heme oxygenase expression in severe pulmonary hypertension. *Chest* **129**, 696-705, doi:10.1378/chest.129.3.696 (2006).
- 79 Bakhshi, F. R. *et al.* Nitrosation-dependent caveolin 1 phosphorylation, ubiquitination, and degradation and its association with idiopathic pulmonary arterial hypertension. *Pulm Circ* **3**, 816-830, doi:10.1086/674753 (2013).
- 80 Jasmin, J. F. *et al.* Lung remodeling and pulmonary hypertension after myocardial infarction: pathogenic role of reduced caveolin expression. *Cardiovasc Res* **63**, 747-755, doi:10.1016/j.cardiores.2004.05.018 (2004).
- 81 Feron, O. *et al.* Endothelial nitric oxide synthase targeting to caveolae. Specific interactions with caveolin isoforms in cardiac myocytes and endothelial cells. *J Biol Chem* **271**, 22810-22814 (1996).
- 82 Chettimada, S., Yang, J., Moon, H. G. & Jin, Y. Caveolae, caveolin-1 and cavin-1: Emerging roles in pulmonary hypertension. *World J Respirol* **5**, 126-134, doi:10.5320/wjr.v5.i2.126 (2015).
- 83 Chen, Z. *et al.* Nitric oxide-dependent Src activation and resultant caveolin-1 phosphorylation promote eNOS/caveolin-1 binding and eNOS inhibition. *Mol Biol Cell* **23**, 1388-1398, doi:10.1091/mbc.E11-09-0811 (2012).
- 84 Garcia-Cardena, G. *et al.* Dissecting the interaction between nitric oxide synthase (NOS) and caveolin. Functional significance of the nos caveolin binding domain in vivo. *J Biol Chem* **272**, 25437-25440, doi:10.1074/jbc.272.41.25437 (1997).
- 85 Trane, A. E. *et al.* Deciphering the binding of caveolin-1 to client protein endothelial nitric-oxide synthase (eNOS): scaffolding subdomain identification, interaction modeling, and biological significance. *J Biol Chem* **289**, 13273-13283, doi:10.1074/jbc.M113.528695 (2014).
- 86 Maniatis, N. A. *et al.* Increased pulmonary vascular resistance and defective pulmonary artery filling in caveolin-1^{-/-} mice. *Am J Physiol Lung Cell Mol Physiol* **294**, L865-873, doi:10.1152/ajplung.00079.2007 (2008).
- 87 Zhao, Y. Y. *et al.* Defects in caveolin-1 cause dilated cardiomyopathy and pulmonary hypertension in knockout mice. *Proc Natl Acad Sci U S A* **99**, 11375-11380, doi:10.1073/pnas.172360799 (2002).

- 88 Murata, T. *et al.* Reexpression of caveolin-1 in endothelium rescues the vascular, cardiac, and pulmonary defects in global caveolin-1 knockout mice. *J Exp Med* **204**, 2373-2382, doi:10.1084/jem.20062340 (2007).
- 89 Hoepfer, M. M. *et al.* Mortality in pulmonary arterial hypertension: prediction by the 2015 European pulmonary hypertension guidelines risk stratification model. *Eur Respir J* **50**, doi:10.1183/13993003.00740-2017 (2017).
- 90 Prins, K. W. & Thenappan, T. World Health Organization Group I Pulmonary Hypertension: Epidemiology and Pathophysiology. *Cardiol Clin* **34**, 363-374, doi:10.1016/j.ccl.2016.04.001 (2016).
- 91 Abe, K. *et al.* Haemodynamic unloading reverses occlusive vascular lesions in severe pulmonary hypertension. *Cardiovasc Res* **111**, 16-25, doi:10.1093/cvr/cvw070 (2016).
- 92 Humbert, M. *et al.* Pathology and pathobiology of pulmonary hypertension: state of the art and research perspectives. *Eur Respir J* **53**, doi:10.1183/13993003.01887-2018 (2019).
- 93 Sztrymf, B. *et al.* Clinical outcomes of pulmonary arterial hypertension in carriers of BMPR2 mutation. *Am J Respir Crit Care Med* **177**, 1377-1383, doi:10.1164/rccm.200712-1807OC (2008).
- 94 Best, D. H., Austin, E. D., Chung, W. K. & Elliott, C. G. Genetics of pulmonary hypertension. *Curr Opin Cardiol* **29**, 520-527, doi:10.1097/hco.000000000000105 (2014).
- 95 Wilkins, M. R. Pulmonary hypertension: the science behind the disease spectrum. *Eur Respir Rev* **21**, 19-26, doi:10.1183/09059180.00008411 (2012).
- 96 Kaneko, F. T. *et al.* Biochemical reaction products of nitric oxide as quantitative markers of primary pulmonary hypertension. *Am J Respir Crit Care Med* **158**, 917-923, doi:10.1164/ajrccm.158.3.9802066 (1998).
- 97 Fagan, K. A. *et al.* The pulmonary circulation of homozygous or heterozygous eNOS-null mice is hyperresponsive to mild hypoxia. *J Clin Invest* **103**, 291-299, doi:10.1172/jci3862 (1999).
- 98 Zhao, Y. Y. *et al.* Persistent eNOS activation secondary to caveolin-1 deficiency induces pulmonary hypertension in mice and humans through PKG nitration. *J Clin Invest* **119**, 2009-2018, doi:10.1172/jci33338 (2009).
- 99 Berger, R. M., Geiger, R., Hess, J., Bogers, A. J. & Mooi, W. J. Altered arterial expression patterns of inducible and endothelial nitric oxide synthase in pulmonary plexogenic arteriopathy caused by congenital heart disease. *Am J Respir Crit Care Med* **163**, 1493-1499, doi:10.1164/ajrccm.163.6.9908137 (2001).
- 100 Konduri, G. G., Bakhutashvili, I., Eis, A. & Pritchard, K., Jr. Oxidant stress from uncoupled nitric oxide synthase impairs vasodilation in fetal lambs with persistent pulmonary hypertension. *Am J Physiol Heart Circ Physiol* **292**, H1812-1820, doi:10.1152/ajpheart.00425.2006 (2007).
- 101 Klinger, J. R., Abman, S. H. & Gladwin, M. T. Nitric oxide deficiency and endothelial dysfunction in pulmonary arterial hypertension. *Am J Respir Crit Care Med* **188**, 639-646, doi:10.1164/rccm.201304-0686PP (2013).

- 102 Daneva, Z., Laubach, V. E. & Sonkusare, S. K. Novel regulators and targets of redox signaling in pulmonary vasculature. *Current Opinion in Physiology* **9**, 87-93, doi:10.1016/j.cophys.2019.04.026 (2019).
- 103 Murphy, M. P. How mitochondria produce reactive oxygen species. *Biochem J* **417**, 1-13, doi:10.1042/bj20081386 (2009).
- 104 Zhang, D. X. & Gutterman, D. D. Mitochondrial reactive oxygen species-mediated signaling in endothelial cells. *Am J Physiol Heart Circ Physiol* **292**, H2023-2031, doi:10.1152/ajpheart.01283.2006 (2007).
- 105 Li, X. *et al.* Mitochondrial Reactive Oxygen Species Mediate Lysophosphatidylcholine-Induced Endothelial Cell Activation. *Arterioscler Thromb Vasc Biol* **36**, 1090-1100, doi:10.1161/atvbaha.115.306964 (2016).
- 106 Sommer, N. *et al.* Mitochondrial Complex IV Subunit 4 Isoform 2 Is Essential for Acute Pulmonary Oxygen Sensing. *Circ Res* **121**, 424-438, doi:10.1161/circresaha.116.310482 (2017).
- 107 Suresh, K. & Shimoda, L. A. Endothelial Cell Reactive Oxygen Species and Ca(2+) Signaling in Pulmonary Hypertension. *Adv Exp Med Biol* **967**, 299-314, doi:10.1007/978-3-319-63245-2_18 (2017).
- 108 Zhang, Z. *et al.* Stabilization of p22phox by Hypoxia Promotes Pulmonary Hypertension. *Antioxid Redox Signal* **30**, 56-73, doi:10.1089/ars.2017.7482 (2019).
- 109 Liu, J. Q., Zelko, I. N., Erbynn, E. M., Sham, J. S. & Folz, R. J. Hypoxic pulmonary hypertension: role of superoxide and NADPH oxidase (gp91phox). *Am J Physiol Lung Cell Mol Physiol* **290**, L2-10, doi:10.1152/ajplung.00135.2005 (2006).
- 110 Nisbet, R. E. *et al.* The role of NADPH oxidase in chronic intermittent hypoxia-induced pulmonary hypertension in mice. *Am J Respir Cell Mol Biol* **40**, 601-609, doi:10.1165/2008-0145oc (2009).
- 111 Zhang, Y. *et al.* An Endothelial Hsp70-TLR4 Axis Limits Nox3 Expression and Protects Against Oxidant Injury in Lungs. *Antioxid Redox Signal* **24**, 991-1012, doi:10.1089/ars.2015.6505 (2016).
- 112 Schroder, K. *et al.* Nox4 is a protective reactive oxygen species generating vascular NADPH oxidase. *Circ Res* **110**, 1217-1225, doi:10.1161/circresaha.112.267054 (2012).
- 113 Lu, X., Gong, J., Dennery, P. A. & Yao, H. Endothelial-to-mesenchymal transition: Pathogenesis and therapeutic targets for chronic pulmonary and vascular diseases. *Biochem Pharmacol* **168**, 100-107, doi:10.1016/j.bcp.2019.06.021 (2019).
- 114 Humbert, M. *et al.* Cellular and molecular pathobiology of pulmonary arterial hypertension. *J Am Coll Cardiol* **43**, 13s-24s, doi:10.1016/j.jacc.2004.02.029 (2004).
- 115 Good, R. B. *et al.* Endothelial to Mesenchymal Transition Contributes to Endothelial Dysfunction in Pulmonary Arterial Hypertension. *Am J Pathol* **185**, 1850-1858, doi:10.1016/j.ajpath.2015.03.019 (2015).

- 116 Kang, Z. *et al.* Ponatinib attenuates experimental pulmonary arterial hypertension by modulating Wnt signaling and vasohibin-2/vasohibin-1. *Life Sci* **148**, 1-8, doi:10.1016/j.lfs.2016.02.017 (2016).
- 117 Stenmark, K. R., Meyrick, B., Galie, N., Mooi, W. J. & McMurtry, I. F. Animal models of pulmonary arterial hypertension: the hope for etiological discovery and pharmacological cure. *Am J Physiol Lung Cell Mol Physiol* **297**, L1013-1032, doi:10.1152/ajplung.00217.2009 (2009).
- 118 Frank, D. B. *et al.* Increased susceptibility to hypoxic pulmonary hypertension in Bmpr2 mutant mice is associated with endothelial dysfunction in the pulmonary vasculature. *Am J Physiol Lung Cell Mol Physiol* **294**, L98-109, doi:10.1152/ajplung.00034.2007 (2008).
- 119 Nozik-Grayck, E. *et al.* Lung EC-SOD overexpression attenuates hypoxic induction of Egr-1 and chronic hypoxic pulmonary vascular remodeling. *Am J Physiol Lung Cell Mol Physiol* **295**, L422-430, doi:10.1152/ajplung.90293.2008 (2008).
- 120 Steiner, M. K. *et al.* Interleukin-6 overexpression induces pulmonary hypertension. *Circ Res* **104**, 236-244, 228p following 244, doi:10.1161/circresaha.108.182014 (2009).
- 121 Jones, R. C. *et al.* A protocol for phenotypic detection and characterization of vascular cells of different origins in a lung neovascularization model in rodents. *Nat Protoc* **3**, 388-397, doi:10.1038/nprot.2007.537 (2008).
- 122 Stenmark, K. R., Fagan, K. A. & Frid, M. G. Hypoxia-induced pulmonary vascular remodeling: cellular and molecular mechanisms. *Circ Res* **99**, 675-691, doi:10.1161/01.RES.0000243584.45145.3f (2006).
- 123 Taraseviciene-Stewart, L. *et al.* Inhibition of the VEGF receptor 2 combined with chronic hypoxia causes cell death-dependent pulmonary endothelial cell proliferation and severe pulmonary hypertension. *Faseb j* **15**, 427-438, doi:10.1096/fj.00-0343com (2001).
- 124 Vitali, S. H. *et al.* The Sugen 5416/hypoxia mouse model of pulmonary hypertension revisited: long-term follow-up. *Pulm Circ* **4**, 619-629, doi:10.1086/678508 (2014).
- 125 Roth, R. A. & Reindel, J. F. Lung vascular injury from monocrotaline pyrrole, a putative hepatic metabolite. *Adv Exp Med Biol* **283**, 477-487, doi:10.1007/978-1-4684-5877-0_64 (1991).
- 126 Schultze, A. E. & Roth, R. A. Chronic pulmonary hypertension--the monocrotaline model and involvement of the hemostatic system. *J Toxicol Environ Health B Crit Rev* **1**, 271-346, doi:10.1080/10937409809524557 (1998).
- 127 Wilson, D. W. *et al.* Mechanisms and pathology of monocrotaline pulmonary toxicity. *Crit Rev Toxicol* **22**, 307-325, doi:10.3109/10408449209146311 (1992).
- 128 Roth, R. A., Dotzlaf, L. A., Baranyi, B., Kuo, C. H. & Hook, J. B. Effect of monocrotaline ingestion on liver, kidney, and lung of rats. *Toxicol Appl Pharmacol* **60**, 193-203, doi:10.1016/0041-008x(91)90223-2 (1981).

- 129 Tallini, Y. N. *et al.* Propagated endothelial Ca²⁺ waves and arteriolar dilation in vivo: measurements in Cx40BAC GCaMP2 transgenic mice. *Circ Res* **101**, 1300-1309, doi:10.1161/CIRCRESAHA.107.149484 (2007).
- 130 Tallini, Y. N. *et al.* Imaging cellular signals in the heart in vivo: Cardiac expression of the high-signal Ca²⁺ indicator GCaMP2. *Proc Natl Acad Sci U S A* **103**, 4753-4758, doi:10.1073/pnas.0509378103 (2006).
- 131 Villalba, N. *et al.* Traumatic brain injury disrupts cerebrovascular tone through endothelial inducible nitric oxide synthase expression and nitric oxide gain of function. *J Am Heart Assoc* **3**, e001474, doi:10.1161/JAHA.114.001474 (2014).
- 132 Bagher, P. *et al.* Low intravascular pressure activates endothelial cell TRPV4 channels, local Ca²⁺ events, and IKCa channels, reducing arteriolar tone. *Proc Natl Acad Sci U S A* **109**, 18174-18179, doi:10.1073/pnas.1211946109 (2012).
- 133 Clifford, P. S. *et al.* Spatial distribution and mechanical function of elastin in resistance arteries: a role in bearing longitudinal stress. *Arterioscler Thromb Vasc Biol* **31**, 2889-2896, doi:10.1161/ATVBAHA.111.236570 (2011).
- 134 Cheng, E. P. *et al.* Restoration of normal L-type Ca²⁺ channel function during Timothy syndrome by ablation of an anchoring protein. *Circ Res* **109**, 255-261, doi:10.1161/CIRCRESAHA.111.248252 (2011).
- 135 Chung, S. H. & Kennedy, R. A. Coupled Markov chain model: characterization of membrane channel currents with multiple conductance sublevels as partially coupled elementary pores. *Math Biosci* **133**, 111-137 (1996).
- 136 Moreno, C. M. *et al.* Ca(2+) entry into neurons is facilitated by cooperative gating of clustered CaV1.3 channels. *Elife* **5**, doi:10.7554/eLife.15744 (2016).
- 137 Navedo, M. F. *et al.* Increased coupled gating of L-type Ca²⁺ channels during hypertension and Timothy syndrome. *Circ Res* **106**, 748-756, doi:10.1161/CIRCRESAHA.109.213363 (2010).
- 138 Ledoux, J. *et al.* Functional architecture of inositol 1,4,5-trisphosphate signaling in restricted spaces of myoendothelial projections. *Proc Natl Acad Sci U S A* **105**, 9627-9632, doi:10.1073/pnas.0801963105 (2008).
- 139 Pires, P. W., Sullivan, M. N., Pritchard, H. A., Robinson, J. J. & Earley, S. Unitary TRPV3 channel Ca²⁺ influx events elicit endothelium-dependent dilation of cerebral parenchymal arterioles. *Am J Physiol Heart Circ Physiol* **309**, H2031-2041, doi:10.1152/ajpheart.00140.2015 (2015).
- 140 Gil, J. in *Textbook of Pulmonary Vascular Disease* (eds J. X. Yuan *et al.*) 13-24 (Springer, 2010).
- 141 Zhang, L., Papadopoulos, P. & Hamel, E. Endothelial TRPV4 channels mediate dilation of cerebral arteries: impairment and recovery in cerebrovascular pathologies related to Alzheimer's disease. *Br J Pharmacol* **170**, 661-670, doi:10.1111/bph.12315 (2013).
- 142 Blum-Johnston, C. *et al.* Developmental acceleration of bradykinin-dependent relaxation by prenatal chronic hypoxia impedes normal development after birth. *Am J Physiol Lung Cell Mol Physiol* **310**, L271-286, doi:10.1152/ajplung.00340.2015 (2016).

- 143 Fike, C. D., Slaughter, J. C., Kaplowitz, M. R., Zhang, Y. & Aschner, J. L. Reactive oxygen species from NADPH oxidase contribute to altered pulmonary vascular responses in piglets with chronic hypoxia-induced pulmonary hypertension. *Am J Physiol Lung Cell Mol Physiol* **295**, L881-888, doi:10.1152/ajplung.00047.2008 (2008).
- 144 Mam, V. *et al.* Impaired vasoconstriction and nitric oxide-mediated relaxation in pulmonary arteries of hypoxia- and monocrotaline-induced pulmonary hypertensive rats. *J Pharmacol Exp Ther* **332**, 455-462, doi:10.1124/jpet.109.160119 (2010).
- 145 Zhang, R. Z., Yang, Q., Yim, A. P., Huang, Y. & He, G. W. Role of NO and EDHF-mediated endothelial function in the porcine pulmonary circulation: comparison between pulmonary artery and vein. *Vascul Pharmacol* **44**, 183-191, doi:10.1016/j.vph.2005.11.005 (2006).
- 146 Harraz, O. F., Brett, S. E. & Welsh, D. G. Nitric oxide suppresses vascular voltage-gated T-type Ca²⁺ channels through cGMP/PKG signaling. *Am J Physiol Heart Circ Physiol* **306**, H279-285, doi:10.1152/ajpheart.00743.2013 (2014).
- 147 Hu, H., Chiamvimonvat, N., Yamagishi, T. & Marban, E. Direct inhibition of expressed cardiac L-type Ca²⁺ channels by S-nitrosothiol nitric oxide donors. *Circ Res* **81**, 742-752 (1997).
- 148 Lohman, A. W. *et al.* S-nitrosylation inhibits pannexin 1 channel function. *J Biol Chem* **287**, 39602-39612, doi:10.1074/jbc.M112.397976 (2012).
- 149 Mistry, D. K. & Garland, C. J. Nitric oxide (NO)-induced activation of large conductance Ca²⁺-dependent K⁺ channels (BK(Ca)) in smooth muscle cells isolated from the rat mesenteric artery. *Br J Pharmacol* **124**, 1131-1140, doi:10.1038/sj.bjp.0701940 (1998).
- 150 Yin, J. *et al.* Negative-feedback loop attenuates hydrostatic lung edema via a cGMP-dependent regulation of transient receptor potential vanilloid 4. *Circ Res* **102**, 966-974, doi:10.1161/CIRCRESAHA.107.168724 (2008).
- 151 Yoshida, T. *et al.* Nitric oxide activates TRP channels by cysteine S-nitrosylation. *Nat Chem Biol* **2**, 596-607, doi:10.1038/nchembio821 (2006).
- 152 Du, J., Wong, W. Y., Sun, L., Huang, Y. & Yao, X. Protein kinase G inhibits flow-induced Ca²⁺ entry into collecting duct cells. *J Am Soc Nephrol* **23**, 1172-1180, doi:10.1681/ASN.2011100972 (2012).
- 153 Parikh, J., Kapela, A. & Tsoukias, N. M. Stochastic model of endothelial TRPV4 calcium sparklets: effect of bursting and cooperativity on EDH. *Biophys J* **108**, 1566-1576, doi:10.1016/j.bpj.2015.01.034 (2015).
- 154 Welsh, D. G. TRPV4 channel cooperativity in the resistance vasculature. *Biophys J* **108**, 1312-1313, doi:10.1016/j.bpj.2015.01.035 (2015).
- 155 Greenberg, B., Rhoden, K. & Barnes, P. J. Endothelium-dependent relaxation of human pulmonary arteries. *Am J Physiol* **252**, H434-438 (1987).
- 156 Konduri, G. G. & Mital, S. Adenosine and ATP cause nitric oxide-dependent pulmonary vasodilation in fetal lambs. *Biol Neonate* **78**, 220-229, doi:14274 (2000).

- 157 Paffett, M. L. *et al.* Altered membrane lipid domains limit pulmonary endothelial calcium entry following chronic hypoxia. *Am J Physiol Heart Circ Physiol* **301**, H1331-1340, doi:10.1152/ajpheart.00980.2010 (2011).
- 158 Lohman, A. W., Billaud, M. & Isakson, B. E. Mechanisms of ATP release and signalling in the blood vessel wall. *Cardiovasc Res* **95**, 269-280, doi:10.1093/cvr/cvs187 (2012).
- 159 Sprague, R. S. & Ellsworth, M. L. Erythrocyte-derived ATP and perfusion distribution: role of intracellular and intercellular communication. *Microcirculation* **19**, 430-439, doi:10.1111/j.1549-8719.2011.00158.x (2012).
- 160 Parker, I. & Smith, I. F. Recording single-channel activity of inositol trisphosphate receptors in intact cells with a microscope, not a patch clamp. *J Gen Physiol* **136**, 119-127, doi:10.1085/jgp.200910390 (2010).
- 161 Everaerts, W., Nilius, B. & Owsianik, G. The vanilloid transient receptor potential channel TRPV4: from structure to disease. *Prog Biophys Mol Biol* **103**, 2-17, doi:10.1016/j.pbiomolbio.2009.10.002 (2010).
- 162 Pankey, E. A., Zsombok, A., Lasker, G. F. & Kadowitz, P. J. Analysis of responses to the TRPV4 agonist GSK1016790A in the pulmonary vascular bed of the intact-chest rat. *Am J Physiol Heart Circ Physiol* **306**, H33-40, doi:10.1152/ajpheart.00303.2013 (2014).
- 163 Leuranguer, V., Gluais, P., Vanhoutte, P. M., Verbeuren, T. J. & Feletou, M. Openers of calcium-activated potassium channels and endothelium-dependent hyperpolarizations in the guinea pig carotid artery. *Naunyn Schmiedebergs Arch Pharmacol* **377**, 101-109, doi:10.1007/s00210-008-0267-x (2008).
- 164 Fleming, I. & Busse, R. Signal transduction of eNOS activation. *Cardiovasc Res* **43**, 532-541 (1999).
- 165 Garvey, E. P. *et al.* 1400W is a slow, tight binding, and highly selective inhibitor of inducible nitric-oxide synthase in vitro and in vivo. *J Biol Chem* **272**, 4959-4963 (1997).
- 166 Zhang, H. Q., Fast, W., Marletta, M. A., Martasek, P. & Silverman, R. B. Potent and selective inhibition of neuronal nitric oxide synthase by N omega-propyl-L-arginine. *J Med Chem* **40**, 3869-3870, doi:10.1021/jm970550g (1997).
- 167 Cook, S. *et al.* Increased eNO and pulmonary iNOS expression in eNOS null mice. *Eur Respir J* **21**, 770-773 (2003).
- 168 Hess, D. T., Matsumoto, A., Nudelman, R. & Stamler, J. S. S-nitrosylation: spectrum and specificity. *Nat Cell Biol* **3**, E46-49, doi:10.1038/35055152 (2001).
- 169 Pankey, E. A. *et al.* Vasodilator responses to acetylcholine are not mediated by the activation of soluble guanylate cyclase or TRPV4 channels in the rat. *Am J Physiol Heart Circ Physiol* **306**, H1495-1506, doi:10.1152/ajpheart.00978.2013 (2014).
- 170 Qi, H. *et al.* Protein kinase G regulates the basal tension and plays a major role in nitrovasodilator-induced relaxation of porcine coronary veins. *Br J Pharmacol* **152**, 1060-1069, doi:10.1038/sj.bjp.0707479 (2007).

- 171 Konduri, G. G. *et al.* P2Y purine receptor responses and expression in the pulmonary circulation of juvenile rabbits. *Am J Physiol Heart Circ Physiol* **287**, H157-164, doi:10.1152/ajpheart.00617.2003 (2004).
- 172 Sprague, R. S. *et al.* Extracellular ATP signaling in the rabbit lung: erythrocytes as determinants of vascular resistance. *Am J Physiol Heart Circ Physiol* **285**, H693-700, doi:10.1152/ajpheart.01026.2002 (2003).
- 173 Leon, C. *et al.* The P2Y1 receptor is an ADP receptor antagonized by ATP and expressed in platelets and megakaryoblastic cells. *FEBS Lett* **403**, 26-30 (1997).
- 174 Maruyama, J. & Maruyama, K. Impaired nitric oxide-dependent responses and their recovery in hypertensive pulmonary arteries of rats. *Am J Physiol* **266**, H2476-2488 (1994).
- 175 Murata, T., Sato, K., Hori, M., Ozaki, H. & Karaki, H. Decreased endothelial nitric-oxide synthase (eNOS) activity resulting from abnormal interaction between eNOS and its regulatory proteins in hypoxia-induced pulmonary hypertension. *J Biol Chem* **277**, 44085-44092, doi:10.1074/jbc.M205934200 (2002).
- 176 Shaul, P. W., Wells, L. B. & Horning, K. M. Acute and prolonged hypoxia attenuate endothelial nitric oxide production in rat pulmonary arteries by different mechanisms. *J Cardiovasc Pharmacol* **22**, 819-827 (1993).
- 177 Lowson, S. M. Alternatives to nitric oxide. *Br Med Bull* **70**, 119-131, doi:10.1093/bmb/ldh028 (2004).
- 178 Balakrishna, S. *et al.* TRPV4 inhibition counteracts edema and inflammation and improves pulmonary function and oxygen saturation in chemically induced acute lung injury. *Am J Physiol Lung Cell Mol Physiol* **307**, L158-172, doi:10.1152/ajplung.00065.2014 (2014).
- 179 Thorneloe, K. S. *et al.* An orally active TRPV4 channel blocker prevents and resolves pulmonary edema induced by heart failure. *Sci Transl Med* **4**, 159ra148, doi:10.1126/scitranslmed.3004276 (2012).
- 180 Villalta, P. C. & Townsley, M. I. Transient receptor potential channels and regulation of lung endothelial permeability. *Pulm Circ* **3**, 802-815, doi:10.1086/674765 (2013).
- 181 Sullivan, M. N. *et al.* Localized TRPA1 channel Ca²⁺ signals stimulated by reactive oxygen species promote cerebral artery dilation. *Sci Signal* **8**, ra2, doi:10.1126/scisignal.2005659 (2015).
- 182 Ju, H., Zou, R., Venema, V. J. & Venema, R. C. Direct interaction of endothelial nitric-oxide synthase and caveolin-1 inhibits synthase activity. *J Biol Chem* **272**, 18522-18525 (1997).
- 183 Straub, A. C. *et al.* Endothelial cell expression of haemoglobin alpha regulates nitric oxide signalling. *Nature* **491**, 473-477, doi:10.1038/nature11626 (2012).
- 184 Brook, M. M. *et al.* Use of ATP-MgCl₂ in the evaluation and treatment of children with pulmonary hypertension secondary to congenital heart defects. *Circulation* **90**, 1287-1293 (1994).
- 185 Lyubchenko, T. *et al.* P2Y1 and P2Y13 purinergic receptors mediate Ca²⁺ signaling and proliferative responses in pulmonary artery vasa vasorum

- endothelial cells. *Am J Physiol Cell Physiol* **300**, C266-275, doi:10.1152/ajpcell.00237.2010 (2011).
- 186 McMillan, M. R., Burnstock, G. & Haworth, S. G. Vasodilatation of intrapulmonary arteries to P2-receptor nucleotides in normal and pulmonary hypertensive newborn piglets. *Br J Pharmacol* **128**, 543-548, doi:10.1038/sj.bjp.0702815 (1999).
- 187 Visovatti, S. H. *et al.* Purinergic dysregulation in pulmonary hypertension. *Am J Physiol Heart Circ Physiol* **311**, H286-298, doi:10.1152/ajpheart.00572.2015 (2016).
- 188 Rummery, N. M., Brock, J. A., Pakdeechote, P., Ralevic, V. & Dunn, W. R. ATP is the predominant sympathetic neurotransmitter in rat mesenteric arteries at high pressure. *J Physiol* **582**, 745-754, doi:10.1113/jphysiol.2007.134825 (2007).
- 189 Yamamoto, K. *et al.* Visualization of flow-induced ATP release and triggering of Ca²⁺ waves at caveolae in vascular endothelial cells. *J Cell Sci* **124**, 3477-3483, doi:10.1242/jcs.087221 (2011).
- 190 Hill-Eubanks, D. C., Gonzales, A. L., Sonkusare, S. K. & Nelson, M. T. Vascular TRP channels: performing under pressure and going with the flow. *Physiology (Bethesda)* **29**, 343-360, doi:10.1152/physiol.00009.2014 (2014).
- 191 Kohler, R. *et al.* Evidence for a functional role of endothelial transient receptor potential V4 in shear stress-induced vasodilatation. *Arterioscler Thromb Vasc Biol* **26**, 1495-1502, doi:10.1161/01.ATV.0000225698.36212.6a (2006).
- 192 Mendoza, S. A. *et al.* TRPV4-mediated endothelial Ca²⁺ influx and vasodilation in response to shear stress. *Am J Physiol Heart Circ Physiol* **298**, H466-476, doi:10.1152/ajpheart.00854.2009 (2010).
- 193 Denninger, J. W. & Marletta, M. A. Guanylate cyclase and the .NO/cGMP signaling pathway. *Biochim Biophys Acta* **1411**, 334-350 (1999).
- 194 Stasch, J. P., Pacher, P. & Evgenov, O. V. Soluble guanylate cyclase as an emerging therapeutic target in cardiopulmonary disease. *Circulation* **123**, 2263-2273, doi:10.1161/CIRCULATIONAHA.110.981738 (2011).
- 195 Goldenberg, N. M. *et al.* TRPV4 Is Required for Hypoxic Pulmonary Vasoconstriction. *Anesthesiology* **122**, 1338-1348, doi:10.1097/ALN.0000000000000647 (2015).
- 196 Villalta, P. C., Rocic, P. & Townsley, M. I. Role of MMP2 and MMP9 in TRPV4-induced lung injury. *Am J Physiol Lung Cell Mol Physiol* **307**, L652-659, doi:10.1152/ajplung.00113.2014 (2014).
- 197 Lai, Y. C., Potoka, K. C., Champion, H. C., Mora, A. L. & Gladwin, M. T. Pulmonary arterial hypertension: the clinical syndrome. *Circ Res* **115**, 115-130, doi:10.1161/circresaha.115.301146 (2014).
- 198 Barst, R. J. *et al.* Updated evidence-based treatment algorithm in pulmonary arterial hypertension. *J Am Coll Cardiol* **54**, S78-84, doi:10.1016/j.jacc.2009.04.017 (2009).
- 199 Lu, T. *et al.* Role of the endothelial caveolae microdomain in shear stress-mediated coronary vasorelaxation. *J Biol Chem* **292**, 19013-19023, doi:10.1074/jbc.M117.786152 (2017).

- 200 Goedicke-Fritz, S. *et al.* Evidence for functional and dynamic microcompartmentation of Cav-1/TRPV4/K(Ca) in caveolae of endothelial cells. *Eur J Cell Biol* **94**, 391-400, doi:10.1016/j.ejcb.2015.06.002 (2015).
- 201 Bowers, R. *et al.* Oxidative stress in severe pulmonary hypertension. *Am J Respir Crit Care Med* **169**, 764-769, doi:10.1164/rccm.200301-147OC (2004).
- 202 Suresh, K. *et al.* Hydrogen peroxide-induced calcium influx in lung microvascular endothelial cells involves TRPV4. *Am J Physiol Lung Cell Mol Physiol* **309**, L1467-1477, doi:10.1152/ajplung.00275.2015 (2015).
- 203 Sonkusare, S. *et al.* AKAP150-dependent cooperative TRPV4 channel gating is central to endothelium-dependent vasodilation and is disrupted in hypertension (678.10). *The FASEB Journal* **28** (2014).
- 204 Peng, H. *et al.* Identification of a Protein Kinase C-dependent phosphorylation site involved in sensitization of TRPV4 channel. *Biochem Biophys Res Commun* **391**, 1721-1725, doi:10.1016/j.bbrc.2009.12.140 (2010).
- 205 Oka, N. *et al.* Caveolin interaction with protein kinase C. Isoenzyme-dependent regulation of kinase activity by the caveolin scaffolding domain peptide. *J Biol Chem* **272**, 33416-33421, doi:10.1074/jbc.272.52.33416 (1997).
- 206 Je, H. D., Gallant, C., Leavis, P. C. & Morgan, K. G. Caveolin-1 regulates contractility in differentiated vascular smooth muscle. *Am J Physiol Heart Circ Physiol* **286**, H91-98, doi:10.1152/ajpheart.00472.2003 (2004).
- 207 Hampl, V. & Herget, J. Role of nitric oxide in the pathogenesis of chronic pulmonary hypertension. *Physiol Rev* **80**, 1337-1372, doi:10.1152/physrev.2000.80.4.1337 (2000).
- 208 Hampl, V. *et al.* Pulmonary vascular iNOS induction participates in the onset of chronic hypoxic pulmonary hypertension. *Am J Physiol Lung Cell Mol Physiol* **290**, L11-20, doi:10.1152/ajplung.00023.2005 (2006).
- 209 Le Cras, T. D., Xue, C., Rengasamy, A. & Johns, R. A. Chronic hypoxia upregulates endothelial and inducible NO synthase gene and protein expression in rat lung. *Am J Physiol* **270**, L164-170, doi:10.1152/ajplung.1996.270.1.L164 (1996).
- 210 Yang, X. R. *et al.* Upregulation of osmo-mechanosensitive TRPV4 channel facilitates chronic hypoxia-induced myogenic tone and pulmonary hypertension. *Am J Physiol Lung Cell Mol Physiol* **302**, L555-568, doi:10.1152/ajplung.00005.2011 (2012).
- 211 Xia, Y. *et al.* TRPV4 channel contributes to serotonin-induced pulmonary vasoconstriction and the enhanced vascular reactivity in chronic hypoxic pulmonary hypertension. *Am J Physiol Cell Physiol* **305**, C704-715, doi:10.1152/ajpcell.00099.2013 (2013).
- 212 Murata, T. *et al.* Genetic evidence supporting caveolae microdomain regulation of calcium entry in endothelial cells. *J Biol Chem* **282**, 16631-16643, doi:10.1074/jbc.M607948200 (2007).
- 213 Geraci, M. W. *et al.* Gene expression patterns in the lungs of patients with primary pulmonary hypertension: a gene microarray analysis. *Circ Res* **88**, 555-562, doi:10.1161/01.res.88.6.555 (2001).

- 214 Chen, F. *et al.* Caveolin-1 is a negative regulator of NADPH oxidase-derived reactive oxygen species. *Free Radic Biol Med* **73**, 201-213, doi:10.1016/j.freeradbiomed.2014.04.029 (2014).
- 215 Lundberg, J. O., Weitzberg, E. & Gladwin, M. T. The nitrate-nitrite-nitric oxide pathway in physiology and therapeutics. *Nat Rev Drug Discov* **7**, 156-167, doi:10.1038/nrd2466 (2008).
- 216 Cosby, K. *et al.* Nitrite reduction to nitric oxide by deoxyhemoglobin vasodilates the human circulation. *Nat Med* **9**, 1498-1505, doi:10.1038/nm954 (2003).
- 217 Wang, S. *et al.* P2Y(2) and Gq/G(1)(1) control blood pressure by mediating endothelial mechanotransduction. *J Clin Invest* **125**, 3077-3086, doi:10.1172/jci81067 (2015).
- 218 Chen, X. *et al.* Endothelial Cell-Specific Deletion of P2Y2 Receptor Promotes Plaque Stability in Atherosclerosis-Susceptible ApoE-Null Mice. *Arterioscler Thromb Vasc Biol* **37**, 75-83, doi:10.1161/atvbaha.116.308561 (2017).
- 219 Syed, N. I., Tengah, A., Paul, A. & Kennedy, C. Characterisation of P2X receptors expressed in rat pulmonary arteries. *Eur J Pharmacol* **649**, 342-348, doi:10.1016/j.ejphar.2010.09.041 (2010).
- 220 Nilius, B., Vriens, J., Prenen, J., Droogmans, G. & Voets, T. TRPV4 calcium entry channel: a paradigm for gating diversity. *Am J Physiol Cell Physiol* **286**, C195-205, doi:10.1152/ajpcell.00365.2003 (2004).
- 221 Good, M. E. *et al.* Emerging concepts regarding pannexin 1 in the vasculature. *Biochem Soc Trans* **43**, 495-501, doi:10.1042/bst20150045 (2015).
- 222 Gavazzi, G. *et al.* Decreased blood pressure in NOX1-deficient mice. *FEBS Lett* **580**, 497-504, doi:10.1016/j.febslet.2005.12.049 (2006).
- 223 Laubach, V. E., Shesely, E. G., Smithies, O. & Sherman, P. A. Mice lacking inducible nitric oxide synthase are not resistant to lipopolysaccharide-induced death. *Proc Natl Acad Sci U S A* **92**, 10688-10692, doi:10.1073/pnas.92.23.10688 (1995).
- 224 Wunderlich, C. *et al.* Chronic NOS inhibition prevents adverse lung remodeling and pulmonary arterial hypertension in caveolin-1 knockout mice. *Pulm Pharmacol Ther* **21**, 507-515, doi:10.1016/j.pupt.2007.11.005 (2008).
- 225 Ferrer-Sueta, G. *et al.* Biochemistry of Peroxynitrite and Protein Tyrosine Nitration. *Chem Rev* **118**, 1338-1408, doi:10.1021/acs.chemrev.7b00568 (2018).